Christoph Schinwald

Validation of tablet coating parameters

Diploma thesis

Institute for Genomics and Bioinformatics
Graz University of Technology
Petersgasse 14, A-8010 Graz
Head: Univ.-Prof. Dipl.-Ing. Dr.techn. Rudolf Stollberger

Supervisor: Dipl.-Ing. Gregor Toschkoff
Evaluator: Ass.-Prof. Dr. Marcel Scheideler

Graz, May, 2011

EIDESSTATTLICHE ERKLÄRUNG

Ich erkläre an Eides statt, dass ich die vorliegende Arbeit selbstständig verfasst, andere als die angegebenen Quellen/Hilfsmittel nicht benutzt und die den benutzten Quellen wörtlich und inhaltlich entnommenen Stellen als solche kenntlich gemacht habe.

Graz, am …… ……..
(Unterschrift)

Englische Fassung:

STATUTORY DECLARATION

I declare that I have authored this thesis independently, that I have not used other than the declared sources / resources and that I have explicitly marked all material which has been quoted either literally or by content from the used sources.

…… ……..
date (signature)

Acknowledgement

This diploma thesis evolved at the Research Center Pharmaceutical Engineering GmbH, under guidance from Mr. Prof. J. Khinast. At this point I want to thank Mr. DI G. Toschkoff and Mr. Dr. D. Koller for their competent supervision.

Likewise, I want to thank Mr. Dr. M. Scheideler at the Institute for Genomics and Bioinformatics, Graz University of Technology, who kindly took on supervision from side of the university.

Furthermore I want to thank Mr. Dr. F. Reiter of G.L. Pharma for providing the required materials and resources for the implementation of the experiments and Mr. Dr. M. Leitner of the Research Center for Non Destructive Testing GmbH for performing the OCT measurements.

Last but not least I want to thank my family for for their kind support during my studies.

Abstract

Tablet coating is widely used in the pharmaceutical industry to provide tablets with a functional thin film. The purposes of the film include the resistance to gastric juice and the control of the release rate of the active pharmaceutical ingredient (API). The process of tablet coating is complex due to the fact that many inter-dependent parameters take influence on the quality of the final product.

In this work, a Design of Experiments (DoE) plan was created to produce tablet batches with three coating process parameters that were Out of Specification. The coating thickness was determined with a μm-caliper and with Optical Coherence Tomography (OCT). Those results served as a reference for the implementation of Multivariate Data Analysis (MVDA) models that are able to predict the coating thickness of tablets from recorded Near-Infrared (NIR) or Raman spectra. The applied methods were compared regarding their potential to serve as a Process Analytical Technology (PAT) tool.

As the last step, the same tablets were investigated in the destructive USP II dissolution test to get information on gastric juice resistance and API release characteristics. Those attributes are the critical quality attributes and decide whether a produced batch goes on sale or not. The two main findings of the dissolution test were that the influence of process parameters on the coating quality is smaller than assumed, and that the film thickness on the band of the tablet is responsible for the API release performance. NIR proved to be a good in-line PAT tool for coating thickness prediction and OCT is the method of choice for coating quality validation.

Keywords: tablet coating, design of experiments, dissolution test, optical coherence tomography (OCT), Near-infrared spectroscopy (NIR)

Kurzfassung

Tablettenbeschichtung ist in der pharmazeutischen Industrie weit verbreitet, um Tabletten mit einem funktionellen Film zu versehen, welcher diese magensaftresistent macht und ihnen die kontrollierte Wirkstofffreisetzung ermöglicht. Der Prozess der Filmbeschichtung ist sehr komplex und viele Parameter haben Einfluss auf die Qualität des Endprodukts.

In dieser Arbeit wurde ein statistischer Versuchsplan aufgestellt, um Tablettenchargen zu produzieren, bei denen drei Prozessparameter außerhalb der Spezifikation lagen. Die Filmschichtdicke wurde mit einer μm-Schraube und mit Optischer Kohärenztomografie (OCT) ermittelt. Diese Resultate dienten als Referenz für die Erstellung von auf multivariater Datenanalyse basierten Modellen, welche mit Hilfe von Nahinfrarot- (NIR) und Ramanspektren die Schichtdicke vorhersagen können. Die angewendeten Methoden wurden hinsichtlich ihres Potentials, als Prozessüberwachungsgerät zu dienen, untersucht.

Im letzten Schritt wurden Magensaftresistenz und Wirkstofffreisetzungsverhalten der untersuchten Tabletten im Auflösungstest geprüft. Diese Attribute sind die entscheidenden Qualitätsmerkmale und bestimmen, ob eine Charge in den Verkauf geht oder nicht. Es hat sich herausgestellt, dass der Einfluss der Prozessparameter auf die Beschichtungsqualität kleiner ist als anfangs angenommen und dass die Filmschichtdicke am Band der Tablette für die Wirkstofffreisetzungsperformance verantwortlich ist. NIR erwies sich als geeignetes Prozessüberwachungsgerät hinsichtlich Filmschichtdickenprognose und OCT ist die Methode erster Wahl für die Überprüfung der Filmschichtqualität.

Schlagworte: Tablettenbeschichtung, Statistische Versuchsplanung, Auflösungstest, Optische Kohärenztomografie (OCT), Nahinfrarot Spektroskopie (NIR)

Table of Contents

Abstract . . . iv
Kurzfassung . . . v
Table of Contents . . . vi
Abbreviations . . . viii

1. Introduction **1**
1.1. Tablet coating process . . . 1
1.2. Process Analytical Technology and Quality by Design . . . 6
1.3. Scope of this work . . . 7

2. Materials and methods **9**
2.1. Materials . . . 9
2.1.1. Film coating suspension . . . 9
2.1.2. Tablet core composition . . . 9
2.2. Methods . . . 10
2.2.1. Design of Experiments . . . 10
2.2.2. Multivariate Data Analysis . . . 12
2.2.3. Near Infrared Spectroscopy . . . 18
2.2.4. Raman Spectroscopy . . . 20
2.2.5. Optical Coherence Tomography . . . 21

3. Results and discussion **23**
3.1. Performing a Design of Experiments . . . 23
3.2. Mechanical survey . . . 31
3.2.1. Determination of film coating thickness . . . 31
3.2.2. Determination of tablet weight . . . 34
3.3. Near Infrared Spectroscopy . . . 38
3.3.1. Monitoring the gain in film coating thickness . . . 38
3.3.2. Selection of batch representative tablets . . . 40
3.4. Raman Spectroscopy . . . 44
3.4.1. Monitoring the gain in film coating thickness . . . 44
3.4.2. Selection of batch representative tablets . . . 46

3.5. Optical Coherence Tomography 48
3.5.1. Determination of image resolution and refractive index 48
3.5.2. Determination of film coating thickness 49
3.6. Dissolution test 63

4. Summary and conclusions **68**

List of Figures 70
List of Tables 73
References 75

A. Appendix **A 1**
A.1. Used devices and programs . . . . . A 1
A.2. Response Surfaces . . . . . A 1
A.3. Histograms . . . . . A 3
A.4. OCT Images . . . . . A 7
A.4. Experimental plan (DoE) . . . . . A 11
A.5. Image processing algorithm . . . . . A 12

Abbreviations

API	Active Pharmaceutical Ingredient
ASA	Acetylsalicylic acid
QbD	Quality by Design
CLSM	Confocal Laser Scanning Microscopy
CQA	Critical Quality Attributes
DoE	Design of Experiments
FDA	US Federal Food and Drug Administration
FT	Fourier-transformed
IPT	Image Processing Toolbox™
LOD	Loss On Drying
MAT	Matlab, determined with Matlab algorithm
MECH	Mechanic, determined with μm-caliper
MVDA	Multivariate Data Analysis
NIR	Near-Infrared Spectroscopy
OCT	Optical Coherence Tomography
OOS	Out Of Specification
PAT	Process Analytical Technology
PC1	First Principal Component
PC2	Second Principal Component
PCA	Principal Component Analysis
PLS	Partial Least Squares Regression
RSME	Root Mean Square Error
SEM	Scanning Electron Microscopy
SNV	Standard Normal Variate
TPI	Terahertz Pulse Imaging
USP	United States Pharmacopeia
UV	Unit Variance

Pilot batch numbers with process parameter in variation:

tablet A		tablet B	
212/10	Replication experiment	226/10	Replication experiment
213/10	High tablet bed temperature	227/10	High tablet bed temperature
214/10	Low tablet bed temperature	228/10	Low supply air power
215/10	High spray rate	229/10	Low spray rate
216/10	Low spray rate	230/10	Replication experiment
217/10	High supply air power	231/10	High supply air power
218/10	Low supply air power	232/10	Replication experiment
224/10	Replication experiment	233/10	High spray rate
225/10	Replication experiment	234/10	Low tablet bed temperature

1. Introduction

1.1. Tablet coating process

Tablet coating is widely used in the pharmaceutical industry to provide tablet cores with a functional thin film as a protection against external influences. The components of one tablet core, most important its active pharmaceutical ingredient (API), may be sensitive to degradation caused by sunlight or exposure to atmospheric oxygen. Other reasons for a film layer could be the resistance against the gastric juice using enteric-coating or the achievement of a specific drug release profile. Apart from that, also non-functional film coating is desired sometimes to cover an unpleasant odour or taste, or to improve visual appearance/distinctiveness of the product. There are different techniques which are used to apply a coating to a tablet core: sugar coating, film coating, particulate/pellet coating and compression coating.[1]

Tablet coating originates from the sugar coating process developed by the confectionery industry for covering candies. The main disadvantages of this process were the long processing time up to 5 days and the high degree of operator skill required for achieving an elegant finish. In sugar coating, syrup was added to the candies moved in an open, bowl-shaped pan and the drying air was shut off. Afterwards the syrup was distributed by tablet to tablet contact until the whole batch was covered and the sugar film started to dry. By switching on the drying air again, a smooth coat was developed. Because of the mentioned disadvantages in time exposure and intricacy, the pharmaceutical industry made efforts to simplify this process by inventing new innovative pan coaters, air suspension techniques in a fluidized bed, spray atomizing techniques and improved drying systems with vented drums. Another alternative developed was the compression coating where the coating material is being compressed around the core. Unfortunately, this method is tainted with several disadvantages. A sufficient bond between coat and core is difficult to obtain. Core expansions causes the coat to split and the process time is relatively long.[1]

The development of new coating materials based on cellulose derivatives made it possible, to produce the first film-coated tablet which was introduced to market by Abbott Laboratories in 1954. It was produced in a fluidized bed coating column based

on the Wurster principle (Wurster, 1953). The most important agent of the cellulose derivatives is hydroxypropyl methylcellulose, which was generally applied in organic solvents. The organic solvents were more and more replaced by the aqueous film solutions because of several reasons, for instance the continuous price escalation, the substitution of coating columns by perforated side-vented pans, the easier suspension handling, the dispensability of recovery systems and environmental considerations.[2]

Nowadays, tablet coating is almost exclusively performed in pan coaters, which will be introduced later in this chapter, and fluidized bed coaters. Figure 1.1 shows the principal functionality of three different fluidized bed coaters. Coater (a) is based on the Wurster principle with bottom spray and draft tube inside the bed, (b) shows a granulator with top spray and (c) is equipped with tangential spray and a rotating disk. The fluidizing air is fed through the gap between rotor and bed wall. It is also called 'Rotor-processor'.[3] The basic principle of applying the coat is similar for all three fluidized bed coaters: the inlet air provides a moving tablet bed, where each tablet should be equally exposed to the spray, and the drying of sprayed on suspension at the same time. The three conceptual phases are similar to those in a pan coater as shown in figure 1.4.[4]

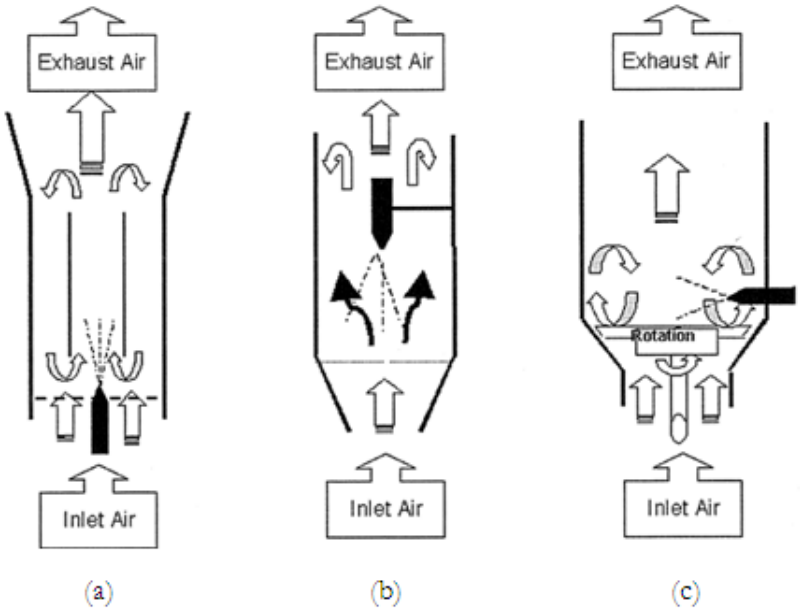

Figure 1.1.: Schematic of a fluidized bed coater.[3]

Film coating materials and their properties:[5]

- *Polymers:* The polymer builds the base of every film coating and dissolves in either water or non-aqueous solvent. Regarding their functionality polymers can be separated in three groups: polymers for conventional film coating, polymers for modified release application and enteric polymers.

- *Polymer characteristics:* There are different physical and chemical attributes that describes a polymer. Those are the grade of solubility depending on the solvent, the viscosity specifying the manner of coating development, the grade of permeability providing a moisture barrier to infiltrating solvent and different mechanical properties like tensile strength or modulus of elasticity.
- *Plasticizers:* Plasticizer are serving the purpose of improving the physical properties of a polymer and to support the polymer in performing its function as film-coating. The plasticizer molecules interpose themselves between the polymer strands and amplifies the polymer-polymer interaction scope. This is chemically enhanced through the stronger polymer-plasticizer interaction compared to the polymer-polymer interaction. In general, the polymer' strands ability to move past each other is improved and the plasticizer makes the suspension softer and more pliable. However, it has to be considered, that a high plasticizer content enlarges the viscosity of the coating suspension.
- *Colorants/opacifiers:* Beside the function of providing tablets an aesthetic appearance, the usage of colorants and opacifiers has several other advantages such as the higher recognition value for patients taking multiple medication, the prevention of counterfeiting and the modified optical characteristics to prevent the pass of sunlight through the coating for protection of the API. Also the application of colorants are modifying permeability and mechanical properties of the coating suspension.
- *Solvents/vehicles:* The solvent/vehicle conveys the coating materials to the surface of the tablet and has to interact adequate with the polymer to prevent a manipulation of the suspensions ability of adhesion and development. Water, alcohol or ketones are usual solvents.

There is a large number of factors that influence the final product quality in a coating process. Regarding the drying air those are the flow rate, the temperature and the moisture content. In case of tablets, the parameters to consider are size, shape, hardness, friability, surface roughness and porosity. For spray consistency the gun design, the number of spray guns, the angle and distance of gun to bed, the spray rate and the pressure settings are of importance. The coating formulation characteristics to consider are mentioned above. When using a pan coater further parameters have to be taken into account. Those are geometry, pan speed, particle load, bed porosity, surface area, mixing baffles, perforation and bed temperature. Although the coating process has a long history, it remains challenging to understand the influence and interaction of all the parameters listed above.[6][7]

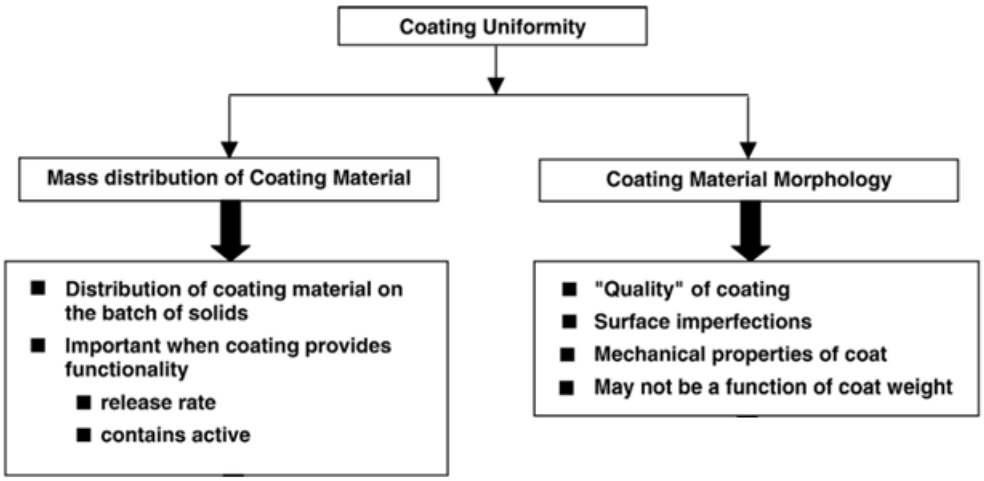

Figure 1.2.: Classification of coating uniformity.[4]

An important quality parameter of coated tablets is the *Coating Uniformity* which can be split up in two categories: the mass distribution of coating material among particles and the coating morphology on each individual particle. This is schematically shown in figure 1.2.[4]

- *Mass Coating Uniformity:* The variation in mass of coating material among the tablets of an identical batch is denoted as mass coating uniformity. The importance of the mass coating variation depends on the purpose of the coating. If the tablet is coated with a non-functional film to improve the appearance for instance, the mass coating uniformity is not indispensable as long as all tablets do not optically differ from each other. On the other hand, if a tablet is provided with a functional film like an enteric coating for the protection of a containing API, the mass coating uniformity is an essential criterion to quality. Unequal distribution of coating in a batch leads to different gastric juice resistance and API release performance during quality testing.

- *Coating Morphology:* The coating quality regarding its distribution on an individual tablet is known as coating morphology. Even if a batch shows a consistent mass coating uniformity, the distribution of the film may differ from tablet to tablet. For example, several tablets may received a thicker film on the band than on the top or bottom or others are not fully covered and the coating is scrappy. Those unequal distributions affect the outcome of the dissolution test. Hence, it is inevitable to quantify the parameters that lead to coating morphology inhomogeneities.

Apart from pan and fluidized bed coating there are other methods using solvent-free coating techniques like hot-melt coating, supercritical fluid spray coating, electrostatic coating, dry powder coating, photocurable coating and compression coating.

In this work we focused on enteric-coated tablets produced in a pan coater using film coating. Figure 1.3 shows the principal functionality of a side-vented pan coater.

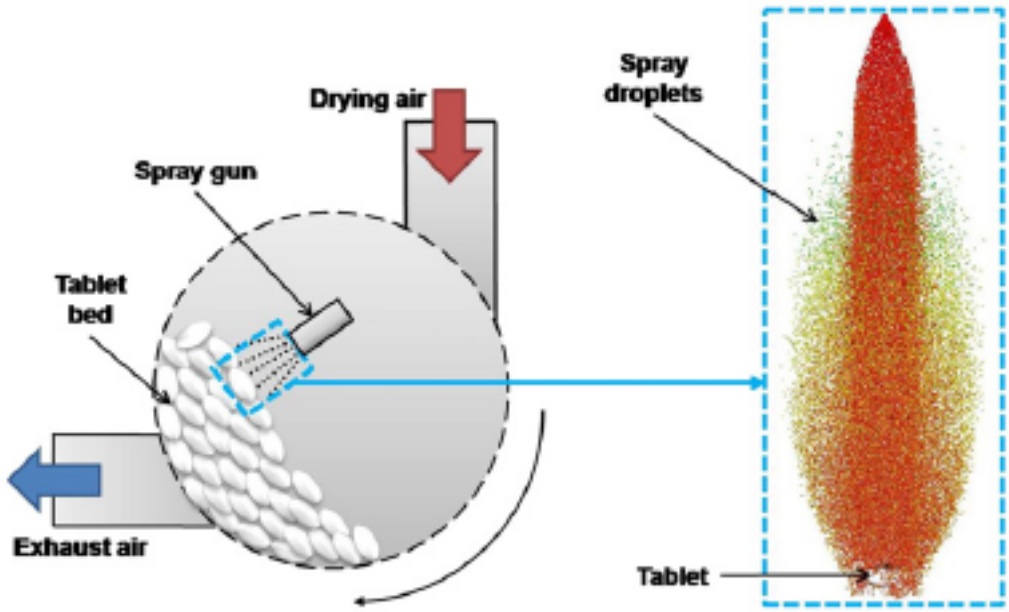

Figure 1.3.: Schematic of a side-vented pan coater and spray anatomy.[2]

The spray gun is atomizing the coating suspension in use and in this way distributing it to the continuously moving tablet bed. Although a single tablet is exposed to the spray only for a fraction of a second, it is necessary to dry the coating solution in order to avoid one tablet sticking to the surrounding tablets.[2] Therefore, drying air is applied, in the shown case directed towards the tablet bed. The exhaust air can exit either through the perforations in the pan as shown in figure 1.3, a side-opening or an integrated immersion tube system.[1][2]

The coating process itself can be broken up into 3 three parts as shown in figure 1.4. In an ideal situation every single tablet passes the spray as often and as long as all the others. In this way, each tablet gets wetted with the same amount of suspension and is sufficiently dried before it is exposed to the spray for the next time.

Generally, the development of a high-quality film coating is specified by the ability of the atomized droplets to coalesce, adhere and cohere. Those properties on the other hand are dependent on characteristics like droplet size, viscosity or surface tension and subsequently defined by process parameters like tablet bed temperature, spray rate, drying air flow, gun-to-bed distance.[1]

At the moment, the ideal process parameters are predefined by the manufactures of pan coaters, but there is little information on how wrong adjustment of a certain process parameter impacts the coating quality and leads to defects like chipping, blistering,

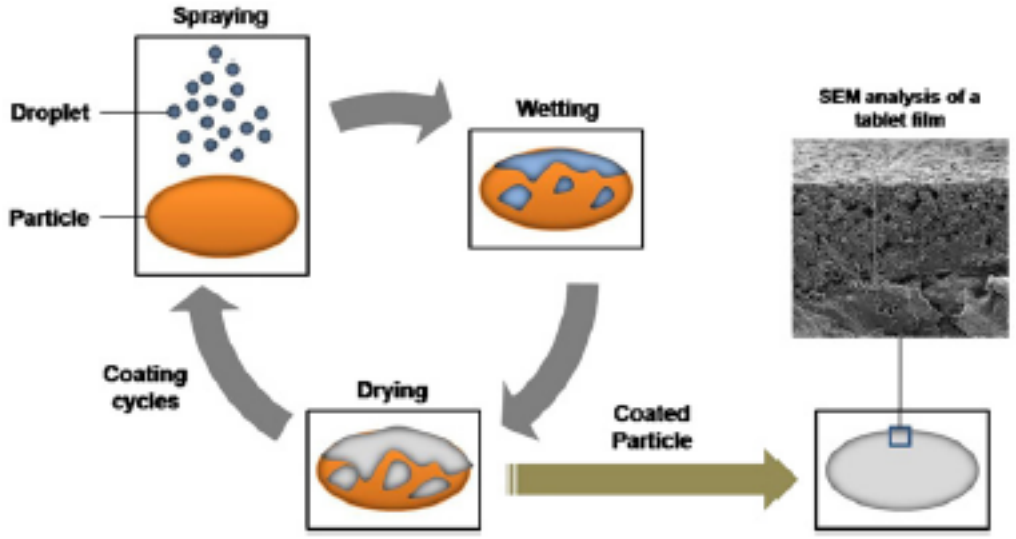

Figure 1.4.: Three conceptual phases of the coating process.[2]

sticking, picking, cratering, pitting, blushing, blooming or film cracking.[2] Due to the fact that the tablet coating process is the last production step, an invalid production goes hand in hand with enormous charges.

1.2. Process Analytical Technology and Quality by Design

Process Analytical Technology (PAT) has been implemented by the pharmaceutical industry in collaboration with the US Federal Food and Drug Administration (FDA) in order to improve the target product quality. In general PAT is 'a systems for analysis and control of manufacturing processes based on timely measurements of critical quality parameters and performance attributes of raw materials and in-process products, to assure acceptable end-product quality at the completion of the process.[8] The big advantage of PAT is that the continuous and non-invasive monitoring of processes in real-time makes it able to intervene and correct in the case of an error.[9][10] This is in conformity with the FDAs Quality by Design (QbD) guidelines. QbD elements include the definition of the target product quality, the designing of product and manufacturing processes, the identification of critical quality attributes, process parameters, and sources of variability and the controlling of manufacturing processes to produce consistent quality over time. In other words, instead of detecting an error by exhaustive testing of final product at the end, out-of-specification parameters leading to decreased product quality should already be discovered during the process and the subsequent reinvention of the process should help to avoid failures.[11]

An established example for a pharmaceutical PAT is the application of Near-infrared spectroscopy (NIR). It is already used to determine both physical and chemical properties of tablet cores and their coating.[12] Furthermore, NIR is used to detect the homogeneity of powder blends.[13] An important tool to handle and analyze the obtained spectral data is Multivariate Data Analysis (MVDA). With Principal Component Analysis (PCA) and Partial Least Squares Regression (PLS), valid process models can be created and Critical Quality Attributes (CQA) can be predicted.[14]

1.3. Scope of this work

In the literature, a wide range of information is available analyzing the quality of film coatings using different methods. The film coating anatomy of double and conventional enteric-coated systems during the United States Pharmacopeia (USP) II dissolution test was analyzed using Scanning Electron Microscopy (SEM) and Confocal Laser Scanning Microscopy (CLSM). Also the drug release performance of tablets out of the same batch has been shown.[15] The roughness of the film coating surface on batches with varying spray gun pressure was illustrated using CLSM. Further, the results were compared to the ones obtained with implemented roughness measuring methods.[16] Both methods are invasive and require a destruction of the tablet under investigation. Additionally they are, due to the long image processing times, difficult to adapt for in process monitoring or as a PAT application.

Another method of analyzing film coatings is NIR. It was used for determining the spectra of tablets coated with different plasticizer content and compressed with varying target hardness. Models predicting film-coating thickness and tablet hardness were built using MVDA and relations to their drug release performance were implemented.[17] The in-line drying end point of a fluidized bed process based on the NIR spectra and Loss On Drying (LOD) humidity determinations was predicted with a PLS model.[18]. In other studies, the influence of varying tablet load and plenum pressure on coating thickness was analyzed and different methods of analysis were compared (X-ray flourescene, Raman and near-infrared spectroscopy).[12] The mentioned Raman spectroscopy was used to implement a PLS model that predicts the tablet's exposure time in a pan coater.[19] A similar approach was used for predicting the film coating thickness for tablets by investigating the Raman spectra of batches with increasing weight gain from zero to six percent. Also the titanium dioxide concentration in suspension was varied.[20] A variety of tablets with different shapes, formulations and coatings were measured with Optical Coherence Tomography (OCT) and the potential of this method was highlighted.[21] The coating of pharmaceutical tablets are analyzed and compared with OCT and Terahertz Pulse Imaging (TPI).[22] In other studies, the coating of

commercially available tablets were investigated with TPI and the results compared to microscopic cut-through photographs.[23] Furthermore, 3D images representing the coating thickness could be implemented.[24][25] The last four methods mentioned (i.e., X-Ray, Raman/NIR, OCT, TPI) are non-invasive and have relatively short processing times. In the available literature, the methods were either applied on tablets produced 'in specification', or a variation of material parameters took place. The influence of varying process parameters like temperature on the coating development was not investigated.

In this work, 'out of specification' batches were produced by controlled variation of different process parameters (tablet bed temperature, spray rate and supply air flow rate). In further consequence, batch-representative tablets were selected, and investigated with a micrometer caliper in order to measure the coating thickness at top and band of the tablet, NIR and Raman spectroscopy in order to predict the coating thickness and separate the tablets regarding their moisture content and OCT in order to validate the film coating quality. Finally, the chosen tablets were tested in the USP II dissolution test, where the resistance to gastric juice and the API release characteristics were determined.[26] This test is the crucial quality feature and decides whether a produced batch goes on sale or not.

Currently, little information about the causality between process parameters, film coating quality and dissolution test results is available in literature. In other words, in some cases there is no clear reason why a batch fails or passes the dissolution test. The aim of this thesis is to evaluate the influence of the different varying process parameters on the film coating quality and further on the tablets USP II dissolution test performance. Therefore, the different methods of analysis are compared regarding their potential to monitor parameters crucial to quality and to serve as a PAT tool. An improved quality monitoring enables the intervention into inferior processes and the prevention of invalid batches.

2. Materials and methods

2.1. Materials

In the presented work, pressed film tablets of bi-convex shape with acetylsalicylic acid (ASA) as active pharmaceutical ingredient were investigated regarding the film coating process. Those tablets are getting enteric-coated to protect the stomach from the harms of the acid. Two different core sizes were examined: tablets cores with a raw weight of 200 mg and 148 mg. In further consequence they are denoted as *tablet A* and *tablet B*.

2.1.1. Film coating suspension

Table 2.1 shows the approximate composition of the coating suspension applied to the raw tablets.

Table 2.1.: Composition of the enteric film coating suspension.

Raw material	(mg)/tablet	(%)
Talcum	3,795	25,3
Glyceryl triacetate	1,020	6,8
Eudragit L30D-55	10,185	67,9
Aqua purificata	38,0	-
Sum	15,0	100

2.1.2. Tablet core composition

The exact composition of the raw tablets is a company secret and can not be disclosed in this work.

2.2. Methods

2.2.1. Design of Experiments

Design of Experiments (DoE) is a tool to perform experiments in a controlled and predefined way. It has a wide range of applications, including the development or improvement of new or existing products and processes, the optimization of quality and performance of a product or the enhancement of existing manufacturing procedures. Using DoE, experiments are performed in a systematic and statistical convincing way and the influence of certain input factors on the monitored output factors are tested.[27]

In many cases there are a lot of input factors to consider and it is therefore necessary to apply a strategy on the experimental plan. In general, DoE offers three different experimental designs: full factorial, fractional factorial and composite design. Based on a standard reference experiment, the so called center point, new experiments are realized by varying their input factors in a symmetrical way around the center point's factors. To gain a better statistical significance and for proving reproducibility the reference experiment is repeated three to five times. Figure 2.1 shows the different factorial designs. The replication experiments are building the base for every design. To perform a full factorial design, the corner experiments have to be realized. For a fractional design it is sufficient to execute the fractional experiments and for optimization issues, corner and axial experiments have to accomplished.[28]

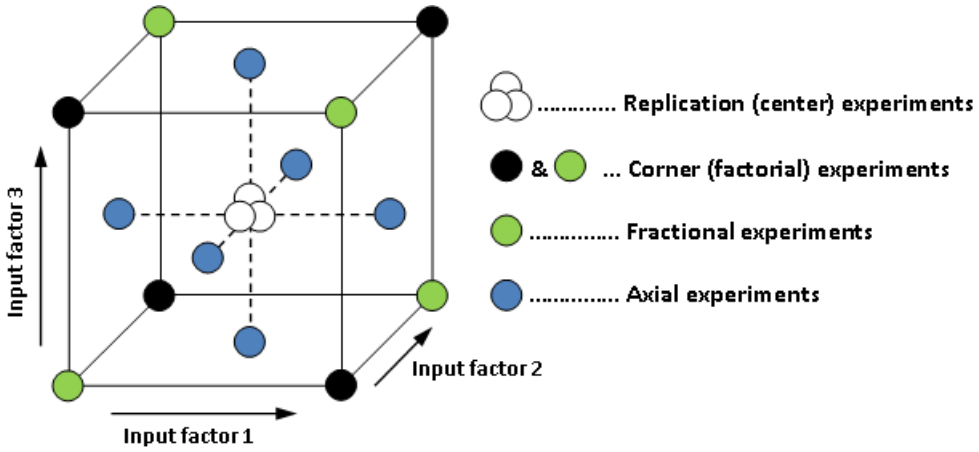

Figure 2.1.: The three factorial designs offered in DoE.

2.2.1.1. Performing a Design of Experiments

There are existing guidelines that an experimental design should should consider[29]:

Recognition of and statement of the problem. Beside the importance of recognizing and defining the problem, it is necessary to think about the desired result and the way of achieving it.

Choice of factors, levels, and ranges. In most cases there is a variety of factors taking influence on the process output. In sophisticated processes and experiments, it would be impossible to consider all of them. Additionally, not every factor is controllable or adjustable. Therefore, it is necessary to figure out the important factors and to chose a reasonable range of variation.

Selection of response variable. It is important that meaningful output factors are chosen. The method of determining this factors and the time this measurement takes should also be considered for selection.

Choice of experimental design. Depending on the chosen factors and the resources that limit the number of experiments, there are several experimental designs that can be taken. Special DoE software provides the established designs and generates the experimental plan.

Performing the experiments.

Statistical analysis of the data. Only results with a statistical significance allow objective conclusions. As explained in chapter 2.2.2, the obtained results were analyzed regarding validity and reproducibility and models for the prediction of outputs were built.

Conclusions and recommendations. Conclusions are made by interpreting graphs that predict the output factors for varying inputs. As a next step it is useful to design validation or follow-up experiments.

2.2.2. Multivariate Data Analysis

Multivariate Data Analysis (MVDA) provides the possibility of handling an enormous set of data and gives one the chance to work out the important information. Because of the increasing importance of spectroscopical methods for process analysis and monitoring in the pharmaceutical industry, the present data are spectral in many cases. With the help of MVDA it is feasible to extract meaningful information from the large amount of raw data and to obtain Critical Quality Attributes (CQA) out of a variety of spectra.[14]

2.2.2.1. Principal Component Analysis

In the first step it is necessary to obtain a concentration of information. Data that carries the relevant information should be spotted while non-informative data should be reduced. The different measured objects can be arranged in clusters and information about the reasons of cluster affinity can be gained. This is done with the help of Principal Component Analysis (PCA). Beforehand it is useful to perform a data pretreatment[30]:

Scaling: Before performing a PCA the data is often pre-treated. Within the variables there is often a big difference in the numerical value and range. Side PCA is a maximum variance projection method, variables with a wide-range value and variance would be expressed more than variables with a low variance. The most common method to provide this is unit variance (UV) scaling. For each variable, the standard deviation is calculated and its inverse is taken as the scaling weight. The variance of each scaled variable is normalized afterwards.

Mean-centering: To improve the interpretability of the model, the mean value of each variable is subtracted from the data.

Figure 2.2 shows a graphical interpretation of the pretreatments.

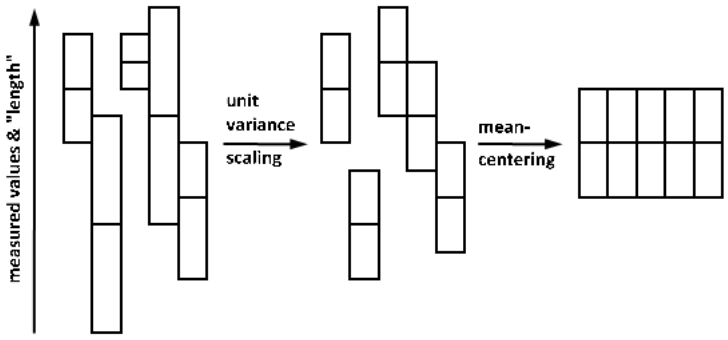

Figure 2.2.: UV-scaled and mean-centered data.

A variable space where each observed variable is represented by a separate coordinate axis is set up. In this space, each observation is represented by a single point, multiple measurements thus leading to a swarm of points. The mean value of the swarm is determined and subtracted from the data. In the last step the mentioned UV-scaling is performed. Figure 2.3 shows this procedure for a three-dimensional variable space.

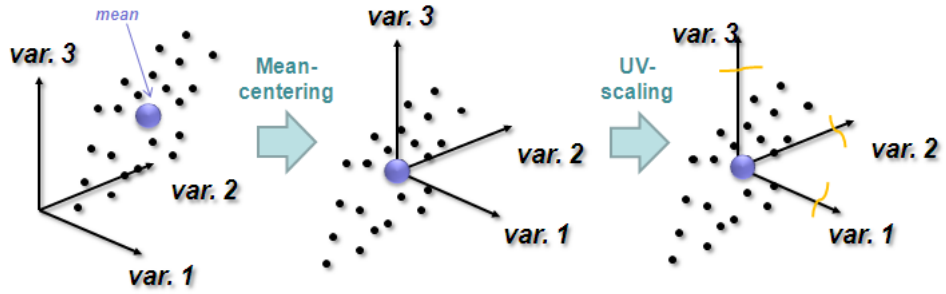

Figure 2.3.: Data set in variable space before and after pretreatment.

The first principal component (PC1) is the line that approximates the data in the least square sense and maximizes the variance of the points along this line. It goes through the mean point as seen in figure 2.4. The value of the observations projection is called score t. The information about the principal components alignment regarding the variable space is carried by the loadings p as shown in figure 2.5. They are providing information about the score's significance.

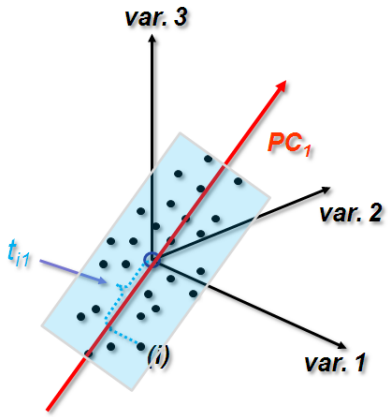

Figure 2.4.: Least square approximation of data lead to PC1.

The second principal component (PC2) is essential to model the systematic variation of the data set. It is orthogonal to PC1 and also passes the mean point as shown in figure 2.6. PC1 and PC2 together define a low-dimensional two-dimensional plane and the projection values of the observations (scores and loadings) represent the data set structure in a simplified way.[30]

In general, the PCA generates new independent latent variables consisting of scores and loadings. The interpretation of scores gives information about the relationships

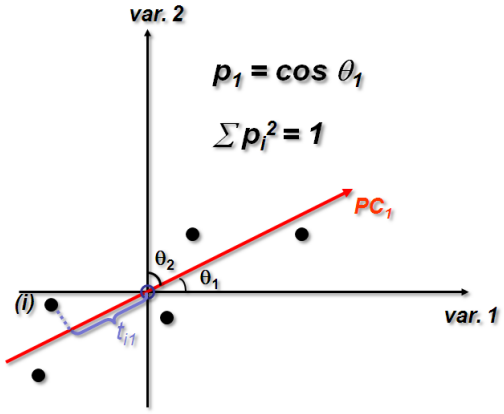

Figure 2.5.: Calculation of loading p_{i1}.

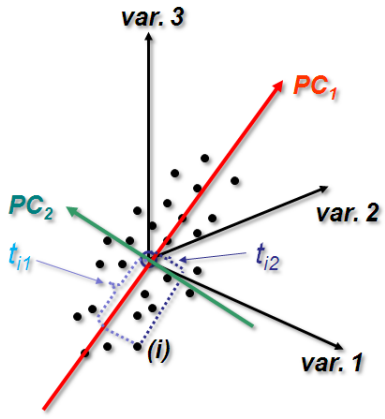

Figure 2.6.: PC1 and PC2 plane in three dimensional space.

between objects (trends, groupings, outliers) and the evaluation of loadings explains patterns in scores.

2.2.2.2. Partial Least Squares Regression

Partial Least Squares (PLS) Regression can be interpreted as a regression extension of PCA, which connects the information contained in two blocks of variable, the predictor X and the response Y, to each other. Compared to PCA, each row of the data table corresponds to two points in each space instead of one. For simplicity, in the following the PLS is further explained for three predictor variables and one response variable. The data space is three-dimensional and the response is represented by a one-dimensional vector as seen in figure 2.7.

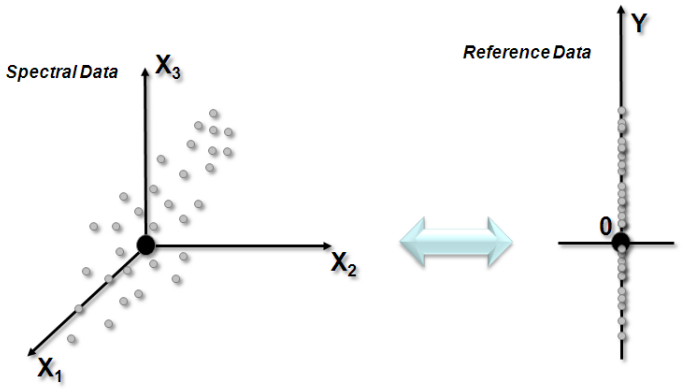

Figure 2.7.: Three prediction and one response variable spaces.

The first PLS component is the best approximation of the data point swarm and provides a good correlation to the y-vector at the same time. The projection of all objects onto the first component forms the score vector t_1 that represents the analytical information. The first model estimate ($\hat{Y}_{(1)}$) is obtained by multiplying the score vector by the the weight of the y-vector (c_1). The residuals are representing the variation that is unexplained by the first PLS component and the projection of this points leads to the residual vector f_1. Figure 2.8 shows a graphical interpretation of this calculation.

The second PLS component is located orthogonal to the first. It also provides a good approximation of the X-data and is in correlation to the weight of the y-vector after the first PLS component, or in other words to the residual vector f_1. Figure 2.9 shows the determination of the second component.

The model estimate ($\hat{Y}_{(2)}$) for a two component PLS regression is obtained by adding up the score/weight multiplications as illustrated in figure 2.10.

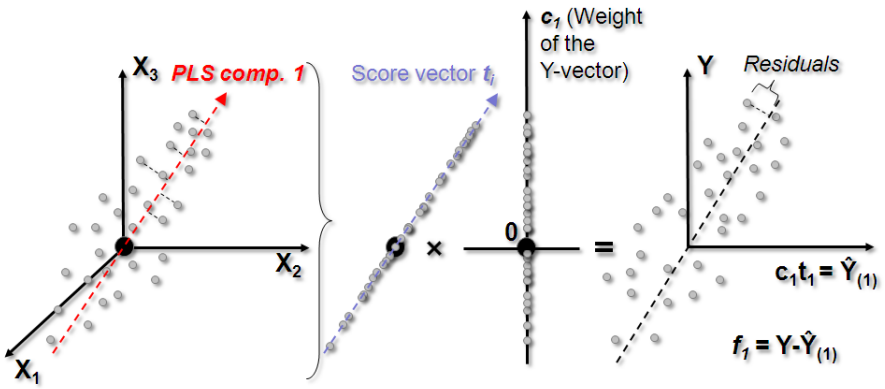

Figure 2.8.: Determination of first PLS component.

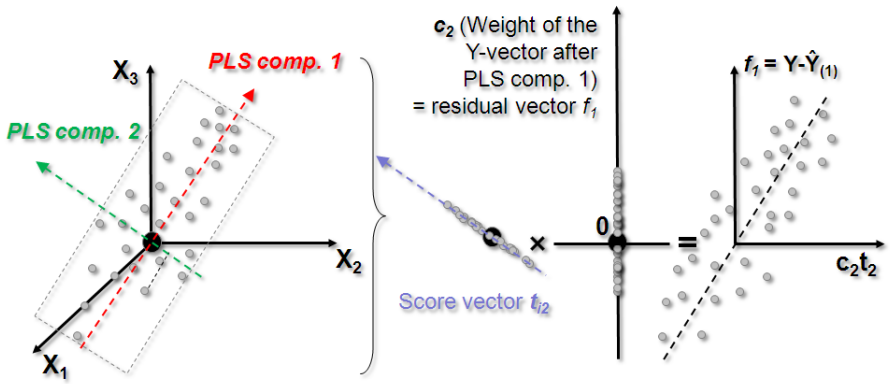

Figure 2.9.: Determination of second PLS component.

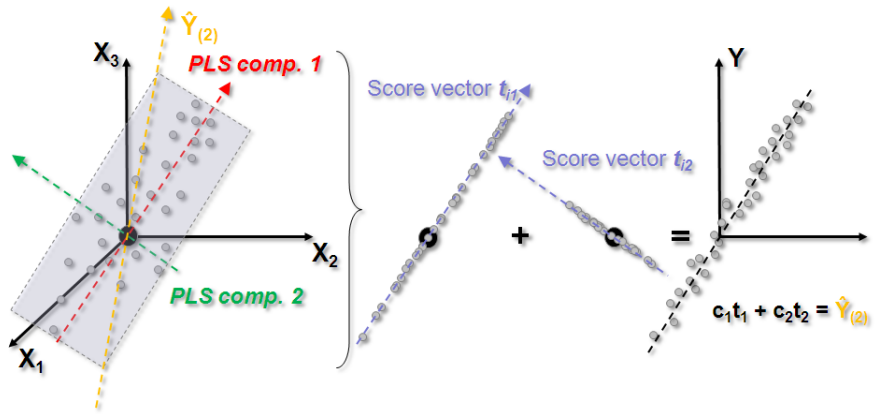

Figure 2.10.: Calculation of two component PLS model.

The response is better modeled by an increasing number of components. This is because of the better agreement between observed and estimated Y-data that leads to smaller residuals. The perfect model of response would have zero residuals.[30]

2.2.2.3. Pretreatments

Before applying a PLS regression on a set of data (e.g. spectra), it is often preprocessed with different correction techniques to enhance the models predictive ability. Undesired systematic variation in the calibration data, for instance baseline drift, scatter effects or regions of low information content that is unrelated to the response, is removed using those techniques and the predictive power is improved. [30] The pretreatments used in this work are [14]:

Baseline Correction: Probe contamination, loss in intensity due to scattering or systematic problems with the measuring arrangement may lead to a systematic deviation between baseline and data set. This drift is removed with the help of 'Baseline Correction'. The whole spectrum a consists of the important information $\tilde{a}$ and of a polynomial that approximates the disturbances as seen in equation (2.1).

$$a = \tilde{a} + \alpha + \beta \cdot x + \dots \tag{2.1}$$

Both constant offset α and linear offset $\beta \cdot x$, if present, are eliminated.

Standard Normal Variate Correction (SNV): The primary function of SNV is the correction of scatter effects. The mean and the variance of each spectrum is calculated. Independently for every spectrum, the measured value at wavelength i is reduced by subtracting the mean and dividing the standard deviation of the row as seen in equation (2.2).

$$x_{\mathrm{i,SNV}} = \frac{(x_{\mathrm{i}} - \overline{x})}{\sqrt{\dfrac{\sum_{i=1}^{p}(x_{\mathrm{i}} - \overline{x})^2}{p-1}}} \tag{2.2}$$

2.2.3. Near Infrared Spectroscopy

Near infrared light covers the range from 780 nm to 2526 nm (wavenumbers 12820 cm^{-}1 to 3959 cm^{-}1) in the electromagnetic spectrum. The Near Infrared Spectroscopy (NIR) is based on the light absorption in this region, that is caused by overtones and combinations of fundamental vibration bands. For identification of a certain substance, the emitted near infrared light frequency should meet the fundamental vibration frequency of its molecules. This vibrational frequency f is explicable with Hooke's law, assuming a harmonic oscillator model. An atom shifts from the equilibrium position with a strength proportional to the shift:

$$f = \frac{1}{2 \cdot \pi \cdot c} \cdot \sqrt{\frac{k}{\mu}} \tag{2.3}$$

where c is the speed of light, k the bonding force of a chemical bond in its normal equilibrium position and m the reduced mass.[31]

Therefore, the probes ability of absorption is frequency (or wavenumber) dependent and material specific adsorption spectra can be obtained.[32] The basic instrument design of a NIR spectrometer is shown in figure 2.11. Here, the reflected light is being measured, which is desired when investigating opaque solids. However, there are also spectrometers for recording transmitted light, e.g. in case of fluids.[33]

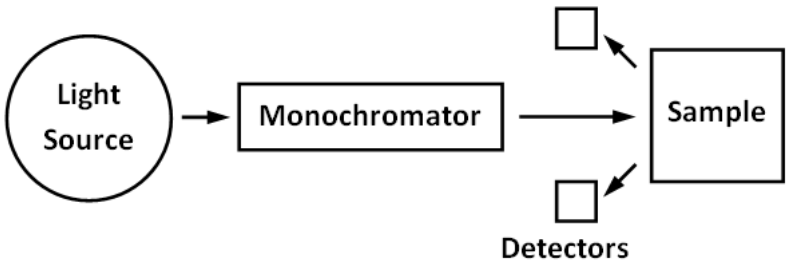

Figure 2.11.: Schematic of a NIR spectrometer for measuring reflectance.

Fourier Transform spectrometers (FT-NIR) are utilizing an interferometer (typically a Michelson-interferometer) for NIR signal modulation and a computer to obtain the materials spectra. Dependent on the beam spacing, which is set by a moving mirror, the corresponding interferograms are recorded. Afterwards, they are Fourier-transformed into intensity value at certain wavelength. The advantages of the FT-NIR compared to a dispersive spectrometer are numerous, a major advantage is that all frequencies of a wide-range spectra can be processed simultaneously and the measuring time is decreased.[33]

NIR diffuse reflectance spectroscopy: When measuring solids, the reflected light consists of two parts, the specular and the diffuse component. Specular reflectance contains little information about the materials composition and is therefore minimized by adjusting the sample-detector position. The more interesting diffuse reflectance is described by the Kubelka-Munk theory, which is rewritten for relative reflectance R (intensity ratio sample to standard):

$$f(R) = \frac{(1-R)^2}{2 \cdot R} = \frac{k}{s} = \frac{\epsilon \cdot \ c \cdot ln(10)}{s} \tag{2.4}$$

where k is the samples absorption coefficient and s its dispersion coefficient, c the concentration of the absorbing analyte and ϵ the specific absorptivity. This equation provides a linear $f(R)$ to c relationship and is valid for weak adsorption bands, or when the absorptivity-concentration product is small. If the analyte exhibits strong adsorption bands, the absorbance A follows Beer's law:

$$A = log\left(\frac{1}{R}\right) = \epsilon \cdot c \cdot d \tag{2.5}$$

where A is proportional to concentration and traveled optical pathlength d.[31] In general, NIR diffusive spectra do not show linearity over a large range of concentration. Therefore, pretreatments as explained in chapter 2.2.2.3 are essential for the analysis of NIR-spectra.

2.2.4. Raman Spectroscopy

Raman spectroscopy is based on the interaction between light and material, where energy is transfered from the former to the latter and vice versa. When gases, liquids or solids are exposed to monochromatic light (in most cases laser light) of a specific wavenumber $\tilde{v}$, the spectrum of scattered light consists of light with wavenumber $\tilde{v} \pm \tilde{v}_i$ (Raman scattering) and with wavenumber $\tilde{v}$ of the incident light (Rayleigh scattering). Figure 2.12 gives a graphical interpretation of Raman scattering.[34]. The energy carried by a photon $E = h \cdot v = \frac{h \cdot c}{\lambda} = h \cdot c \cdot \tilde{v}$ may cause a transition from a lower vibrational energy level to a higher one. In further consequence, a photon of smaller energy is created and light of lower wavenumber is scattered (Stokes line). If the system is in an upper excited level, an incident photon with the interacting wavenumber is re-emitted as a photon of higher energy, resulting in the emission of light with a higher wavenumber (Anti-Stokes line). Those wavenumber shifts are called Raman shifts and are material-specific. Therefore, the qualitative and quantitative identification of matters is provided and chemical mapping is possible.

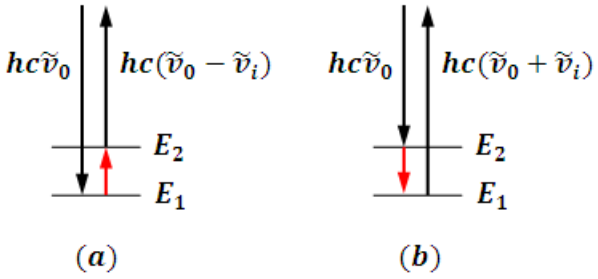

Figure 2.12.: Schematic vibrational energy level diagram for Raman scattering: (a) Stokes line; (b) Anti-Stokes line.

Similar as explained in chapter 2.2.3, the FT-Raman spectrometry makes use of a Michelson-interferometer and the recorded interferograms are Fourier-transformed by a computing unit. This provides a faster spectra processing. Nevertheless, the fast measuring time of NIR can not be reached when measuring with Raman. For further method comparison the reader is referred to Siesler et al. [34].

2.2.5. Optical Coherence Tomography

Optical Coherence Tomography (OCT) is a nondestructive imaging method that is the optical analogy to ultrasound imaging. Cross-sectional images can be processed by measuring the echo time delay and intensity of reflected or backscattered light. The image shows differences in contrast where inhomogeneities in the refractive index of the sample occur. Those varieties are often caused by the boundary of two materials.[21]

The high velocity of light makes it very difficult to measure the echo time delay directly. Therefore, OCT makes use of low-coherence interferometry realized with a Michelson interferometer as seen in figure 2.13. The light of a super luminescent diode is split up in two paths. The first is the reference path where the light travels a known variable length and has a known time delay. The second is the sample path where the light is directed to the object under investigation. The backscattered and the reference beam are then recombined in the interferometer and read out with a photodetector. If both light beams have traveled the same optical distance (less than a coherence length), a constructive interference pattern is recorded meaning that a boundary is detected. From this pattern, depth information can be demodulated using Fourier transformation. 2D and even 3D gray scale images can be obtained by transverse scanning of the sample.[35]

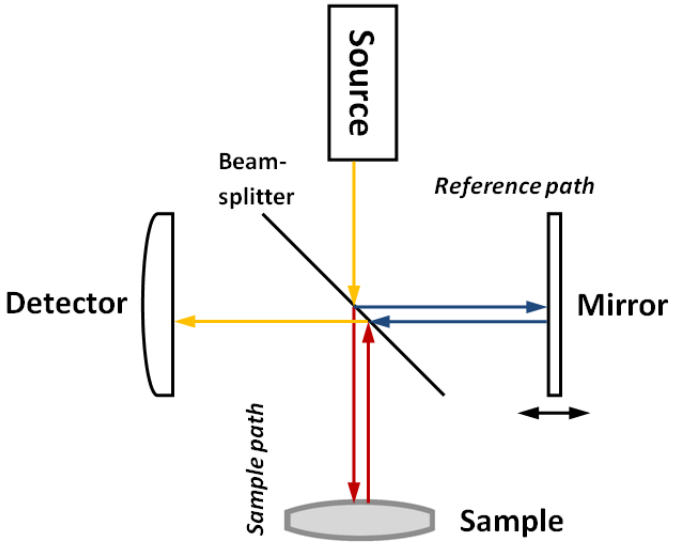

Figure 2.13.: Schematic setup of an OCT system realized with Michelson interferometer.

Resolution: In OCT the axial image resolution is limited by the coherence length of the light source l_c[21]:

$$l_c = \frac{2 \cdot ln(2)}{\pi} \cdot \frac{\bar{\lambda}}{\Delta\lambda} \tag{2.6}$$

where λ is the mean wavelength and $\Delta\lambda$ the spectral bandwidth of the source. In OCT the transversal resolution is independent from the axial one and defined as the full width at half maximum diameter Δd_{FWHM} of the probe beam amplitude distribution at the beam waist of the focused probe beam:

$$\Delta d_{\mathrm{FWHM}} = 2 \cdot \sqrt{ln(2)} \frac{\bar{\lambda}}{\pi \cdot \Theta_{\mathrm{s}}} \tag{2.7}$$

where Θ_{s} is the angular spread of the Gaussian beam. Therefore, the transverse resolution is also dependent on the scanning depth.[21]

3. Results and discussion

3.1. Performing a Design of Experiments

Recognition of and statement of the problem. Because the coating process is the last step in tablet production, an invalid film coating that fails the USP II dissolution test goes hand in hand with enormous economic losses. There was little information about the influence of coating process parameters on the quality of the final product and in further consequence on the output of the USP II dissolution test. Therefore, the objective was to gain a better process understanding, to identify parameters crucial to quality, and to avoid invalid batches.

Choice of factors, levels, and ranges. A crucial criterion for the formation of the film coating is the drying velocity of the applied suspension.[1] For this reason, three parameters that have an direct effect on this drying time were chosen for variation:

- the tablet bed temperature,
- the spray rate,
- the supply air power.

The range of variation is limited by several environmental factors and device specifications.

Selection of response variable. In our case, the most important quality attribute is the USP II dissolution test that decides whether a batch goes on sale or not. It can be broken up into two parts: the disintegration test and the release performance test.[36] Hence, the first output chosen was the coating thickness that takes influence on the gastric juice resistance. Obviously the second one was the release performance or in other words the percentage of API release after certain times. The third output factor was the moisture content of the tablets. It was hypothesized that moisture trapped between coating layer and tablet core caused the API to degrade before it could be released in the dissolution test. For reason of integrity, the tablet weight and process time were monitored as well.

Choice of experimental design. For validation of the influence of each input factor we decided to take the one-factor-at-a-time approach, where a certain input factor was changed while the others were kept in the center point. In other words, the axial experiments as seen in figure 2.1 were implemented. Figure 3.1 and 3.2 are showing the experimental design for tablet A and tablet B. 'Out-of-specification' batches are marked with blue and red colored circles. The exhaustive table with all input factors and responses can be found in chapter A.4.

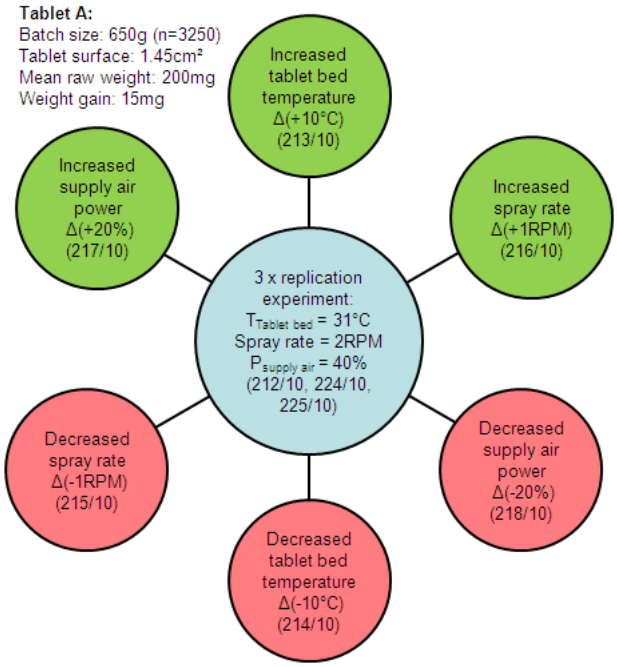

Figure 3.1.: Axial experiments of tablet A.

Performing the experiments. The experiments were realized on a tablet coater in the pilot plant of G.L. Pharma GmbH (Graz, Austria) as seen in figure 3.3. Based on the settings of the replication experiment that was repeated three times, every input factor was changed both to a higher and lower value. The spray rate was modified by increasing or decreasing the rotation velocity of a peristaltic pump by 1 round per minute (RPM). The supply air power was adjusted at the control unit and the tablet bed temperature was controlled using the possibility of modifying the supply air temperature. The process was terminated after a gain in weight of 15 mg for tablet A and 13 mg for tablet B batches.

Statistical analysis of the data. The analysis was done with the help of the software MODDE (Umetrics AB, Sweden). The replication plots state the reproducibility of the performed experiments. The maximum statistical fluctuation within the replication experiments should be at least smaller than the variation within the experiments. In that way, it is assured that the influence of the parameters is distinguishable from random changes. In figure 3.4 it can be seen that this

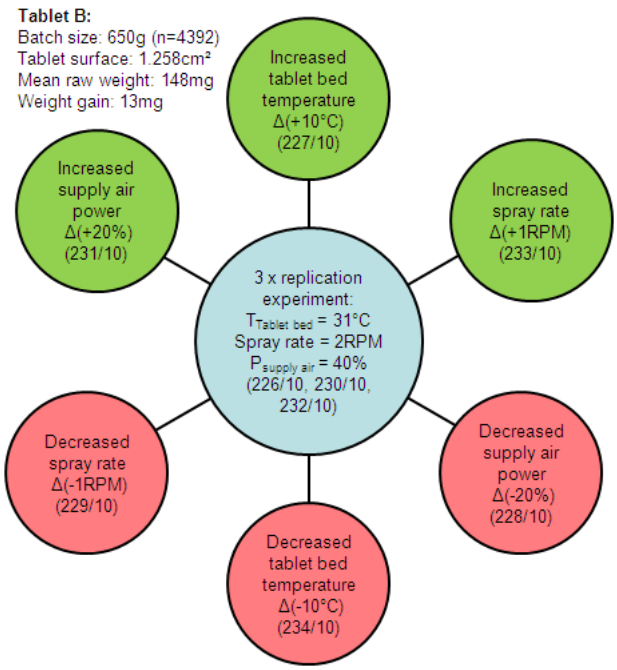

Figure 3.2.: Axial experiments of tablet B.

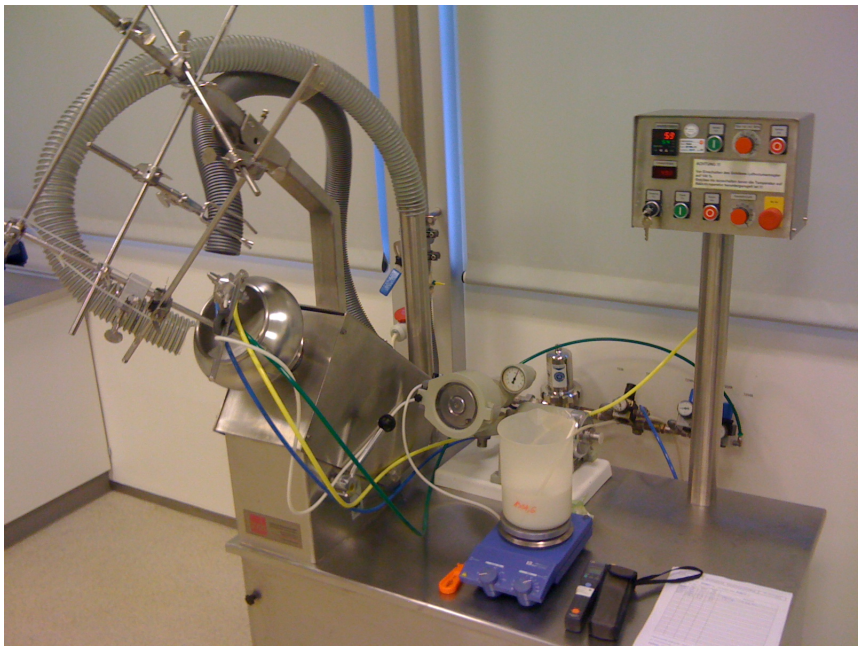

Figure 3.3.: Experiment set-up with coating pan, supply and exhaust air, atomization nozzle, tube pump, coating suspension and control unit.

condition is not fulfilled for the observed output factors. The output factor variations within the replication experiments (1, 8 and 9) are almost as big as the variations within the performed experiments (2 to 7). The variation within the replication experiments of tablet B (1 to 3) could be decreased as seen in figure 3.5.

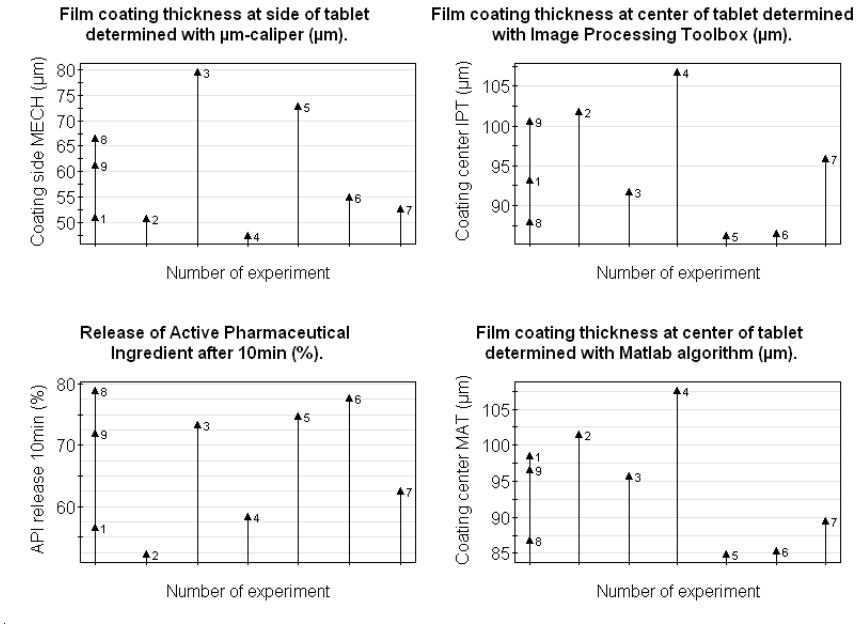

Figure 3.4.: Replication Plots of tablet A.

At the beginning, a model using Partial Least Square Regression (PLS) was built regarding all input factors and their squares. Afterwards, the model performance was refined by excluding certain input factors. For model interpretation, the following performance parameters are to consider [28]:

- R^2*:* Also called the 'Goodness of fit'. Indicates how good an output factor is explained by the model. Zero stands for no model at all and one for the perfect model.
- Q^2*:* Also called the 'Goodness of prediction'. Represents the prediction capability of the model and is therefore a more realistic performance indicator.
- *Model Validity:* Shows if the model is appropriate in a general sense.
- *Reproducibility:* Is an indicator of how well experiments can be reproduced and is in general a numeric value representing the replication plot.
- *Evaluation of parameters:* For a model to be judged as good, the difference between R^2 and Q^2 should not be bigger than 0.2 to 0.3, R^2 and the Reproducibility at least 0.5 and the Model validity not smaller than 0.25.

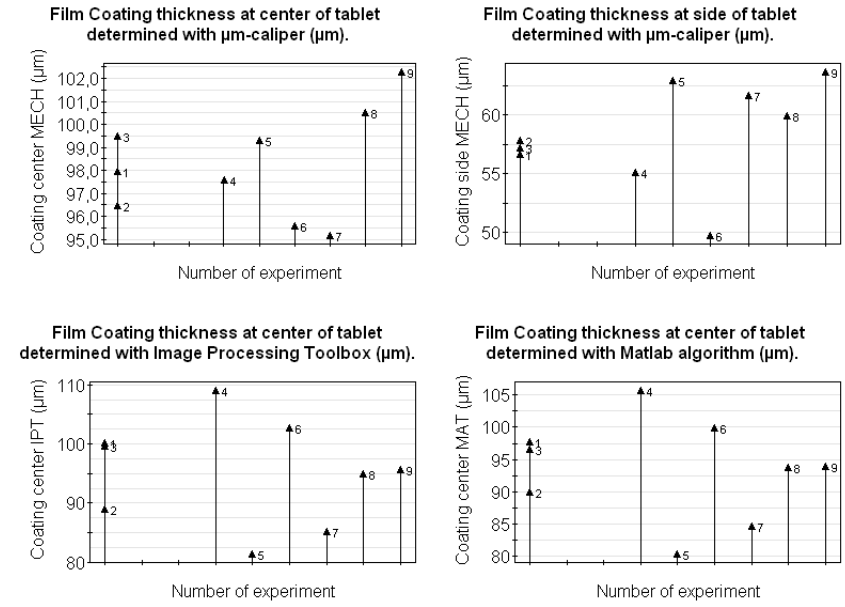

Figure 3.5.: Replication Plots of tablet B.

Tables 3.1 and 3.2 show the performance values obtained for the tablet A and tablet B experiments using the optimized models. Figures 3.6 and 3.7 provide a graphical overview. It can be seen, that the investigated output factors are having a R^2 of around 0.8 and are therefore relatively good explained by the model. However, the predicting capability of the models is poor because of the rather big difference between Q^2 (around 0.45) and R^2. The value of reproducibility can be easily explained with a view on the replication plots. Matching replication experiments lead to a high reproducibility as seen for the coating thickness at the side of tablet B. In general the tablet B experiments show a better reproducibility. Nevertheless the model validity for every output factor is good, a balanced performance parameter characteristic describes a good model.

Table 3.1.: Model performance for output factors of tablet A.

	R^2	Q^2	Model validity	Reproducibility
Coating side MECH	0,8140	0,4367	0,9501	0,4934
Coating center IPT	0,7908	0,4756	0,9734	0,2473
API release 10min	0,6554	0,2827	0,9861	-0,2000
Coating center MAT	0,8301	0,4379	0,9214	0,3696

Table 3.2.: Model performance for output factors of tablet B.

	R^2	Q^2	Model validity	Reproducibility
Coating center MECH	0,8854	0,4377	0,9117	0,5820
Coating side MECH	0,9621	0,4629	0,3076	0,9815
Coating center IPT	0,8575	0,4381	0,9908	0,4922
Coating center MAT	0,9066	0,5068	0,9646	0,7231

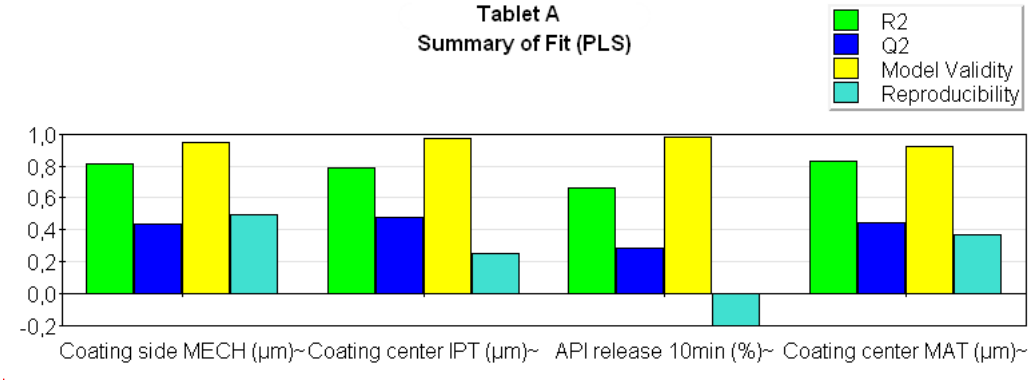

Figure 3.6.: Summary of model, tablet A.

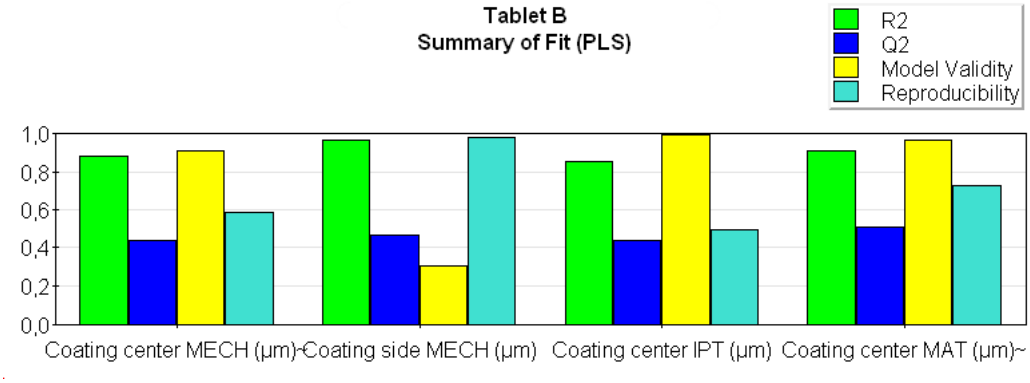

Figure 3.7.: Summary of model, tablet B.

The surface response plot of the coating thickness on the side of tablet B is shown in figure 3.8. It can be seen that there is a maximum coating development when the process is driven with a high spray rate at a low tablet bed temperature. A view on the surface response of the coating thickness at the top of the tablet shows the converse case (Figure 3.9). An exhaustive listing of response surface plots can be found in the appendix A.2.

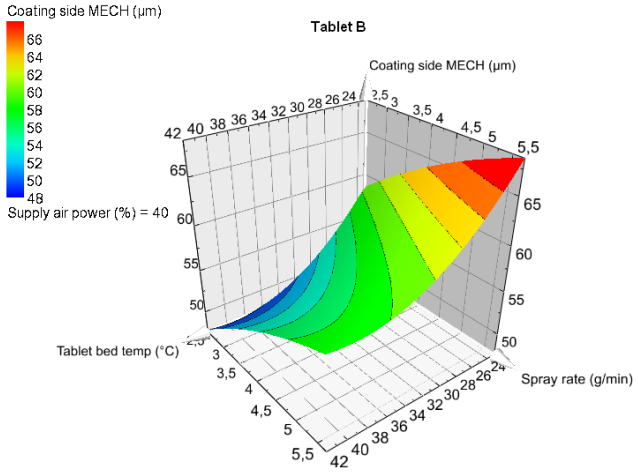

Figure 3.8.: Surface response plot of Coating thickness at side of tablet B, determined with μm-caliper.

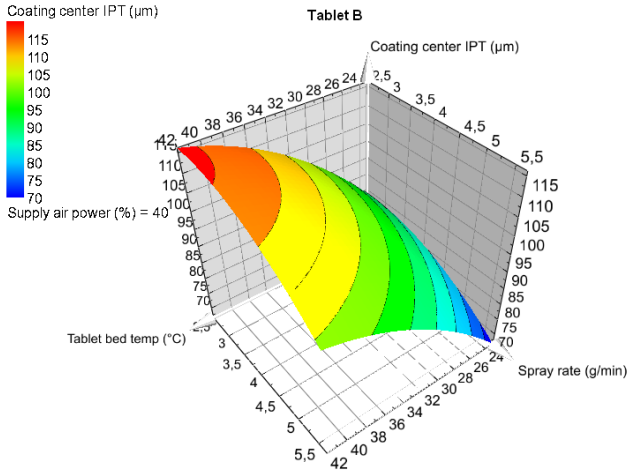

Figure 3.9.: Surface response plot of Coating thickness at top of tablet B, determined with Image Processing Toolbox^{TM}.

Discussion: The reproducibility of the performed experiments turned out to be relatively low. The high variation within the replication experiments, especially for tablet A, can partially be explained with the operator error. At the very beginning of the

experiments, the operator was not familiar with the process and its equipment. This missing continuity in handling led to a bigger variation within the batches. With more experience, this error was minimized and the variation within the replication experiments could be decreased. Especially the coating thickness for the band of the tablet determined with the μm-caliper shows a good reproducibility. It also has to be considered that the difference in coating thickness within the performed experiments is not significant. This is because the equal process end point was enforced for every batch and it was a challenge to exactly determine the final point of the process. Also, the variation of tablet weight within a batch made it impossible to terminate the process exactly at a gain in weight of 15 mg. Therefore, the reproducibility of the models regarding the thickness is relatively low.

In the response surface plots, the maximum coating developed when the process is driven with a high spray rate at a low tablet bed temperature. This can be explained by the slower drying process of the suspension. It is known that in most pan coating processes, the bi-convex sides of the tablet have more exposure to the spray and therefore the film thickness is higher at the top and bottom. However, the undried suspension can be passed to the surrounding tablets during the movement in the pan, leading to a more homogeneous coating distribution on the tablet. In the warmer environment, or in other words at high tablet bed temperature and low spray rate, the suspension dries immediately after application and the development of coating reaches a maximum.

The models regarding the thickness show a quite reasonable performance, whereas the model values for the API release are insufficient caused by the strong replication experiment variation.

The adaption of an experimental design is very useful when analyzing varying input factors. It provides a strategical approach for performing experiments, a statistical validation of the obtained results and it allows convincing interpretations. In the literature, a DoE was applied on an aqueous film coating process varying the amount of suspension applied, the drying inlet air temperature, the spray rate, the atomizing air pressure, the pan speed and the number of spray guns. The output factors observed in this study were the coating uniformity, the loss of weight during LOD, the coating process efficiency. The process exhaust temperature, the surface roughness and the gloss were also recorded but not further analyzed. All listed output factors were determined with calculations out of weight measurements. The magnitude of influence of input factors on the observed results were presented.[37] Different parameters, experimental plans and methods of analysis in this work makes it difficult to compare the obtained results with the literature.

3.2. Mechanical survey

3.2.1. Determination of film coating thickness

At the present time it is a commonly accepted method to determine the film coating thickness of tablets with a μm-caliper (Digimatic outside micrometer 293-821, Mitutoyo Inc., Japan). For an easier investigation of the coating thickness at the top of the tablet a height gauge was used (Absolute Digimatic dial gauge ID-S 543-690B, Mitutoyo Inc., Japan). Figure 3.10 shows both devices, on the left the μm-caliper for measuring the coating thickness at the band (side) of the tablet and on the right the height gauge. Equation (3.1) shows the calculation of the film coating thickness d_{coating} where diameter and height of the uncoated tablets d_{core} are measured, subtracted from the values for the coated ones d_{batch} and finally divided by two. For a better statistical accuracy, 10 tablets per batch were taken and the diameter was measured three times for each tablet. Figure 3.11 shows the points of measuring. The standard deviation for the coating thickness is calculated with the use of equation (3.2), where σ_{core} and σ_{batch} are the standard deviations of the thickness measurements of uncoated and coated tablets, respectively.

$$d_{\text{coating}} = \frac{d_{\text{batch}} - d_{\text{core}}}{2} \tag{3.1}$$

$$\sigma_{\text{coating}} = \frac{1}{2} \cdot \sqrt{\sigma_{\text{core}}^2 + \sigma_{\text{batch}}^2} \tag{3.2}$$

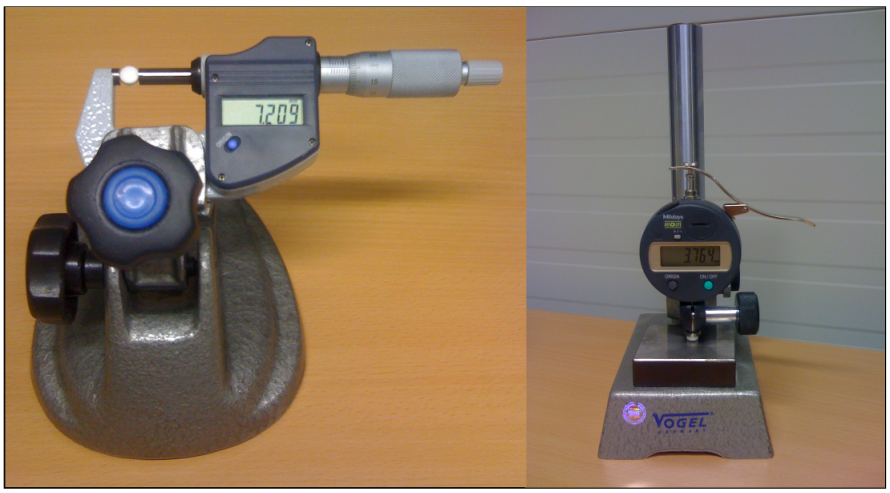

Figure 3.10.: The μm caliper (left) and height gauge (right) measurement devices used in the coating thickness investigations.

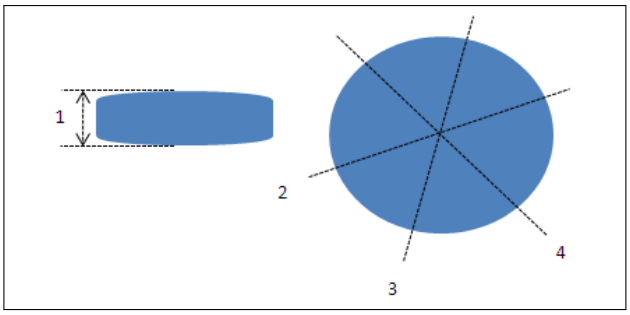

Figure 3.11.: Measuring points for coating thickness determination.

Table 3.3 shows the results for film coating thickness and standard deviation for both top and side of tablet A and table 3.4 lists the same for tablet B. Figure 3.12 and figure 3.13 provide a graphical interpretation.

Table 3.3.: Film coating thickness of tablet A batches, determined with μm-caliper.

	Top of tablet			Side of tablet		
Batch	$d_{top}(\mu m)$	$\sigma_{top}(\mu m)$	$\sigma_{top}(\%)$	$d_{side}(\mu m)$	$\sigma_{side}(\mu m)$	$\sigma_{side}(\%)$
212/10	91,60	11,08	12,10	51,02	4,25	8,33
213/10	87,35	12,23	14,00	50,98	4,52	8,87
214/10	94,65	12,90	13,63	79,60	4,42	5,55
215/10	84,25	15,57	18,48	47,47	3,57	7,52
216/10	75,65	15,92	21,04	72,75	6,69	9,20
217/10	80,45	14,69	18,26	55,10	5,67	10,29
218/10	90,65	13,06	14,41	52,73	4,93	9,35
224/10	77,95	11,25	14,43	66,53	5,23	7,87
225/10	84,45	15,86	18,78	61,42	4,84	7,87

For both tablet types the error was bigger for the coating thickness at the top of the tablet (up to 32,62 μm). This is explicable by the fact that only one measurement of the thickness per tablet is possible in axial direction, and by the higher variation in height of compacted tablet cores compared to diameter. Tablet B showed a more homogeneous film coating at top and side of the tablet than tablet A. The processes driven with a low tablet bed temperature (214/10) and with a high spray rate (216/10) led to a more equal distribution of film on the top and the side and therefore to a more uniform coating thickness for tablet A. The complementary processes driven with high tablet bed temperature (213/10) and low spray rate (216/10) show a higher coating development at the top of the tablet than on the side. Varying supply air power (217/10 and 218/10) did not seem to affect the coating distribution on the tablet in a specific way. The batches of tablet B show a uniform film coating for both top and side of tablet.

For a part of the tablet A batches (212/10 to 218/10), it was possible to test their gastric juice resistance in the disintegration testing part of the USP II dissolution test. For

Table 3.4.: Film coating thickness of tablet B batches, determined with μm-caliper.

	Top of tablet			Side of tablet		
Batch	$d_{top}(\mu m)$	$\sigma_{top}(\mu m)$	$\sigma_{top}(\%)$	$d_{side}(\mu m)$	$\sigma_{side}(\mu m)$	$\sigma_{side}(\%)$
226/10	97,95	15,33	15,65	56,63	5,66	10,00
227/10	97,60	25,59	26,22	55,12	4,96	8,99
228/10	102,30	11,58	11,32	63,70	5,39	8,46
229/10	95,60	32,62	34,12	49,70	4,93	9,91
230/10	96,45	14,46	14,99	57,82	5,97	10,32
231/10	100,50	14,36	14,29	59,97	5,46	9,11
232/10	99,50	15,61	15,69	57,23	5,70	9,95
233/10	95,15	21,40	22,49	61,67	5,39	8,74
234/10	99,30	11,99	12,07	62,98	6,72	10,67

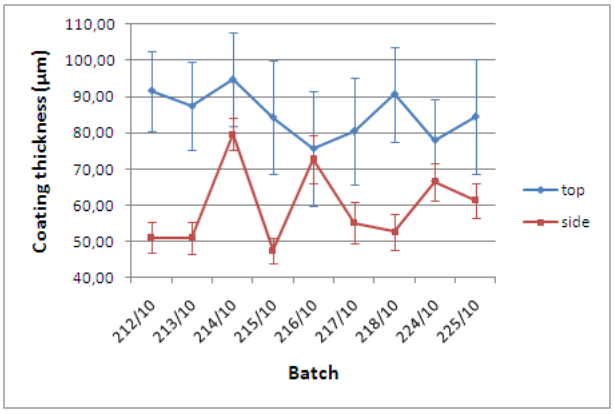

Figure 3.12.: Film coating thickness of tablet A batches, determined with μm-caliper.

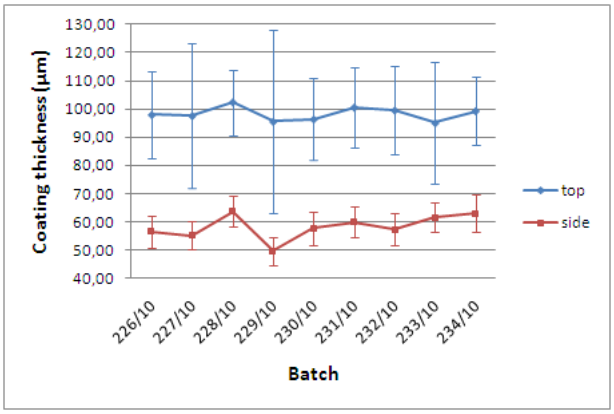

Figure 3.13.: Film coating thickness of tablet B batches, determined with μm-caliper.

that, 6 tablets of each batch were placed in 0,1 molar hydrochloric acid and constantly kept in motion for 2 hours to simulate the gastric environment. All 7 batches showed resistance (i.e., did not disintegrate). After the disintegration test, the dimension of the tablet was measured again as seen in table 3.5 and figure 3.14.

Table 3.5.: Film coating thickness of tablet A batches after disintegration test, determined with μm-caliper.

	Top of tablet			Side of tablet		
Batch	$d_{top}(\mu m)$	$\sigma_{top}(\mu m)$	$\sigma_{top}(\%)$	$d_{side}(\mu m)$	$\sigma_{side}(\mu m)$	$\sigma_{side}(\%)$
212/10	111,90	13,82	12,35	75,40	4,64	6,15
213/10	124,10	12,80	10,31	78,10	4,17	5,33
214/10	121,80	15,30	12,56	98,00	5,29	5,39
215/10	119,10	11,43	9,60	75,40	3,43	4,55
216/10	99,70	15,64	15,69	91,40	6,47	7,08
217/10	107,60	17,88	16,62	76,70	4,62	6,03
218/10	113,00	12,94	11,45	78,40	4,28	5,46

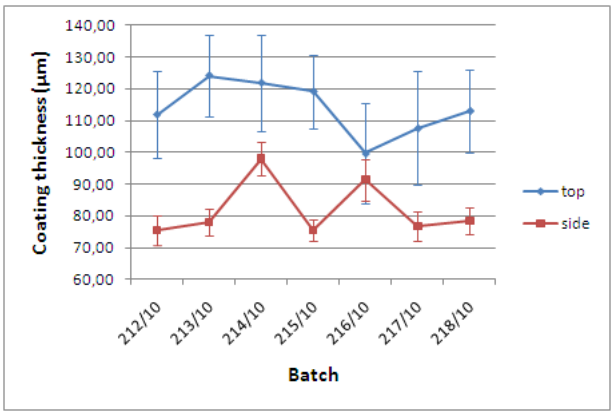

Figure 3.14.: Film coating thickness of disintegration tested tablet A batches, determined with μm-caliper.

Compared to the tablets of the batches not investigated in the disintegration test, a significant change in volume could be observed. The coating thickness both at top and side of the tablet seemed to increase around around 30μm for each batch. Figure 3.15 illustrates this fact for the coating thickness at the top, figure 3.16 for the thickness at the side.

3.2.2. Determination of tablet weight

The increase of film thickness during the coating process goes hand in hand with the gain in weight. Therefore, samples were taken during the process and the weight was monitored at certain times. The process endpoint for our DoE was a gain in weight of 15 mg for the tablet A and 13 mg for tablet B batches. For every batch, the average of

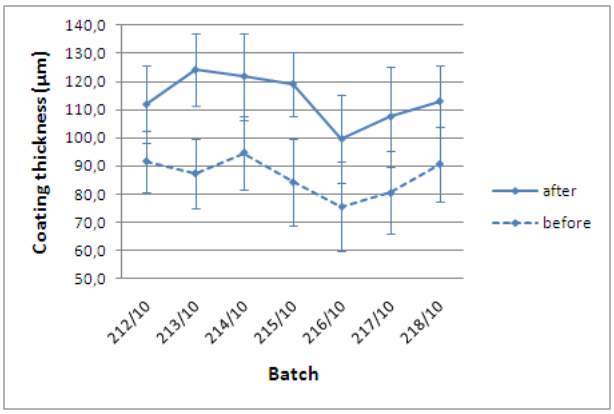

Figure 3.15.: Film coating thickness top of tablet A batches before and after disintegration test, determined with μm-caliper.

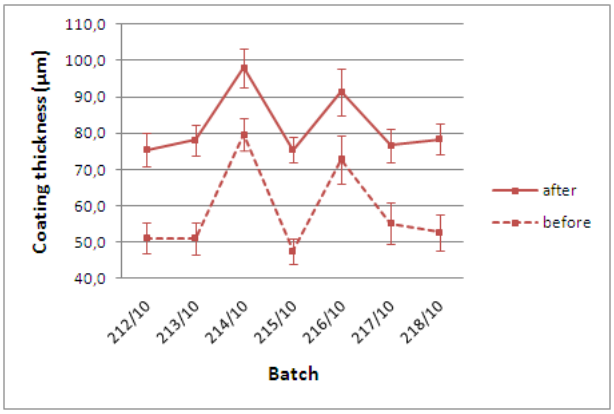

Figure 3.16.: Film coating thickness side of tablet A batches before and after disintegration test, determined with μm-caliper.

the measurements of 10 different tablets was determined 5 times. Table 3.6 and table 3.7 show the results.

Table 3.6.: Weight of tablet A batches.

Batch	$m_{tablet}(mg)$	$\sigma_{tablet}(mg)$	$m_{coating}(mg)$	$\sigma_{coating}(mg)$
Raw tablet	199,93	0,68	0	0
212/10	215,27	0,53	15,34	0,86
213/10	215,67	0,63	15,74	0,93
214/10	216,40	0,91	16,47	1,14
215/10	215,14	0,60	15,20	0,91
216/10	216,17	0,72	16,24	0,99
217/10	215,74	0,32	15,80	0,75
218/10	215,36	1,03	15,43	1,24
224/10	215,00	0,88	15,07	1,11
225/10	215,95	0,29	16,02	0,74

Table 3.7.: Weight of tablet B batches.

Batch	$m_{tablet}(mg)$	$\sigma_{tablet}(mg)$	$m_{coating}(mg)$	$\sigma_{coating}(mg)$
Raw tablet	147,76	0,54	0	0
212/10	161,55	0,76	11,90	0,93
213/10	161,61	1,43	12,95	1,52
214/10	161,93	0,56	13,82	0,78
215/10	161,06	0,91	13,87	1,06
216/10	161,37	0,67	11,95	0,86
217/10	162,00	0,43	13,65	0,69
218/10	162,43	0,75	13,54	0,92
224/10	162,24	0,65	14,29	0,84
225/10	160,98	0,90	11,98	1,05

Also, the weight of the tablets investigated in the disintegration test was measured before and after the test. Table 3.8 and figure 3.17 illustrate a significant gain in tablet weight upon treatment with 0.1 molar hydrochloric acid for 2 hours. The average was calculated with 6 tablets each batch.

Discussion: A possible reason for the more uniform coating thickness distribution at moist driven processes is the longer drying time of the coating suspension and the associated distribution of coating liquid from a freshly coated tablets to the surrounding tablets due to the tablet bed movement. In warm processes the applied coating dries immediately and the bi-convex sides of the tablet receive a higher coating thickness than the band.

In the literature, the tablets increase in volume and weight after 2h testing for gastric resistance in 0.1 N HCl was investigated regarding different coating suspensions.[38] The

Table 3.8.: Weight of tablet A batches before and after disintegration test.

Batch	$m_{before}(mg)$	$m_{after}(mg)$	Gain in weight(mg)
212/10	216,37	221,93	5,57
213/10	216,43	222,38	5,95
214/10	216,15	221,30	5,15
215/10	214,88	220,80	5,92
216/10	217,53	221,68	4,15
217/10	216,36	220,98	4,62
218/10	214,92	220,07	5,15

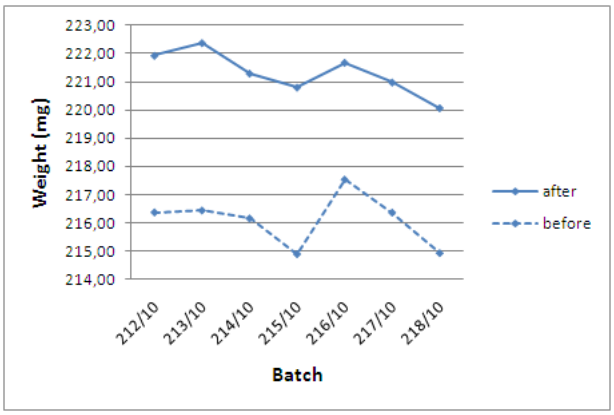

Figure 3.17.: Weight of tablet A batches before and after disintegration test.

swelling can only be explained by the diffusion of gastric juice into the tablet during the disintegration test. With the μm-caliper no clear declaration can be made, whether it took place in the coating or in the core. Also it can not be said yet if this diffusion leads to API dissolution in the tablet core.

3.3. Near Infrared Spectroscopy

3.3.1. Monitoring the gain in film coating thickness

We were able to take samples at different time points during an industrial coating process of tablet A performed on a Bohle Tablet Coater (BTC400, L.B. Bohle Maschinen + Verfahren GmbH, Germany). The weight and dimensions of the tablet samples were investigated as described in chapter 3.2. Table 3.9 shows the dimensions and table 3.10 the increase in weight of the tablets. For the determination of the weight, an average of 20 tablets for each time point was measured.

Table 3.9.: Time-related film coating thickness of tablet A, determined with μm-caliper.

	Top of tablet			Side of tablet		
Progress	$d_{top}(\mu m)$	$\sigma_{top}(\mu m)$	$\sigma_{top}(\%)$	$d_{side}(\mu m)$	$\sigma_{side}(\mu m)$	$\sigma_{side}(\%)$
10 min	15,95	9,54	59,81	6,03	6,45	106,92
37 min	29,05	10,19	35,08	14,93	5,56	37,22
70 min	41,90	9,74	23,24	30,00	5,81	19,37
96 min	50,35	10,78	21,41	40,23	7,12	17,69
127 min	78,45	14,59	18,60	58,73	7,13	12,14
155 min	88,20	9,42	10,68	69,85	7,59	10,86
180 min	94,10	13,15	13,97	77,98	7,77	9,97

Table 3.10.: Time-related weight of tablet A.

Progress	$m_{tablet}(mg)$	$m_{coating}(mg)$
0 min	198,85	0
10 min	201,90	3,05
37 min	204,85	6,00
70 min	207,85	9,00
96 min	210,15	11,30
127 min	214,35	15,50
155 min	216,20	17,35
180 min	217,40	18,55

In the next step, the spectra of the samples were measured with an NIR spectrometer (FT-NIR Spectrum 400, Perkin Elmer, USA) spectrometer and the obtained spectra were analyzed with the software Unscrambler® (CAMO Software AS., Norway). For every time point, the spectra of ten different tablets were recorded. With progressing process time, the NIR spectra show an increasing peak at wavenumber 7184 cm^{-1}. Figure 3.18 displays the spectra with time-dependent changes during the coating progress. For a better visualization, only the section from wavenumber 7260 cm^{-1} to 7110 cm^{-1} is shown. The spectra were pretreated with 'baseline offset correction'. A comparison with the raw material spectra of the different coating suspension ingredients indicates

that this peak results from the talcum component of the applied film coating. Figure 3.19 illustrates the NIR spectra of an uncoated tablet, a completely coated tablet and talcum. The whole range from wavenumber 10000 cm^{-1} to 3001 cm^{-1} is shown and the baseline offset was eliminated.

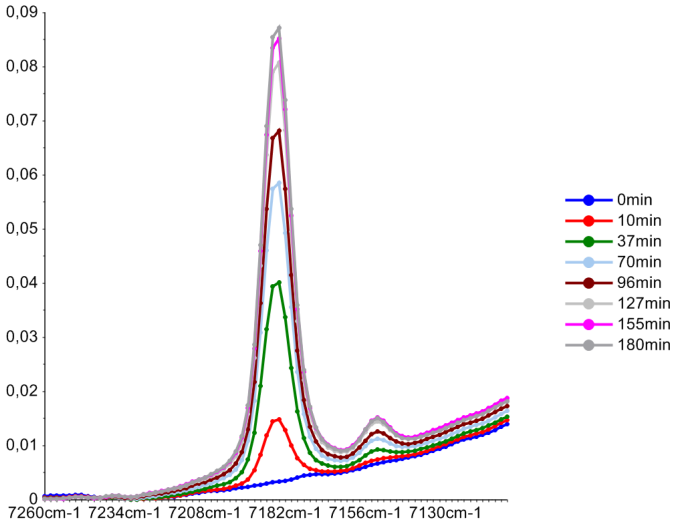

Figure 3.18.: NIR spectra of increasing talcum peak for certain time points during the coating process.

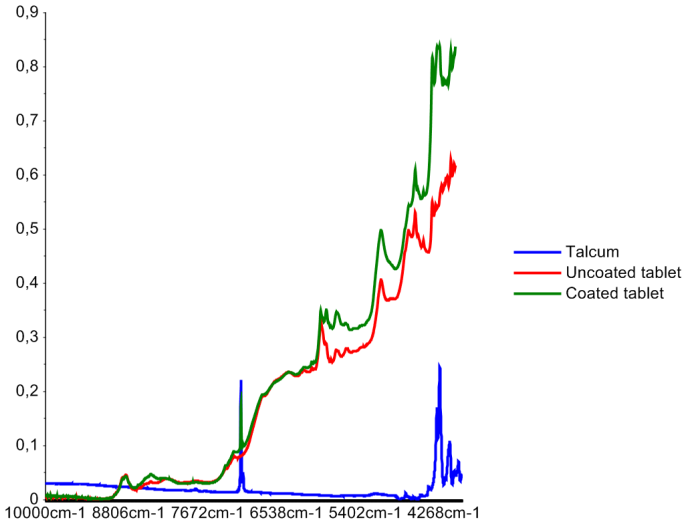

Figure 3.19.: NIR spectra of an uncoated tablet, a completely coated tablet and talcum.

With the obtained NIR spectra and the measured values for weight and coating dimensions as a reference, a PLS model for coating thickness prediction could be built. The range from wavenumber 7254cm^{-1} to 4100cm^{-1} was used. Different pretreatments (SNV, Area normalizations, differentiations, smoothing filters) were tried, where the pretreatment of the data with 'baseline correction' led to best results. The number of

PLS-factors was set to 6. The tables 3.11, 3.12 and 3.13 show the model parameters and performance for weight, coating thickness at top and at side for PLS-factor 5.

Table 3.11.: Model performance for gain in weight.

	Slope	Offset	RMSE	R-Square
Calibration	0,9723	4,9428	0,9808	0,9763
Prediction	0,9679	6,6601	1,1104	0,9704

Table 3.12.: Model performance for coating thickness, top of tablet.

	Slope	Offset	RMSE	R-Square
Calibration	0,9623	1,8744	6,2811	0,9623
Prediction	0,9510	2,2137	7,2105	0,9519

Table 3.13.: Model performance for coating thickness, side of tablet.

	Slope	Offset	RMSE	R-Square
Calibration	0,9623	1,4023	5,3621	0,9623
Prediction	0,9535	1,5748	6,1657	0,9514

Discussion: The model's low RMSE of prediction in combination with the fast measuring time of NIR spectrometers could be applied as a PAT tool for in-line monitoring of coating thickness growth. It represents a respectable alternative to the present-day used monitoring of gain in weight. Several studies that investigated tablet coatings with NIR come to the same conclusion.[12][32][31]

3.3.2. Selection of batch representative tablets

One of the main aims in this work was to establish a connection between the results of the different methods of analysis and the results of the dissolution test. Therefore it was important to first execute all available measurements on tablets which are representative for the batch, and then investigate exactly those tablets in the dissolution test. To this end, ten tablets of each batch were picked and their NIR spectra were determined. Based on the theory that the dissolution performance is related to the trapped moisture between film coating and tablet core, the spectra were cut to the wavelength range of the OH^--bands using Unscrambler®. This area from 5600cm^{-1} to 4600cm^{-1} carries information about the trapped moisture in the sample. Furthermore, the data was pretreated with SNV and a PCA-analysis was executed. Figure 3.20 shows the PCA plot of the tablet A batches and their clustering. The reason that each batch is present with 20 points is that both front and back of one tablet were investigated using the NIR probe of the spectrometer.

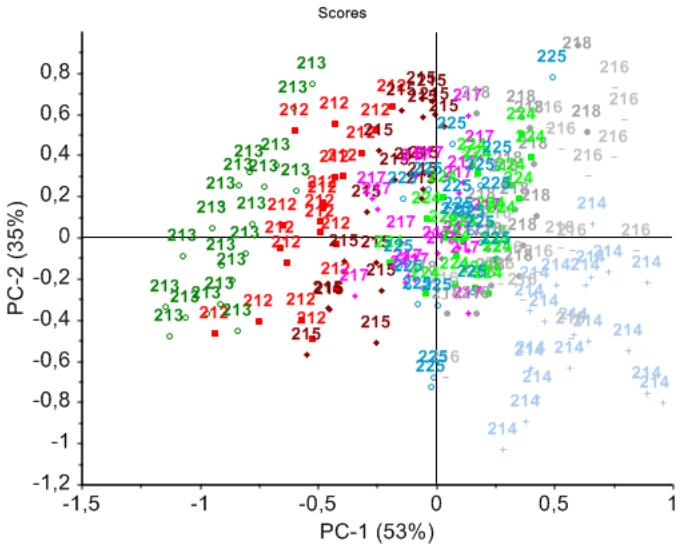

Figure 3.20.: PCA plot of the first and second principal component of tablet A, focused on the OH-bands.

It can be observed that the batches produced in processes where the coating suspension is drying relatively fast are located on the left-hand side of the plot. Examples for those batches are 213/10 (produced with high tablet bed temperature), 215/10 (produced with low spray rate) and 217/10 (produced with high supply air power). The right-hand side of the plot is populated with batches where the process parameters were deflected into the other direction (214/10, 216/10 and 218/10). The replication experiments (224/10 and 225/10) driven with the standard parameters are located along the y-axis and do not differ from each other. Batch 212/10 shows the same attributes as the batches with a high suspension drying rate, even though it is a replication experiment. Finally, the tablet located in the center of a batchs cluster was picked as a representative for the whole batch and was further investigated with μm-caliper, scale, Raman, OCT and dissolution test as described in chapters 3.2, 2.2.4, 2.2.5 and 3.6.

The same procedure was deployed to tablet B (figure 3.21) and the disintegration-tested batches (figure 3.22). For the latter, only 12 measurement points are visible, corresponding to the front and back of the 6 tested tablets.

Also the tablet B batches showed notable clustering. The ones with high suspension drying rate (227/10 - high tablet bed temperature and 229/10 - low spray rate) are located on the upper left side of the plot, whereas the complementary experiments are on the lower right side (234/10, 233/10). For the batches driven with increased and decreased supply air power (231/10 and 228/10) no significant difference could be observed. The replication experiments (226/10, 230/10 and 232/10) are, like expected, allocated in the middle of the plot and between the other clusters.

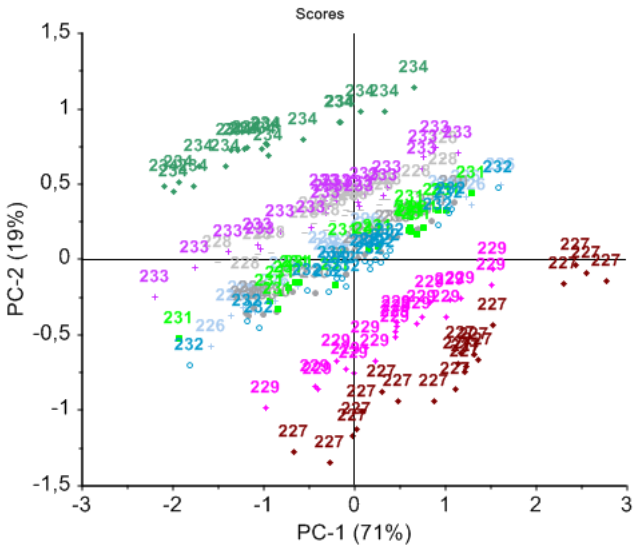

Figure 3.21.: PCA plot of tablet B, focused on the OH-bands.

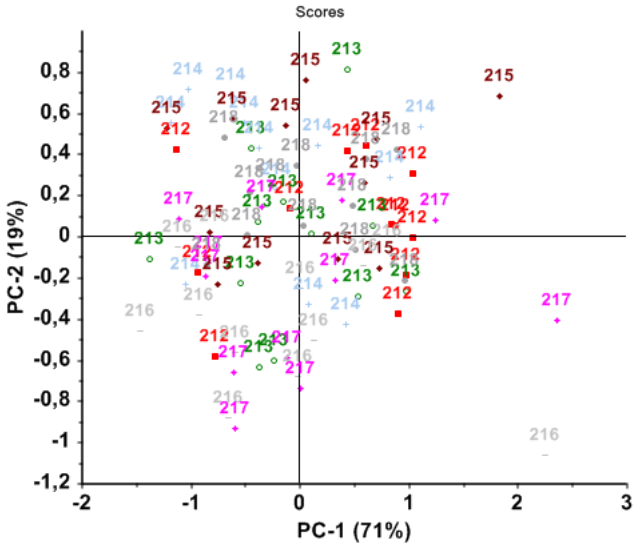

Figure 3.22.: PCA plot of disintegration tested tablet B batches, focused on the OH-bands.

After the disintegration test the tablet A batches were not distinguishable from each other any more. On the PCA plot the batches were not building clusters if the same pretreatments like for the other batches that were used. Nevertheless, it is important to subject them to the same selection procedure to achieve an objective result.

Discussion: A possible reason for the fact that replication batch 212/10 shows an equivalent clustering to batches with a high suspension drying rate could be that this batch was the first batch produced and has therefore a bigger operator error than the others.

After disintegration testing, tablet A batches were not clustering in the PCA plot as they did before. The gastric juice that diffuses into the tablet during the test seemed to affect the moisture content of the tablets and makes it impossible to differentiate them from each other.

When applying the appropriate pretreatments, PCA is a very good method to distinguish tablets with smallest differences in spectra. It makes it possible to find the average and therefore representative tablet out of an amount of similar tablets. By adding reference values for moisture content (e.g. determination with LOD) to the data, a PLS model predicting the moisture could be built. In the literature, NIR in combination with MVDA has not been applied so far for moisture investigations.

3.4. Raman Spectroscopy

3.4.1. Monitoring the gain in film coating thickness

The used Raman spectrometer (RamanStation 400, Perkin Elmer, USA) offers different possibilities of determining a sample spectrum: *Single Point*, *Super Macro Point*, *Line Scan* and *Mapping*. Because of the weak statistical significance of a single point measurement and the very long processing time of mapping mode, only super macro point and line scan spectra were used. The super macro point scan mode consists of a center point plus nine surrounding measurement points and therefore of ten spectra. The focus is adjusted only for the center point and the surrounding ones are measured with the same settings. In the line scan mode 15 points and their spectra are recorded along a line over the tablets surface. For each point, the focus is reset to account for the tablet curvature.

When the Raman spectra of uncoated and coated tablets were compared to the raw spectra of their ingredients, it could be seen that most of the observable peaks belong to ASA. This is illustrated in figure 3.23 where the data was pretreated with 'Area Normalization' and 'Baseline Offset' correction and the spectra from wavenumber 1800 cm^{-1} to 200 cm^{-1} is shown. Furthermore, a decrease in intensity of the spectra with increasing film coating thickness is notable, especially in the range from wavenumber 1670 cm^{-1} to 1550 cm^{-1}. Figure 3.24 shows the spectra of this area and their decrease in intensity for increasing film coating thickness. As pretreatment the 'Baseline Offset' correction was used.

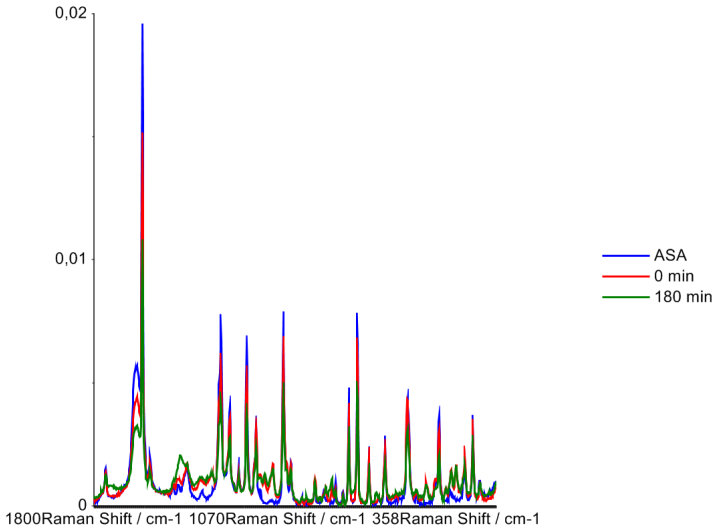

Figure 3.23.: Raman spectra of an uncoated tablet, a completely coated tablet and ASA.

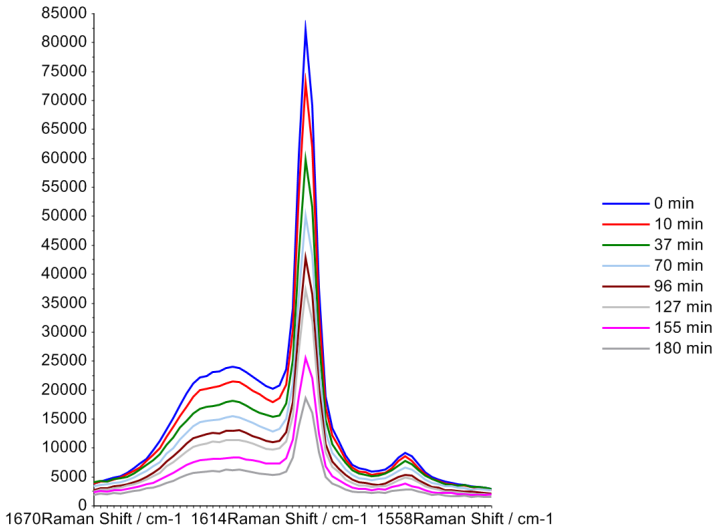

Figure 3.24.: Raman spectra with decreasing intensity for certain time points during coating process.

Similar to the procedure described in chapter 3.3.1 the prediction models were calculated using a software for multivariate data analysis (The Unscrambler®, Camo, Norway). The values of dimensions and weight are the model references and are taken out of tables 3.9 and 3.10. The best model performance for the line scan spectra could be achieved by highlighting the section from wavenumber 1590 cm^{-1} to 200 cm^{-1} and pretreat them with 'Baseline Correction' and 'Area Normalization'. Tables 3.14, 3.15 and 3.16 show the model parameters obtained with PLS at PLS-factor 6. Pretreating the data with 'Baseline Correction' and cutting down the spectra from wavenumber 1590cm^{-1} to 200cm^{-1} led to the best model performance for super macro point. The model parameters received with PLS regarding factor 6 are shown in tables 3.17, 3.18 and 3.19. For both Raman models the obtained parameters are showing a worse performance than the ones calculated with the NIR data (Chapter 3.3.1).

Table 3.14.: Model performance for gain in weight, line scan mode.

	Slope	Offset	RMSE	R-Square
Calibration	0,9435	11,8114	1,4988	0,9446
Prediction	0,9284	15,1822	2,2889	0,8727

Table 3.15.: Model performance for coating thickness, top of tablet, line scan mode.

	Slope	Offset	RMSE	R-Square
Calibration	0,9528	2,3479	7,0298	0,9528
Prediction	0,9283	4,6991	11,3143	0,8794

Table 3.16.: Model performance for coating thickness, side of tablet, line scan mode.

	Slope	Offset	RMSE	R-Square
Calibration	0,9535	1,7322	5,9598	0,9535
Prediction	0,9259	3,6700	9,4985	0,8836

Table 3.17.: Model performance for gain in weight, super macro point mode.

	Slope	Offset	RMSE	R-Square
Calibration	0,9519	10,0636	1,3850	0,9517
Prediction	0,9156	17,6582	2,0280	0,8989

Table 3.18.: Model performance for coating thickness, top of tablet, super macro point mode.

	Slope	Offset	RMSE	R-Square
Calibration	0,9347	3,2876	8,1931	0,9347
Prediction	0,8922	5,5230	11,7232	0,8691

Table 3.19.: Model performance for coating thickness, side of tablet, super macro point mode.

	Slope	Offset	RMSE	R-Square
Calibration	0,9314	2,5862	7,1979	0,9314
Prediction	0,8825	4,4559	10,5312	0,8562

Discussion: Raman spectroscopy proved to be a good tool for coating thickness prediction. However, compared to NIR, the RSME values obtained for prediction were worse for every parameter. Additionally, the measuring and processing time of a Raman spectrometer is approximately 10 time longer than of a NIR spectrometer.

In other studies, models with a low RSME for prediction were presented and were applied for monitoring the gain of coating thickness.[20]

3.4.2. Selection of batch representative tablets

Both the front and back face of 10 different tablets from each batch were investigated with the Raman spectrometer and their spectra analyzed with MVDA using CAMOs Unscrambler®. Different pretreatments were tested to distinguish the batches regarding

the trapped moisture between film coating and core tablet. Unfortunately, none of the tried variations in data pretreatment led to satisfying PCA plots similar to the ones obtained with the MVDA analysis of the NIR spectra. Therefore, the batch representative tablets were selected as described in chapter 3.3.2, and their Raman spectra were recorded for the sake of completeness.

Discussion: Raman spectroscopy does not seem to be applicable for determination of the moisture content of a tablet. In the literature, no studies regarding the examination of moisture content in coated tablets with Raman spectroscopy could be found.

3.5. Optical Coherence Tomography

The OCT measurements were performed by RECENDT (Research Center for Non Destructive Testing GmbH, Linz, Austria).

3.5.1. Determination of image resolution and refractive index

First of all, it was important to determine both resolution and refractive index for the present images to enable an accurate analysis. When measuring in air, the size of an image is 4 mm in lateral and 2,6 mm in medial direction. If the digital image size of 1000 times 1025 pixel is taken into account, the resolution is calculated by dividing the image size of one direction d_{image} by its belonging number of pixels n_{pixel}. In equation 3.3 the medial resolution R_{y} of an image of air is calculated:

$$R_{\text{y}} = \frac{d_{\text{image}}}{n_{\text{pixel}}} = \frac{2,6}{1025} \cong 2,54, \qquad \text{units: } \frac{\mu\text{m}}{\text{px}} \tag{3.3}$$

This is only possible due to the fact, that air has an refractive index of one. For materials with a refractive index different from one, the obtained value for geometric distance has to be divided by this index. In our case the refractive index of the dried coating suspension had to be ascertained. This was done by using the image of a tablet showing an approximately 1 mm^2 big piece of missing coating. The distance coating-tablet measured in coating d_{coating} had to be put in relation to the distance coating-tablet measured in air d_{air}. Figure 3.25 gives an optical explanation for this relation and equation 3.4 shows the calculation of the refractive index n_{ref}:

$$n_{\text{ref}} = \frac{d_{\text{coating}}}{d_{\text{air}}}, \qquad \text{units: } \frac{\text{px}}{\text{px}} \tag{3.4}$$

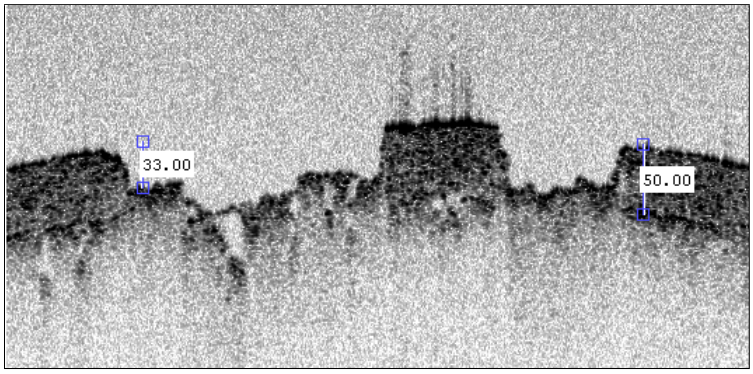

Figure 3.25.: Determination of refractive index.

For a better statistical accuracy the refractive index was determined eight times in four different images and the mean value (1,52) was taken for further calculations. Equation 3.5 shows how the film coating thickness d_{coating} in an OCT image is determined:

$$d_{\text{coating}} = \frac{d_{\text{pixel}} \cdot R_{\text{y}}}{n_{\text{ref}}}, \qquad \text{units: } \frac{\text{px} \cdot \frac{\mu\text{m}}{\text{px}}}{1} \tag{3.5}$$

where d_{pixel} is the coating thickness in pixel.

3.5.2. Determination of film coating thickness

Two possibilities of determining the film coating thickness of a tablet in an OCT image were realized. The first one was to measure the pixel count of the coating layer manually using Matlabs Image Processing Toolbox™ (MathWorks Inc., USA). The coating thickness was measured at least ten times in every OCT image. Therefore, the measuring time is rather long. Moreover, this procedure is relatively subjective, as the start and end point of the coating in the image is not clearly defined and has to be estimated by the user. However, it is a good method to get a rough benchmark for the coating thickness that can be used for calibration.

The second possibility was using an automatic image analysis with a self-written Matlab algorithm. Several methods for obtaining the film coating thickness were implemented such as threshold treatment, smoothing windows, edge detection techniques and coating reconstruction fits. It showed that the algorithm is an objective and reliable way of measuring the coating thickness in an OCT image.

3.5.2.1. Image Processing Toolbox™

For determining the film coating thickness with the Image Processing Toolbox™ included in Matlab, two images for each batch have been chosen and the number of pixels from the coating/air to the coating/tablet boundary was measured. This was done five times for every bitmap as seen in 3.26 to get a better statistical significance. Equation 3.5 was then used to calculate the coating thickness. Tables 3.20, 3.21 and 3.22 show the results for the three different batches.

The film coating thickness of tablet A batches determined with the Image Processing Toolbox™ are in most cases bigger than the ones determined with the μm-caliper. For the tablet B cores the situation is converse. Figures 3.27 and 3.28 are showing this relation.

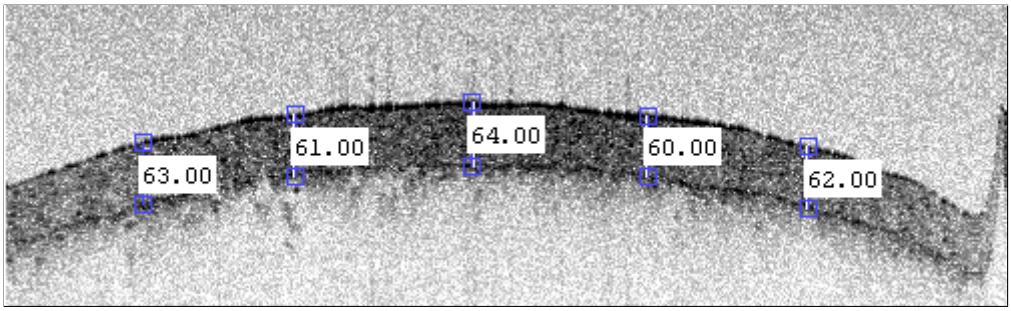

Figure 3.26.: Determination of coating thickness with Image Processing Toolbox™.

Table 3.20.: Film coating thickness of tablet A batches, determined with Image Processing Toolbox™.

Batch	$d_{top}(\mu m)$	$\sigma_{top}(\mu m)$	$\sigma_{top}(\%)$
212/10	93,19	2,82	3,02
213/10	101,76	2,63	2,58
214/10	91,69	4,47	4,87
215/10	106,84	3,19	2,99
216/10	86,19	3,97	4,61
217/10	86,44	2,11	2,44
218/10	95,85	2,37	2,47
224/10	88,02	5,33	6,05
225/10	100,68	1,94	1,93

Table 3.21.: Film coating thickness of tablet A batches after disintegration test, determined with Image Processing Toolbox™.

Batch	$d_{top}(\mu m)$	$\sigma_{top}(\mu m)$	$\sigma_{top}(\%)$
212/10	94,35	2,75	2,91
213/10	91,77	4,26	4,64
214/10	76,11	4,46	5,86
215/10	88,11	2,71	3,08
216/10	80,28	3,22	4,01
217/10	81,61	3,33	4,08
218/10	90,27	4,21	4,67

Table 3.22.: Film coating thickness of tablet B batches, determined with Image Processing Toolbox™.

Batch	$d_{top}(\mu m)$	$\sigma_{top}(\mu m)$	$\sigma_{top}(\%)$
226/10	100,18	4,28	4,28
227/10	109,01	3,15	2,89
228/10	95,68	2,79	2,91
229/10	102,68	2,89	2,81
230/10	89,02	4,11	4,61
231/10	94,93	2,00	2,11
232/10	99,60	2,92	2,93
233/10	85,27	2,89	3,39
234/10	81,36	3,04	3,74

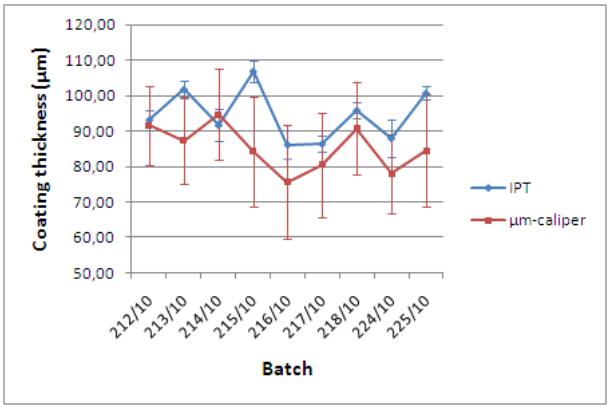

Figure 3.27.: Film coating thickness of tablet A batches, determined with Image Processing Toolbox™.

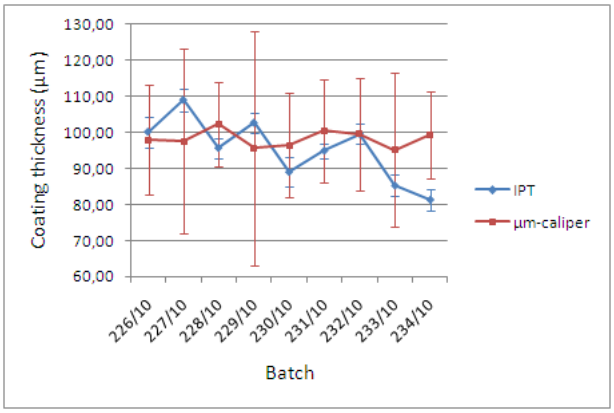

Figure 3.28.: Film coating thickness of tablet B batches, determined with Image Processing Toolbox™.

In figure 3.14 (chapter 3.2.1) it could be seen that there had been an increase in volume of the tablets caused by the disintegration test. At this stage, there could not be made a clear declaration whether the coating or the tablet core gained volume. The Image Processing Toolbox^{TM} thickness determination of the mentioned tablets showed that it was not the coating that increased its volume, it therefore must have been the core. In figure 3.29 showing the film coating thicknesses, even a decrease in coating can be seen for tablets tested for disintegration.

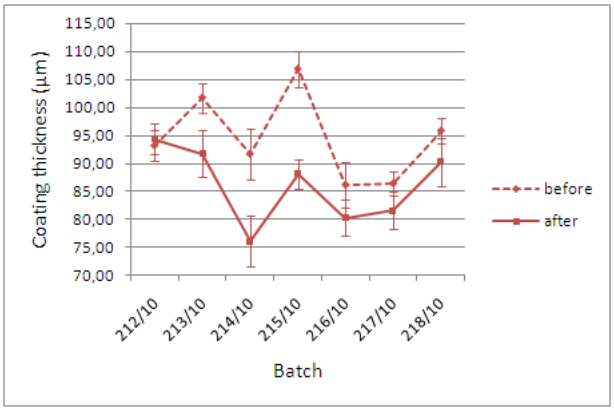

Figure 3.29.: Film coating thickness of tablet A batches before and after disintegration test, determined with Image Processing Toolbox^{TM}.

Discussion: When measuring the thickness via OCT images and Image Processing Toolbox^{TM}, the sources of error are an inaccurate refractive index and the operator error regarding the subjectivity selecting a measuring point. The advantage is that the thickness is measured directly, variations in the tablet core size have no effect on the result. The sources of error are more diverse when measuring with the μm-caliper. In addition to the operator error, the diameter had to be measured twice at tablet core and at coated tablet to calculate an result for the thickness. Therefore, it can be assumed that the values achieved using the Image Processing Toolbox^{TM}are closer to the true coating thickness.

3.5.2.2. Matlab Algorithm

In general, the images are obtained by OCT are gray-scale and every pixel carries a value from zero (black) to 255 (white). The big challenge of analyzing the present OCT images automatically was to create an algorithm that can deal with the different attributes a specific image comes with. Among others, challenges were that the bitmaps of different batches have strongly varying brightness, the contrast between coating, tablet and air is weak and differing as well, and the coating edges are not clearly defined. Several different methods and algorithms were written and tested on the different images. In

the following, the image of the batch produced with increased tablet core temperature (215/10, figure 3.30) is taken to show the results of the algorithms progression and to provide reproducibility. An exhaustive listing of batch representative OCT images can be found in the appendix A.4.

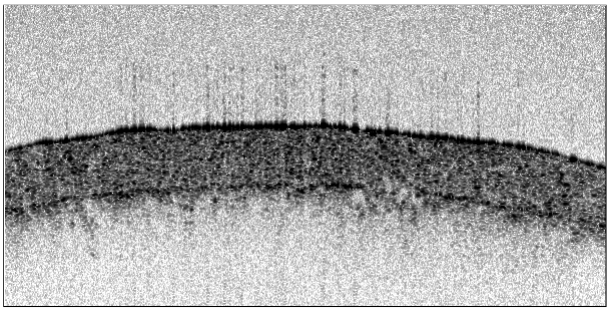

Figure 3.30.: Original OCT image of batch 215/10, increased tablet bed temperature production.

Version 1: Application of threshold and smoothing window in vertical direction. In the first version of the algorithm, the image was converted from gray-scale to black-white, using a theshhold value. Everything above 127 was set white, everything below to black, as shown in figure 3.31. In the next step, the image was treated with a so called smoothing window. Starting from a center pixel at the upper left corner of the image, the previous and next 20 pixels in vertical direction are checked and added up. If the window embraces more ones than zeroes, or in other words the sum is bigger than 20, the center pixel is set to one and the window is moving down the column one pixel. This is repeated until the bottom of the image is reached. In this way, each column is treated. Figure 3.32 shows the smoothed image. In the last step all zeros (black) were added up and divided by 600 to obtain a mean value for the coating thickness over all columns. This last calculation of thickness stayed the same for all versions up to 4.

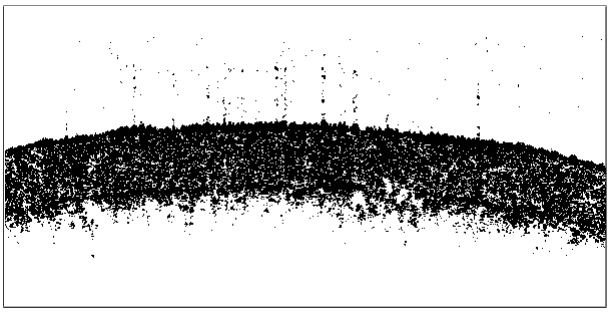

Figure 3.31.: OCT image of batch 215/10 after treatment with preset threshold.

Version 2: Application of smoothing window in vertical direction and adapting threshold. Because of the problem with the varying brightness, the idea of calculating

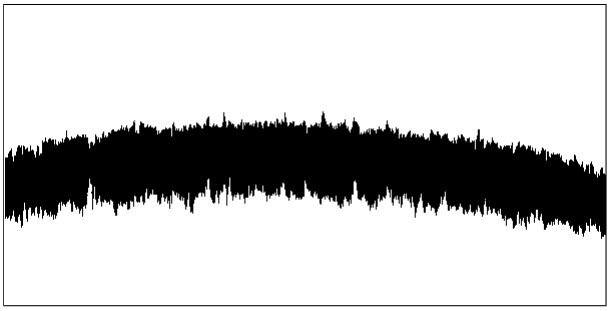

Figure 3.32.: Image 3.31 of batch 215/10 after treatment with smoothing window.

an adapting threshold came up. Therefore, the order of the treatments described above was interchanged. The smoothing was done like before but on the original image. The previous and next 20 pixels were added up, divided by the number of pixels and the center pixel was set to this mean value. Figure 3.33 shows the original image treated with the smoothing window. Afterwards, the background noise was determined by placing a window with an adequate size (30x30px) on the upper left corner of the image and calculating the mean pixel value. The threshold was then defined as 60% of this value. After converting the image to black-and-white via adapting the threshold on the smoothed image, the processed bitmap appeared as seen in figure 3.34.

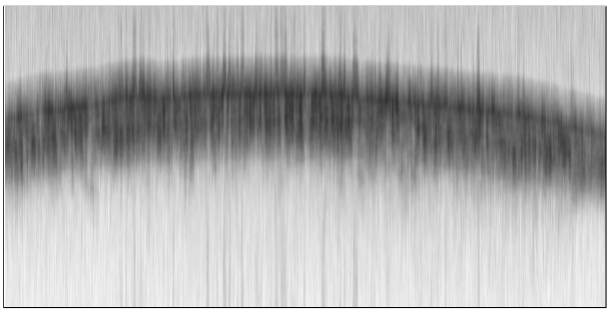

Figure 3.33.: Original OCT image of batch 215/10 after treatment with smoothing window.

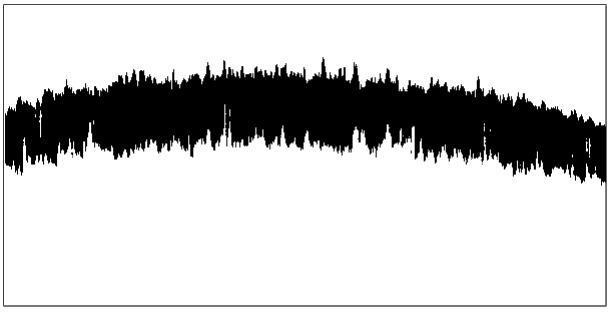

Figure 3.34.: Image 3.33 of batch 215/10 after treatment with self calculated threshold.

Version 3: Application of smoothing window in horizontal direction and adapting threshold. To gain a better reconstruction of the coating and tablet surface, the

smoothing window was adapted in the lateral direction this time. The size of the window was reduced such that the ten previous and ten next pixel were checked. The order of the other treatments was the same as in version 2. Figure 3.35 shows the obtained lateral smoothed image. The calculation of threshold was done like in the version before. In figure 3.36 the resulting image used for thickness calculation is shown.

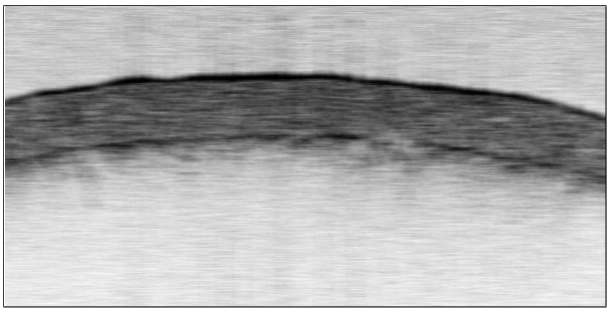

Figure 3.35.: Original OCT image of batch 215/10 after treatment with lateral smoothing window.

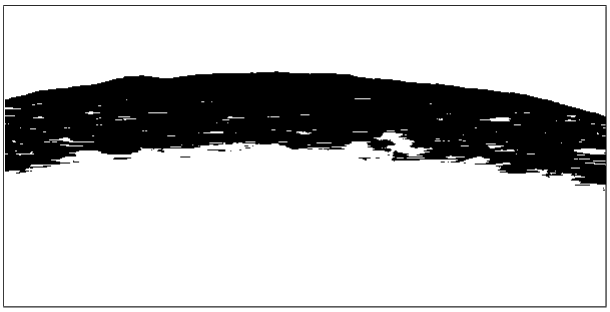

Figure 3.36.: Image 3.35 of batch 215/10 after treatment with self calculated threshold.

Version 4: Application of smoothing window in horizontal direction and improved adapting threshold. The smoothing of the image was done in the same way as in the version before (Figure 3.35). Due to the variation in contrast, it became necessary to also consider the brightness of the coating itself for the calculation of the threshold. Therefore, the window for calculating the background noise from before was taken and moved in medial direction pixel by pixel down the image. The mean area values were saved in a 'brightness-vector'. The best value for the threshold is somewhere between the maximum value (background) and minimum value (coating) of the vector. Hence, the threshold was calculated by adding half of the difference between maximum and minimum to the minimum value. Figure 3.37 shows the processed image used for thickness determination.

The result shown in Fig. 3.37 was the best that could be obtained by using smoothing window and threshold conversion.

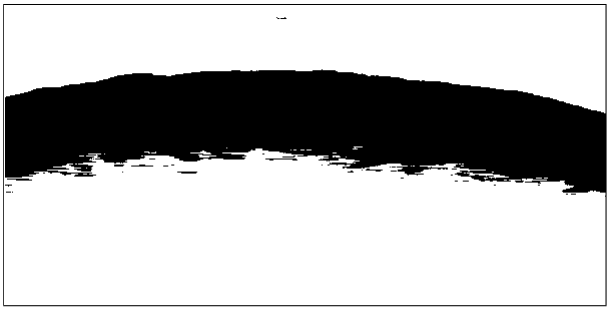

Figure 3.37.: Image 3.35 of batch 215/10 after treatment with advanced threshold.

Version 5: Boundary detection and reconstruction of film coating edges. The last version is based on a detection of the two boundaries (air/coating and coating/tablet) and the reconstruction of it by fitting a polynomial. The original image was investigated with a two pixel window along the medial direction. Starting from the top of the bitmap, the window sampled downwards, stopped and saved its position once the sum of the pixels was lower than 200. This was selective enough to identify coating and skip artifacts. Afterwards, a second order polynomial was fitted through the detected points. In the next step, every point that was located outside a tolerance range of plus or minus ten pixels from the fit was excluded (Figure 3.38). With the remaining values, another polynomial of order 20 was fitted to reconstruct the upper edge of the coating (Figure 3.39).

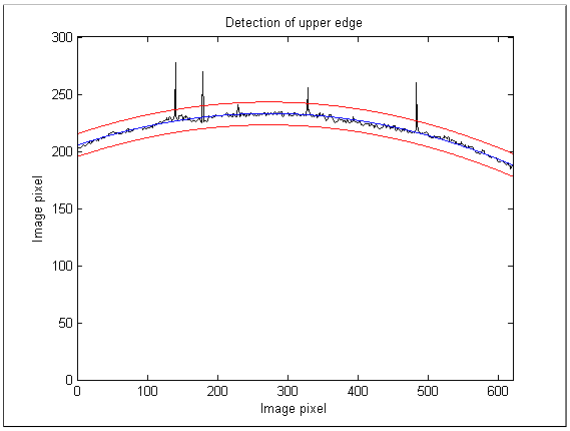

Figure 3.38.: Detection of air/coating boundary in image 3.35 of batch 215/10.

In most cases, the lower boundary (coating/tablet) in the images is not as well-defined as the upper one (air/coating), demanding an increased effort in the detection algorithm. Here, the sampling window was starting at the bottom of the bitmap and moving upwards until the sum of the pixel was smaller than 100. The reason for that smaller value compared to the one before is that only the actual coating should be identified as coating and not the previously mentioned artifacts. In the next step a band was defined to determine expressive detections. The polynomial fit of the upper boundary minus a calibration value that corresponds to a known estimate of the thickness. Every

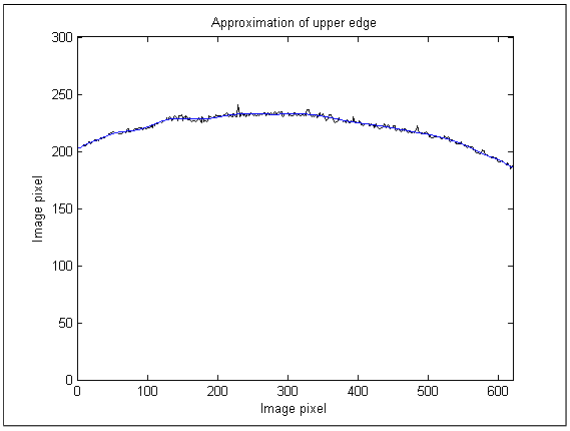

Figure 3.39.: Approximation of polynomial for air/coating boundary in image 3.35 of batch 215/10.

point outside plus or minus 20 pixels of this base was excluded and set zero (Figure 3.40). Like before, the remaining values were fitted with a polynomial of order 20 and the lower edge of the coating was rebuilt (Figure 3.41).

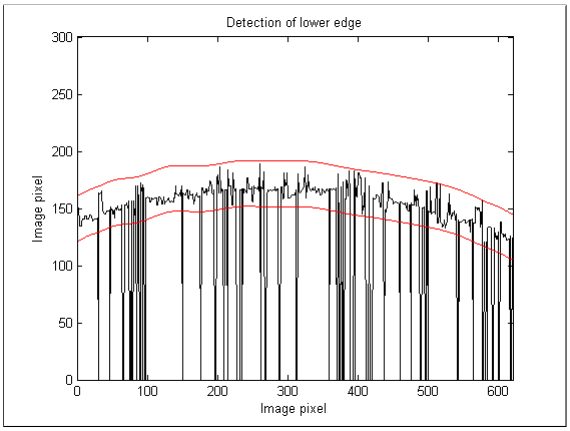

Figure 3.40.: Detection of coating/tablet boundary in image 3.30 of batch 215/10.

In figure 3.42 the reconstruction of the film coating for an image of batch 215/10 is shown. The thickness, its distribution and the surface character could be emulated very well and the algorithm was applicable to all batch images. To provide a good statistical interpretation, the thickness distributions were plotted in a histogram and the data was compared regarding skewness and standard deviation. After fitting with Normal-, Weibull, and Cauchy-distribution it could be seen, that in most cases the data was fitted best with a Weibull distribution. Therefore, the different batches were compared regarding skewness and standard deviation of the Weibull distribution. Tables 3.23, 3.24 and 3.25 show the mean coating thickness, the standard deviation and the skewness of the experiments. Figures 3.43, 3.45 and 3.44 show the corresponding diagrams. The histogram of thickness distribution for batch 215/10 is shown in 3.46. An exhaustive listing of histograms can be found in the appendix A.3.

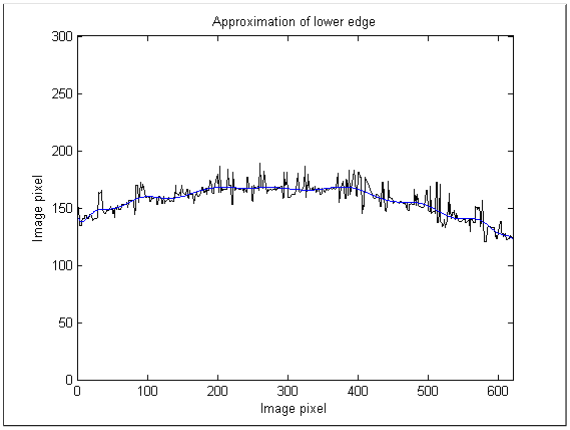

Figure 3.41.: Approximation of polynomial for coating/tablet boundary in image 3.30 of batch 215/10.

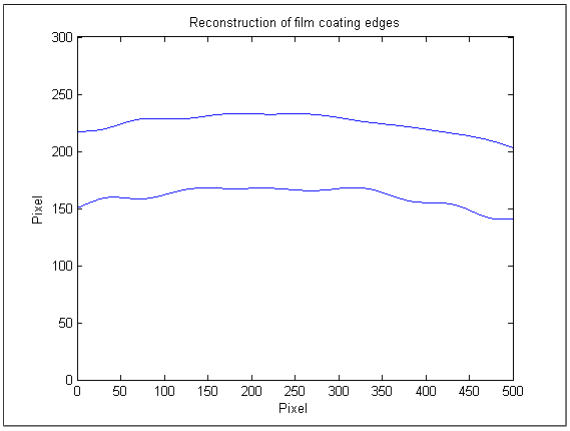

Figure 3.42.: Reconstruction of film coating for image 3.30 of batch 215/10.

Table 3.23.: Film coating thickness of tablet A batches, determined with Matlab algorithm.

Batch	$d_{top}(\mu m)$	$\sigma_{top}(\mu m)$	$\sigma_{top}(\%)$	$Skewness(1)$
212/10	98,62	1,79	1,82	0,35
213/10	101,58	2,33	2,29	-0,06
214/10	95,78	2,66	2,78	0,99
215/10	107,66	3,11	2,89	0,12
216/10	84,86	4,28	5,04	-0,77
217/10	85,40	1,78	2,08	-0,64
218/10	89,57	4,38	4,89	-1,13
224/10	86,84	5,66	6,52	-0,63
225/10	96,60	2,65	2,74	-0,24

Table 3.24.: Film coating thickness of tablet A batches after disintegration test, determined with Matlab algorithm.

Batch	$d_{top}(\mu m)$	$\sigma_{top}(\mu m)$	$\sigma_{top}(\%)$	$Skewness(1)$
212/10	102,79	3,04	2,96	-0,79
213/10	93,81	2,38	2,54	-0,78
214/10	78,59	5,91	7,52	-0,73
215/10	91,17	2,30	2,52	-0,30
216/10	75,36	4,44	5,89	-0,29
217/10	78,18	4,22	5,40	-0,67
218/10	86,99	4,33	4,98	0,74

Table 3.25.: Film coating thickness of tablet B batches, determined with Matlab algorithm.

Batch	$d_{top}(\mu m)$	$\sigma_{top}(\mu m)$	$\sigma_{top}(\%)$	$Skewness(1)$
226/10	97,75	4,29	4,39	0,02
227/10	105,73	3,75	3,55	-0,05
228/10	93,91	4,38	4,66	-0,27
229/10	94,85	5,48	5,78	-0,64
230/10	90,05	5,38	5,97	-0,09
231/10	93,81	3,40	3,62	-0,33
232/10	96,56	5,03	5,21	0,14
233/10	84,69	4,18	4,94	-0,54
234/10	80,35	4,37	5,44	-1,31

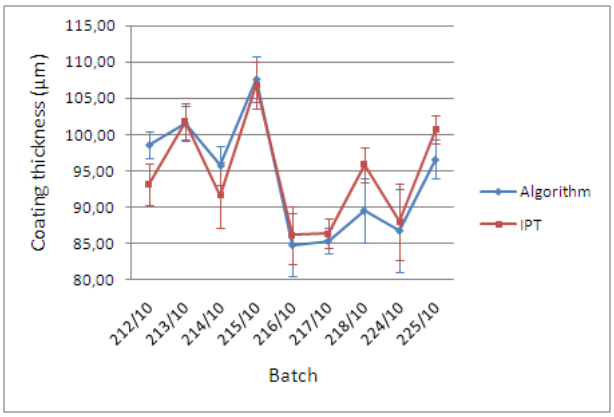

Figure 3.43.: Film coating thickness of tablet A batches, determined with Matlab algotithm.

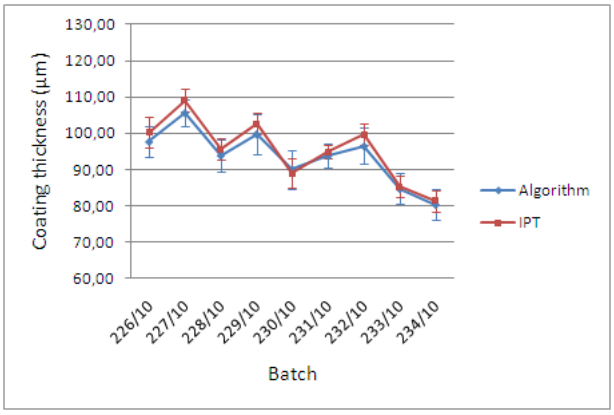

Figure 3.44.: Film coating thickness of tablet B batches, determined with Matlab algotithm.

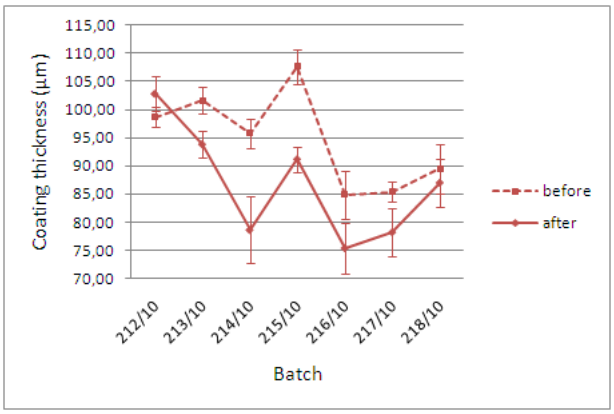

Figure 3.45.: Film coating thickness of tablet A batches before and after disintegration test, determined with Matlab algotithm.

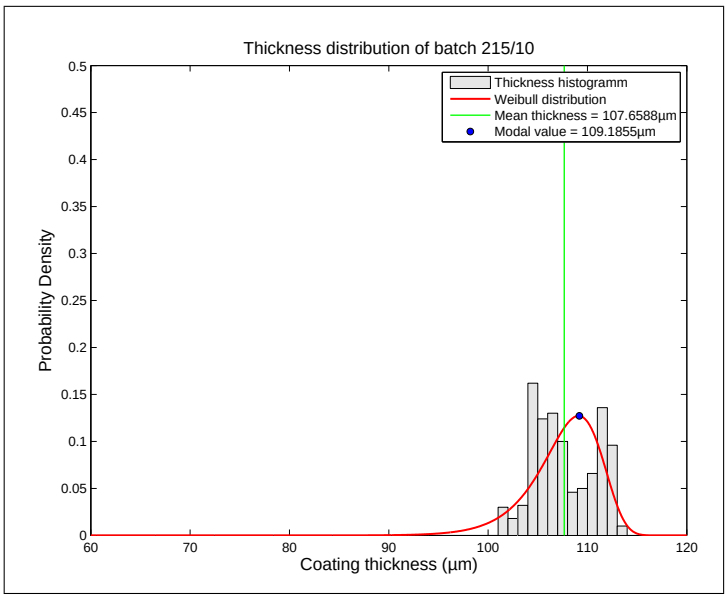

Figure 3.46.: Thickness distribution histogram with mean and modal value of batch 215/10.

Discussion: The reason for the consecutive development of the algorithm were:

- **Version 1: Application of threshold and smoothing window in vertical direction.** The main problem for this solution was that the differences in brightness of the specific bitmaps would have forced us to manually reset the threshold value for every image.
- **Version 2: Application of smoothing window in vertical direction and adapting threshold.** The average coating thickness in the previous algorithm may be predicted quite well, but in both figures 3.32 and 3.34 it can be seen that the reconstruction of the coating surface is lacking, and that there is no meaningful information about planarity or thickness distribution on the tablet.
- **Version 3: Application of smoothing window in horizontal direction and adapting threshold.** In this version, a good reconstruction of the surfaces could be implemented and thickness distribution data was collected. After trying the algorithm on different batches it could be seen that in some cases the coating does not appear solid. This is caused by the large variations in brightness inside the coating layer, making it impossible to apply the algorithm on all OCT results without unwanted manual adjusting.
- **Version 4: Application of smoothing window in horizontal direction and improved adapting threshold.** Both, a good film thickness calculation and an appropriate reconstruction of surfaces, could be implemented for every batch. However, there were some problems with artifacts caused by the coating/tablet boundary that manifested as dark regions located at some distance underneath this boundary. In some cases, those artifacts are identified as coating by the algorithm, although they definitively do not belong to it.
- **Version 5: Boundary detection and reconstruction of film coating edges.** The results obtained with the algorithm are correlating well with the ones received with the Image Processing Toolbox^{TM}. The advantages of the algorithm are the faster processing and the improved statistical interpretation.

3.5.2.3. Damaged film coating

It was possible to process a 3D image of the before mentioned damaged tablet out of the tablet A experiments (224/10), which was used to determine the refractive index. Figure 3.47 shows the coating of the tablet. It can be seen that a piece of coating of approximately 1 mm^2 has broken out. This tablet was out of a replication experiment and so we still can provide a gapless analysis of the batches in the dissolution test.

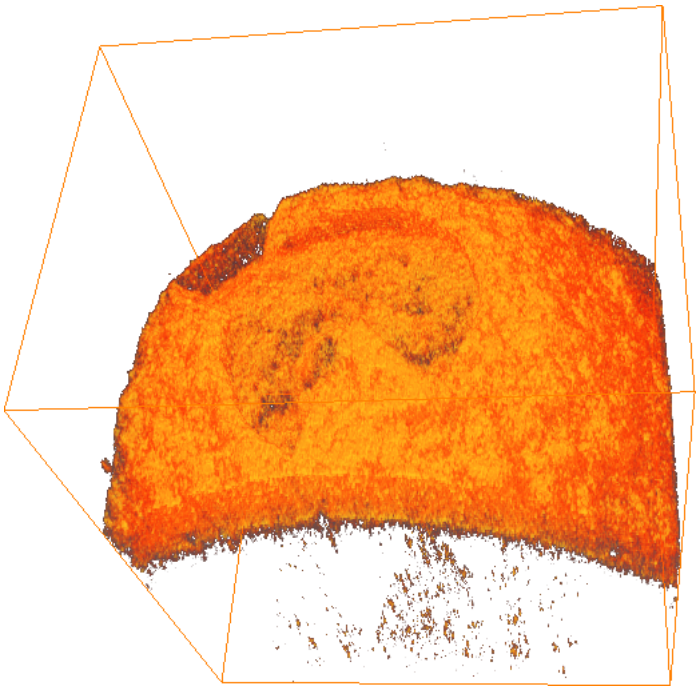

Figure 3.47.: 3D image of damaged coating at batch 224/10 of tablet A experiments.

Discussion: In other studies, single tablets were investigated with OCT and the potential of this method was highlighted [21]. Therefore we used OCT for the non-destructive imaging of the tablets under investigation. OCT provides a fast image processing and measuring time. In combination with the developed automatic post-processing algorithms, it can be applied as a in-line PAT tool for monitoring the coating thickness and as a device for end product quality testing regarding its capability of detecting film coating damages.

3.6. Dissolution test

After the non-destructive measurements described above, the last, destructive step was the investigation of the chosen tablets in a dissolution tester (DT 800, ERWEKA®, Germany) regarding the USP II dissolution test guidelines. This test measures the crucial quality features, i.e. resistance to gastric juice and API release characteristics. The result decides whether a produced batch goes on sale or not. The test consists of two steps. In the first step, the tablets are kept in motion for 2 hours in 0,1 molar hydrochloric acid (pH=1) to simulate the movement in gastric juice in the stomach. After this gastric juice resistance test, the API concentration in a sample taken from the solution has to be lower than 10 %. As a reference, an equivalent solution of hydrochloric acid that contains 100 % dissolved API is prepared. Both, sample and reference, are investigated in an UV-VIS spectrometer (Agilent 8453, Agilent Technologies Inc., USA), the absporption at 280 nm is measured and the percentage of release is calculated as seen in equation (3.6). In the second step, the hydrochloric acid is neutralized (phosphate buffer of pH=6.8) to simulate the environment in the intestinal tract and the tablets are moved for another 30 minutes in the buffer solution. Solution samples are taken every ten minutes and are compared to a reference phosphate buffer with 100 % API in solution. The absorption at a wavelength of 265 nm is measured and the release percentage is determined via Equation (3.7). After 30 minutes in phosphate buffer, an API release of at least 75 % is necessary to pass the dissolution test. Table 3.26 and figure 3.48 show the test results for the tablet A experiment. All batches passed both the disintegration and release test, with the exception of the tablet with the damaged coating (224/10) who failed the disintegration test as could be expected. Additionally, the release performance of the tablets already investigated in the disintegration test after production was tested. The results are shown in table 3.27 and figure 3.49. Those batches had a perfect API release as well.

$$Release[\%] = \frac{Abs_{\text{Sample}}[1] \cdot ASA_{\text{actual}}[mg] \cdot 750 \cdot 100 \cdot API_{\text{content}}[\%]}{Abs_{\text{Reference}}[1] \cdot 1000 \cdot ASA_{\text{nominal}}[mg]} \tag{3.6}$$

$$Release[\%] = \frac{Abs_{\text{Sample}}[1] \cdot ASA_{\text{actual}}[mg] \cdot 1000 \cdot 100 \cdot API_{\text{content}}[\%]}{Abs_{\text{Reference}}[1] \cdot 1000 \cdot ASA_{\text{nominal}}[mg]} \tag{3.7}$$

In the dissolution test, it was observed that the tablets start to crack at their band, where the coating thickness has its thinnest point. Figure 3.50 shows the progress of dissolution in the dissolution tester. After initial cracking, the tablet breaks in two halves and the API is released rapidly. A breakup pattern different than this was only shown by the tablet with the damaged film coating (224/10) that was also tested in the dissolution test. It broke up during the test of gastric juice resistance at the location of

Table 3.26.: Dissolution performance of tablet A batches in 0,1 molar hydrochloric acid of pH 1 (gastric) and phosphate buffer of pH 6.8 (intestinal).

$t(min)$	212/10 API release(%)	213/10 API release(%)	214/10 API release(%)
120 (gastric)	0,4	0,2	0,6
10 (intestinal)	56,6	52,2	73,3
20 (intestinal)	97,8	95,6	98,8
30 (intestinal)	104,7	100,9	102,2
$t(min)$	215/10 API release(%)	216/10 API release(%)	217/10 API release(%)
120 (gastric)	0,9	0,1	0,6
10 (intestinal)	58,4	74,7	77,8
20 (intestinal)	94,4	99,0	100,0
30 (intestinal)	103,4	103,2	105,3
$t(min)$	218/10 API release(%)	224/10 API release(%)	225/10 API release(%)
120 (gastric)	1,4	37,2	2,3
10 (intestinal)	62,5	79,0	71,9
20 (intestinal)	102,3	106,0	95,9
30 (intestinal)	104,0	107,6	99,8

Table 3.27.: Release performance of disintegration tested tablet A batches in 0,1 molar hydrochloric acid of pH 1 (gastric) and phosphate buffer of pH 6.8 (intestinal).

$t(min)$	212/10 API release(%)	213/10 API release(%)	214/10 API release(%)
10 (intestinal)	91,0	83,8	86,8
20 (intestinal)	106,9	97,8	101,9
30 (intestinal)	108,7	103,7	102,2
$t(min)$	215/10 API release(%)	216/10 API release(%)	217/10 API release(%)
10 (intestinal)	66,5	49,2	70,7
20 (intestinal)	99,8	95,9	101,1
30 (intestinal)	105,3	103,2	106,8
$t(min)$	218/10 API release(%)		
10 (intestinal)	74,4		
20 (intestinal)	95,7		
30 (intestinal)	102,0		

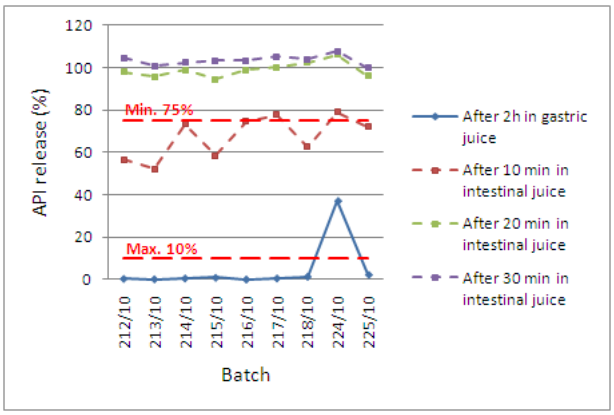

Figure 3.48.: Dissolution performance of tablet A batches in 0,1 molar hydrochloric acid of pH 1 (gastric) and phosphate buffer of pH 6.8 (intestinal).

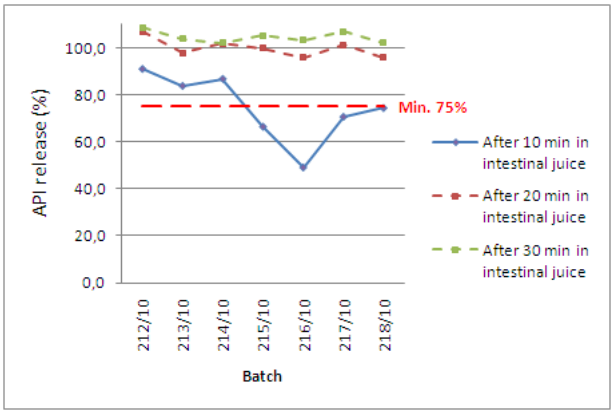

Figure 3.49.: Release performance of disintegration tested tablet A batches.

the missing coating. Therefore, it already released 37,2 % of its API at the end of this test. In the following API release test, the tablet disintegrated different than the other batches as seen in figure 3.51. Beside the mentioned tablet all other batches showed a similiar behaviour.

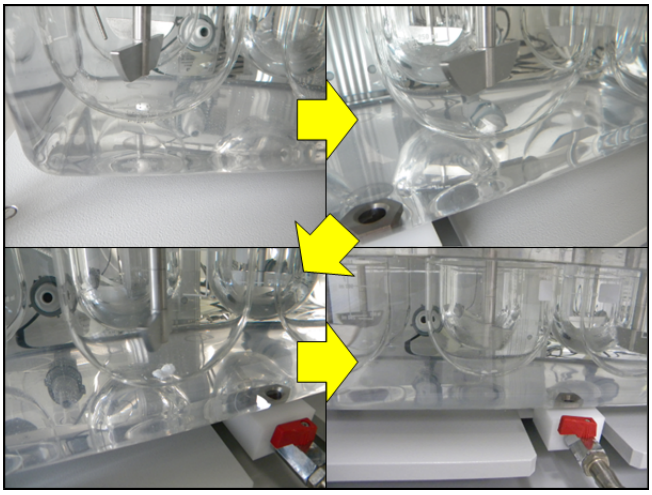

Figure 3.50.: Progress of dissolution over time.

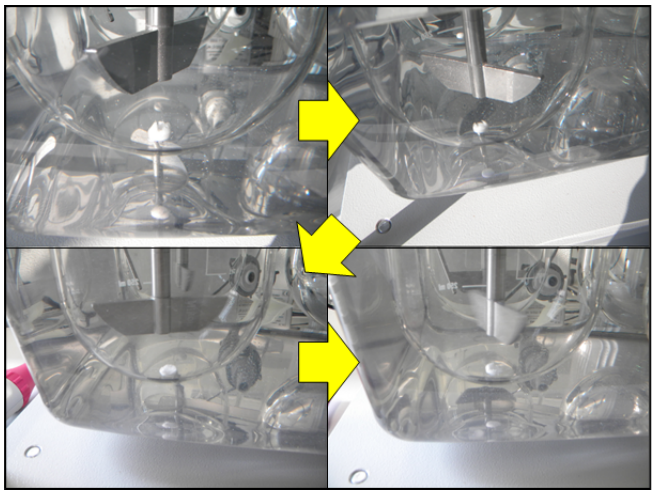

Figure 3.51.: Disintegration of tablet with damaged film coating (224/10).

Discussion: In the literature, tablets with different enteric-coatings were analyzed with the USP II dissolution test and destructive imaging methods (CLSM, SEM) [15], with the obvious limitation that different tablets had to be used for the destructive investigations. The relation of coating anatomy and dissolution behavior could be shown in this work using the non-destructive OCT.

It seems that the varying process parameters do not affect the dissolution test performance of tablets. It could also be seen that trapped moisture in between film coating and tablet did not lead to API dissolution as assumed before. Also, the diffusion of

gastric juice into the tablet during the disintegration test did not harm the release behavior. However, tablets with even small damages in film coating do not resist the disintegration test. It could be observed that a gastric juice resistive tablet always start to crack at its band. Therefore it could be possible that the coating thickness there is responsible for the velocity of API release.

4. Summary and conclusions

The film coating of tablets produced with OOS parameters were analyzed using different non-destructive methods. The coating thickness was determined with a μm-caliper and OCT. Models for predicting the gain in film coating thickness were built with the help of MVDA and NIR/Raman spectra. Finally, the obtained results were compared with each other and the relationship to the outcome of the final (destructive) inspection, the dissolution test, was investigated.

The measurement of the film coating thickness with a μm-caliper proved to be relatively time-consuming. The variance of weight and dimensions within a batch of raw tablets made it necessary to measure at least ten tablets for gaining a reasonable statistical variance. Especially the thickness at the top of the tablet was error-prone, as it can only be measured once per tablet, whereas the thickness on the side can be measured for several diagonals. Another disadvantage of this method is that the coating thickness is determined indirectly by subtracting the diameter of the raw tablet from the diameter of the coated tablet and dividing by two. As a consequence, when an increase in tablet volume between the original tablets and the ones already investigated in the disintegration test could be observed, the μm-caliper measurements allowed no decision whether this increase in volume happened in the coating or the core. In contrast, OCT directly provides images of the tablet coating and with the help of an algorithm developed in this work the film coating thickness was ascertainable very fast and with a good statistical significance. Additionally, OCT images carry information about the thickness distribution on the tablet and the coating homogeneity. From this it could be seen that the coating thickness of the disintegration tested tablets decreased. In combination with the μm-caliper results it could be determined that the tablet core gained volume due to osmotic processes. The fast processing time of the OCT method in combination with the algorithm allows a potential application as a reliable and useful in-line PAT tool for coating process monitoring.

The results obtained with both μm-caliper and OCT served as a reference for the development of PLS models of recorded NIR and Raman spectra. NIR proved to be qualified for film coating thickness prediction because of its good model RMSE (6.17 %). At the moment, the gain in coating thickness is monitored by controlling the tablet's

gain in weight. However, even the uncoated tablet cores show a significant variation in weight. Thus, the uncoated weight of an individual coated tablet is unknown, making it impossible to exactly determine the coating thickness from a weight measurement. Those errors can be circumvented by using NIR because it quantifies the increasing amount of coating ingredients directly. Due to the short processing time, NIR could be used as a PAT tool for in-line process monitoring and could replace the weight measurement. The model obtained with Raman spectra had a slight worse RMSE (9.5 %) and the processing time is slower in comparison to NIR.

Summarizing, it can be said that the method of choice for in-line monitoring of a film coating process is OCT. In addition to an accurate coating thickness value, it provides information about coating distribution and its homogeneity and is fast enough.

All tablets tested in the USP II dissolution apparatus showed a perfect gastric juice resistance and API release performance. It seemed that OOS process parameters affect neither the resistance nor the API release significantly. The previous stated theory of API decomposition in case of a humid coating process therefore turned out to be wrong. This is affirmed by the measurement of tablets that have already been subjected to a disintegration test prior to the full measurement procedure and final dissolution test. While the core of these tablets even gained volume due to osmosis, they still fully released the API.

It is assumed that the most important parameter affecting the gastric juice resistance and API release is the film coating thickness. In the second part of the dissolution test, the release test, the tablet starts to crack at its band. This indicates that the coating thickness at the side of the tablet has the main influence on the velocity of API release. In case of a coating thickness that is well above average, it is to be expected that the API will only be fully released after the time limit of 30 minutes that is usually chosen for the investigation. Based on the presented thesis, further experiments with varying coating thicknesses and an increased observation time window for the release test could be a logical next step.

List of Figures

1.1. Schematic of a fluidized bed coater.[3] 2
1.2. Classification of coating uniformity.[4] 4
1.3. Schematic of a side-vented pan coater and spray anatomy.[2] 5
1.4. Three conceptual phases of the coating process.[2] 6

2.1. The three factorial designs offered in DoE. 10
2.2. UV-scaled and mean-centered data. 12
2.3. Data set in variable space before and after pretreatment. 13
2.4. Least square approximation of data lead to PC1. 13
2.5. Calculation of loading p_{i1}. 14
2.6. PC1 and PC2 plane in three dimensional space. 14
2.7. Three prediction and one response variable spaces. 15
2.8. Determination of first PLS component. 16
2.9. Determination of second PLS component. 16
2.10. Calculation of two component PLS model. 16
2.11. Schematic of a NIR spectrometer for measuring reflectance. 18
2.12. Schematic vibrational energy level diagram for Raman scattering: (a) Stokes line; (b) Anti-Stokes line. 20
2.13. Schematic setup of an OCT system realized with Michelson interferometer. 21

3.1. Axial experiments of tablet A. 24
3.2. Axial experiments of tablet B. 25
3.3. Experiment set-up with coating pan, supply and exhaust air, atomization nozzle, tube pump, coating suspension and control unit. 25
3.4. Replication Plots of tablet A. 26
3.5. Replication Plots of tablet B. 27
3.6. Summary of model, tablet A. 28
3.7. Summary of model, tablet B. 28
3.8. Surface response plot of Coating thickness at side of tablet B, determined with μm-caliper. 29
3.9. Surface response plot of Coating thickness at top of tablet B, determined with Image Processing Toolbox™. 29

3.10. The μm caliper (left) and height gauge (right) measurement devices used in the coating thickness investigations. 31
3.11. Measuring points for coating thickness determination. 32
3.12. Film coating thickness of tablet A batches, determined with μm-caliper. 33
3.13. Film coating thickness of tablet B batches, determined with μm-caliper. 33
3.14. Film coating thickness of disintegration tested tablet A batches, determined with μm-caliper. 34
3.15. Film coating thickness top of tablet A batches before and after disintegration test, determined with μm-caliper. 35
3.16. Film coating thickness side of tablet A batches before and after disintegration test, determined with μm-caliper. 35
3.17. Weight of tablet A batches before and after disintegration test. 37
3.18. NIR spectra of increasing talcum peak for certain time points during the coating process. 39
3.19. NIR spectra of an uncoated tablet, a completely coated tablet and talcum. 39
3.20. PCA plot of the first and second principal component of tablet A, focused on the OH-bands. 41
3.21. PCA plot of tablet B, focused on the OH-bands. 42
3.22. PCA plot of disintegration tested tablet B batches, focused on the OH-bands. 42
3.23. Raman spectra of an uncoated tablet, a completely coated tablet and ASA. 44
3.24. Raman spectra with decreasing intensity for certain time points during coating process. 45
3.25. Determination of refractive index. 48
3.26. Determination of coating thickness with Image Processing Toolbox^{TM}. . 50
3.27. Film coating thickness of tablet A batches, determined with Image Processing Toolbox^{TM}. 51
3.28. Film coating thickness of tablet B batches, determined with Image Processing Toolbox^{TM}. 51
3.29. Film coating thickness of tablet A batches before and after disintegration test, determined with Image Processing Toolbox^{TM}. 52
3.30. Original OCT image of batch 215/10, increased tablet bed temperature production. 53
3.31. OCT image of batch 215/10 after treatment with preset threshold. . . . 53
3.32. Image 3.31 of batch 215/10 after treatment with smoothing window. . . 54
3.33. Original OCT image of batch 215/10 after treatment with smoothing window. 54
3.34. Image 3.33 of batch 215/10 after treatment with self calculated threshold. 54

3.35. Original OCT image of batch 215/10 after treatment with lateral smoothing window. 55
3.36. Image 3.35 of batch 215/10 after treatment with self calculated threshold. 55
3.37. Image 3.35 of batch 215/10 after treatment with advanced threshold. . 56
3.38. Detection of air/coating boundary in image 3.35 of batch 215/10. . . . 56
3.39. Approximation of polynomial for air/coating boundary in image 3.35 of batch 215/10. 57
3.40. Detection of coating/tablet boundary in image 3.30 of batch 215/10. . . 57
3.41. Approximation of polynomial for coating/tablet boundary in image 3.30 of batch 215/10. 58
3.42. Reconstruction of film coating for image 3.30 of batch 215/10. 58
3.43. Film coating thickness of tablet A batches, determined with Matlab algotithm. 59
3.44. Film coating thickness of tablet B batches, determined with Matlab algotithm. 60
3.45. Film coating thickness of tablet A batches before and after disintegration test, determined with Matlab algotithm. 60
3.46. Thickness distribution histogram with mean and modal value of batch 215/10. 60
3.47. 3D image of damaged coating at batch 224/10 of tablet A experiments. 62
3.48. Dissolution performance of tablet A batches in 0,1 molar hydrochloric acid of pH 1 (gastric) and phosphate buffer of pH 6.8 (intestinal). . . . 65
3.49. Release performance of disintegration tested tablet A batches. 65
3.50. Progress of dissolution over time. 66
3.51. Disintegration of tablet with damaged film coating (224/10). 66

A.1. Response surface plots of tablet A batches. . . . . A 2
A.2. Response surface plots of tablet B batches. . . . . A 2
A.3. Thickness distribution histogram with mean and modal value of tablet A batches. . . . . A 4
A.4. Thickness distribution histogram with mean and modal value of disintegration tested tablet A batches. . . . . A 5
A.5. Thickness distribution histogram with mean and modal value of tablet B batches. . . . . A 7
A.6. Batch representative OCT images of tablet A experiments. . . . . A 8
A.7. Batch representative OCT images of disintegration tested tablet A experiments. . . . . A 9
A.8. Batch representative OCT images of tablet B experiments. . . . . A 10

List of Tables

2.1. Composition of the enteric film coating suspension. 9

3.1. Model performance for output factors of tablet A. 27
3.2. Model performance for output factors of tablet B. 28
3.3. Film coating thickness of tablet A batches, determined with μm-caliper. 32
3.4. Film coating thickness of tablet B batches, determined with μm-caliper. 33
3.5. Film coating thickness of tablet A batches after disintegration test, determined with μm-caliper. 34
3.6. Weight of tablet A batches. 36
3.7. Weight of tablet B batches. 36
3.8. Weight of tablet A batches before and after disintegration test. 37
3.9. Time-related film coating thickness of tablet A, determined with μm-caliper. 38
3.10. Time-related weight of tablet A. 38
3.11. Model performance for gain in weight. 40
3.12. Model performance for coating thickness, top of tablet. 40
3.13. Model performance for coating thickness, side of tablet. 40
3.14. Model performance for gain in weight, line scan mode. 45
3.15. Model performance for coating thickness, top of tablet, line scan mode. 45
3.16. Model performance for coating thickness, side of tablet, line scan mode. 46
3.17. Model performance for gain in weight, super macro point mode. 46
3.18. Model performance for coating thickness, top of tablet, super macro point mode. 46
3.19. Model performance for coating thickness, side of tablet, super macro point mode. 46
3.20. Film coating thickness of tablet A batches, determined with Image Processing Toolbox^{TM}. 50
3.21. Film coating thickness of tablet A batches after disintegration test, determined with Image Processing Toolbox^{TM}. 50
3.22. Film coating thickness of tablet B batches, determined with Image Processing Toolbox^{TM}. 51

3.23. Film coating thickness of tablet A batches, determined with Matlab algorithm. 58
3.24. Film coating thickness of tablet A batches after disintegration test, determined with Matlab algorithm. 59
3.25. Film coating thickness of tablet B batches, determined with Matlab algorithm. 59
3.26. Dissolution performance of tablet A batches in 0,1 molar hydrochloric acid of pH 1 (gastric) and phosphate buffer of pH 6.8 (intestinal). . . . 64
3.27. Release performance of disintegration tested tablet A batches in 0,1 molar hydrochloric acid of pH 1 (gastric) and phosphate buffer of pH 6.8 (intestinal). 64

References

[1] Cole G, Hogan J, Aulton M: *Pharmaceutical coating technology*. Informa Healthcare 1995.

[2] Suzzi D, Radl S, Khinast J: **Local Analysis of the Tablet Coating Process: Impact of Operation Conditions on Film Quality**. *Chemical Engineering Science* 2009.

[3] Levin M: *Pharmaceutical process scale-up*. Drugs and the pharmaceutical sciences, Marcel Dekker, Inc. 2002.

[4] Turton R: **Challenges in the modeling and prediction of coating of pharmaceutical dosage forms**. *Powder Technology* 2008, (2).

[5] Hogan JE: *Film-coating materials and their properties*. Informa Healthcare 1995.

[6] Shelukara S, Hoa J, Zegaa J, Rolandc E, Yeh N, Quiramb D, Nole A, Katdarea A, Reynolds S: **Identification and characterization of factors controlling tablet coating uniformity in a Wurster coating process**. *Powder Technology* 2000.

[7] Wilson KE, Crossman E: **The Influence of Tablet Shape and Pan Speed on Intra-tablet Film Coating Uniformity**. *Drug Development and Industrial Pharmacy* 1997.

[8] Food, Administration D: **PAT - A Framework for Innovative Pharmaceutical Manufactoring and Quality Assurance (Draft Guideline)**. Food and Drug Administration 2003, [http://www.fda.gov/ohrms/dockets/ac/04/briefing/2004-4052B1_15_GFI-Draft-PAT-Guidance.pdf].

[9] Lopes J, Costa P, Alves T, Menezes J: **Chemometrics in bioprocess engineering: process analytical technology (PAT) applications**. *Chemometrics and Intelligent Laboratory Systems* 2004.

[10] Balboni M: *Pharmaceutical Technology*. Advanstar Communications, Duluth, MN, ETATS-UNIS 2003.

[11] Yu L: **Pharmaceutical Quality by Design: Product and Process Development, Understanding, and Control**. *Pharmaceutical Research* 2008.

[12] Cahyadi C, Karande A, Chan L, Heng P: **Comparative study of non-destructive methods to quantify thickness of tablet coatings**. *International Journal of Pharmaceutics* 2010.

[13] El-Hagrasy A, Morris H, D'Amico F, Lodder R, Drennen J: **Near-infrared spectroscopy and imaging for the monitoring of powder blend homogeneity**. *Journal of Pharmaceutical Sciences* 2001.

[14] Kessler W: *Multivariate Datenanalyse*. WILEY-VCH Verlag 2007.

[15] Liu F, Lizio R, Schneider U, Petereit HU, Blakey P, Basit A: **SEM/EDX and confocal microscopy analysis of novel and conventional enteric-coated systems**. *International Journal of Pharmaceutics* 2008.

[16] Ruotsalainen M, Heinämäki J, Guo H, Laitinen N, Yliruusi J: **A novel technique for imaging film coating defects in the film-core interface and surface of coated tablets**. *European Journal of Pharmaceutics and Biopharmaceutics* 2003.

[17] Kirsch J, Drennen J: **Determination of film-coated tablet parameters by near-infrared spectroscopy**. *Journal of Pharmaceutical and Biomedical Analysis* 1995.

[18] Peinado A, Hammond J, Scott A: **Development, validation and transfer of a Near Infrared Method to determine in-line the end point of a fluidised drying process for comercial production batches of an approved oral solid dose pharmaceutical product**. *Journal of Pharmaceutical and Biomedical Analysis* 2011.

[19] Romero-Torres S, Pérez-Ramos J, Morris K, Grant E: **Raman spectroscopic measurement of tablet-to-tablet coating variability**. *Journal of Pharmaceutical and Biomedical Analysis* 2005.

[20] Kauffmann J, Dellibovi M, Cunningham C: **Raman spectroscopy of coated pharmaceutical tablets and physical models for multivariate calibration to tablet coating thickness**. *Journal of Pharmaceutical and Biomedical Analysis* 2006.

[21] Mauritz J, Morrisby R, Hutton R, Legge C, Kaminski C: **Imaging pharmaceutical tablets with optical coherence tomography**. *Journal of Pharmaceutical Sciences* 2010.

[22] Zhong S, Shen YC, Ho L, May RK, Zeitler JA, Evans M, Taday PF, Pepper M, Rades T, Gordon KC, Müller R, Kleinebudde P: **Non-destructive quantification of pharmaceutical tablet coatings using terahertz pulsed imaging and optical coherence tomography**. *Optics and Lasers in Engineering* 2010.

[23] Fitzgerald A, Cole B, Taday P: **Nondestructive Analysis of Tablet Coating Thickness Using Terahertz Pulsed Imaging**. *Wiley InterScience* 2004.

[24] Ho L, Muller R, Romer M, Gordon KC, Heinamaki J, Kleinebudde P, Pepper M, Rades T, Shen YC, Strachan CJ, Taday PF, Zeitler JA: **Analysis of sustained-release tablet film coats using terahertz pulsed imaging**. *Journal of Controlled Release* 2007.

[25] May R, Evans M, Zhong S, Warr I, Gladden L, Shen Y, Zeitler J: **Terahertz in-line sensor for direct coating thickness measurement of individual tablets during film coating in real-time**. *Journal of Pharmaceutical Sciences* 2010.

[26] Cox D, Wells C, Furman W, Savage T, KING A: **Systematic Error Associated with Apparatus 2 of the USP Dissolution Test 11: Effects of Deviations in Vessel Curvature from That of a Sphere**. *Journal of Pharmaceutical Sciences* 1982.

[27] Siebertz K, Van Bebber D, Hochkirchen T: *Statistische Versuchsplanung - Design of Experiments (DoE)*. Springer Verlag Berlin Heidelberg 2010.

[28] Eriksson L, Johansson E, Kettaneh-Wold N, Wikström C, Wold S: *Design of Experiments - Principals and Applications*. Umetrics Academy 2008.

[29] Montgomery C: *Design and analysis of experiments*. Wiley VCH 1996.

[30] Eriksson L, Johansson E, Kettaneh-Wold N, Trygg J, Wikström C, Wold S: *Multi- and Megavariate Data Analysis*. Umetrics Academy 2006.

[31] Blanco M, Coello J, Iturriaga H, Maspoch S, De La Pezuela C: **Near-infrared spectroscopy in the pharmaceutical industry**. *The Analyst* 1998.

[32] Reich G: **Near-infrared spectroscopy and imaging: Basic principles and pharmaceutical applications**. *Advanced Drug Delivery Reviews* 2005.

[33] Burns D, Ciurczak E: *Handbook fo Near-Infrared Analysis*. CRC Press 2008.

[34] Siesler H, Ozaki Y, Kawata S, Heise H: *Near-Infrared Spectroscopy*. Wiley VCH 2002.

[35] Fujimoto J: **Optical coherence tomography**. *Comptes Rendus de l'Académie des Sciences - Series IV* 2001.

[36] Baxter J, Kukura J, FJ M: **Hydrodynamics-induced variability in the USP apparatus II dissolution test**. *International Journal Of Pharmaceutics* 2005.

[37] Porter SC, Verseput RP, Cunningham CR: **Process Optimization Using Design of Experiments**. *Pharmaceutical Technology* 1997, **1**:1–7.

[38] Thoma K, Bechtold K: **Influence of aqueous coatings on the stability of enteric coated pellets and tablets**. *European Journal Of Pharmaceutics And Biopharmaceutics* 1998.

A. Appendix

A.1. Used devices and programs

- *Spectrum 400 FT-IR/FT-NIR Spectrometer:* Perkin Elmer; 940 Winter Street; Walthm; Massachusetts 02451; USA
- *Raman Station 400F/Raman Spectrometer:* Perkin Elmer; 940 Winter Street; Walthm; Massachusetts 02451; USA
- *Digimatic outside micrometer 293-821:* Mitutoyo, Inc., Japan
- *Absolute Digimatic dial gauge ID-S 543-690B:* Mitutoyo, Inc., Japan
- *MODDE 9.0.0.0:* Umetrics AB, Box 7960, SE-907 19 Umea, Sweden
- *The Unscrambler, V10.0.1:* CAMO Software AS, Nedre Vollgate 8, N-0158 Oslo, Norway
- *MATLAB R2009b, V7.9.0.529:* MathWorks, Inc., USA
- *Microsoft Office Excel 2007:* Microsoft, Inc., USA

A.2. Response Surfaces

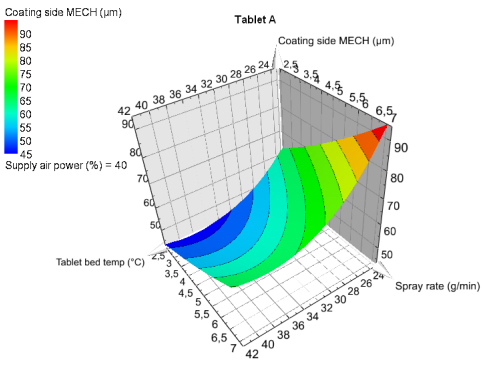

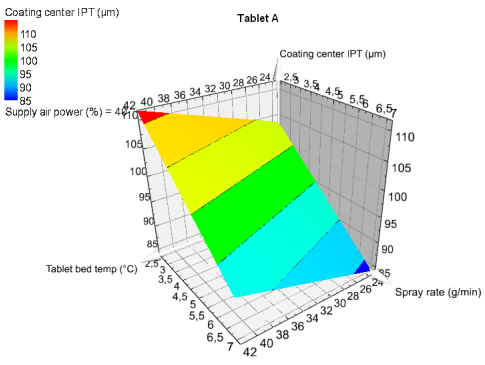

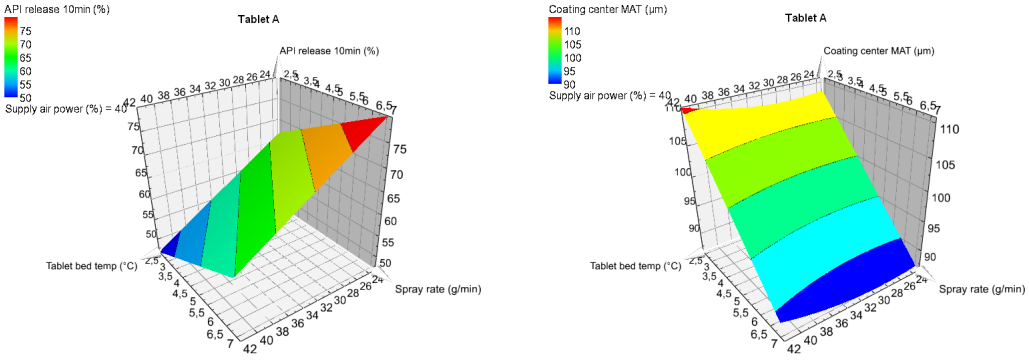

Figure A.1.: Response surface plots of tablet A batches.

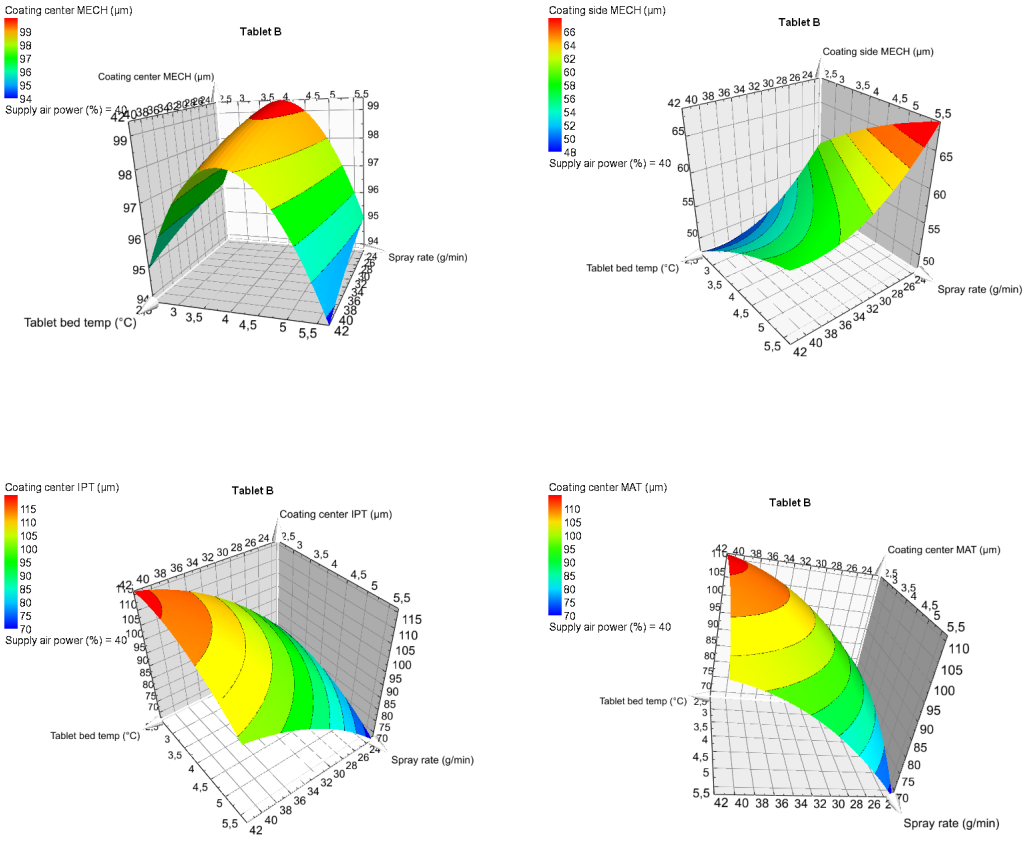

Figure A.2.: Response surface plots of tablet B batches.

A.3. Histograms

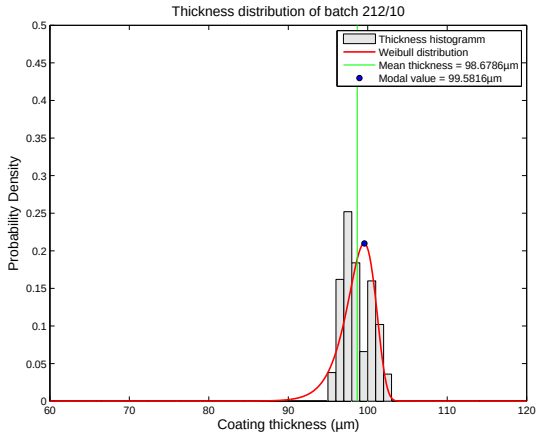

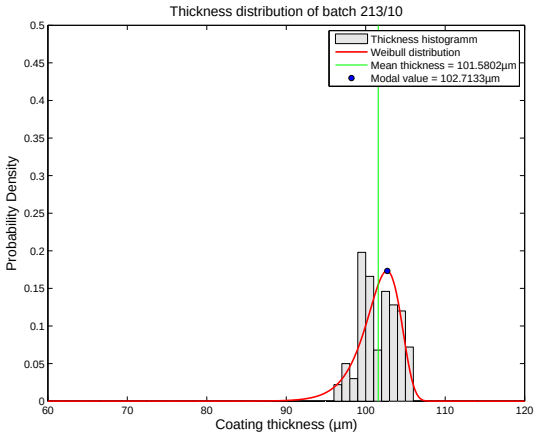

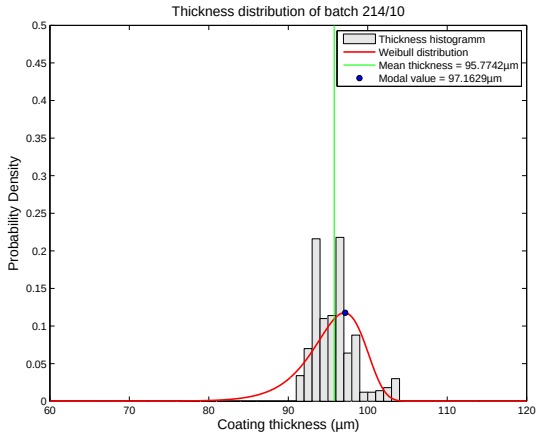

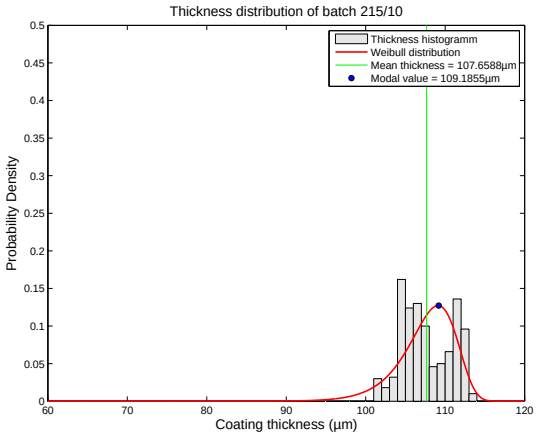

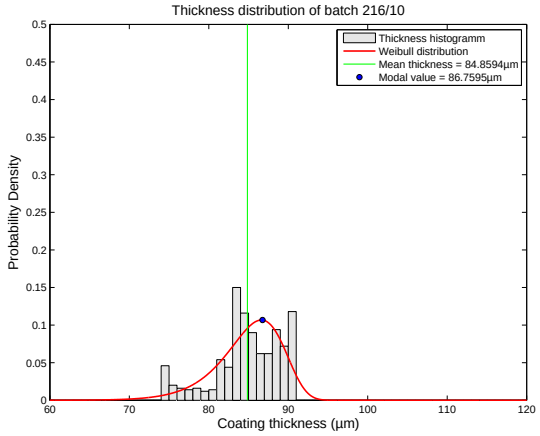

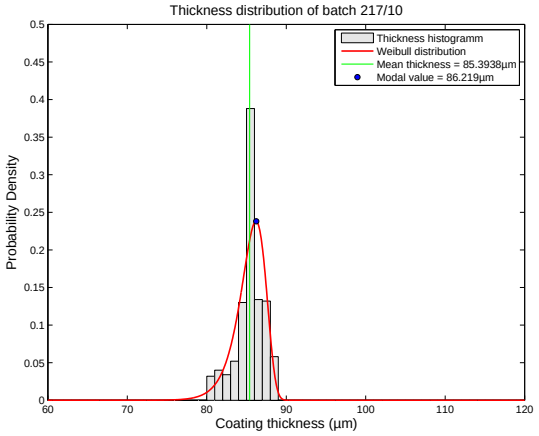

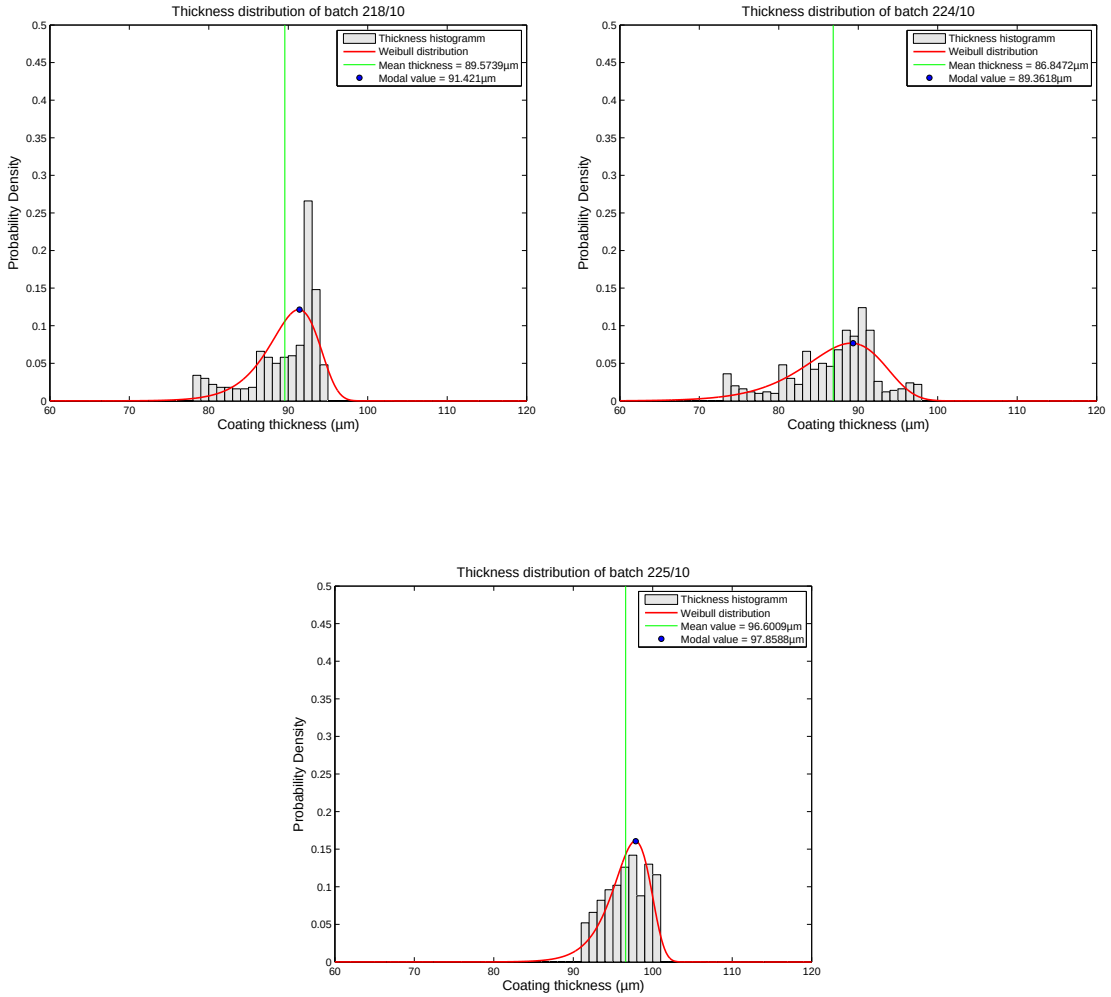

Figure A.3.: Thickness distribution histogram with mean and modal value of tablet A batches.

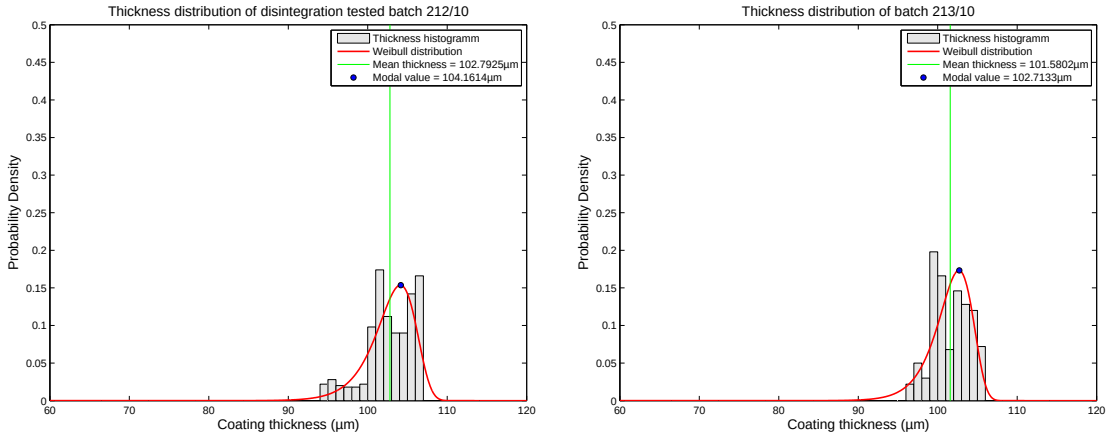

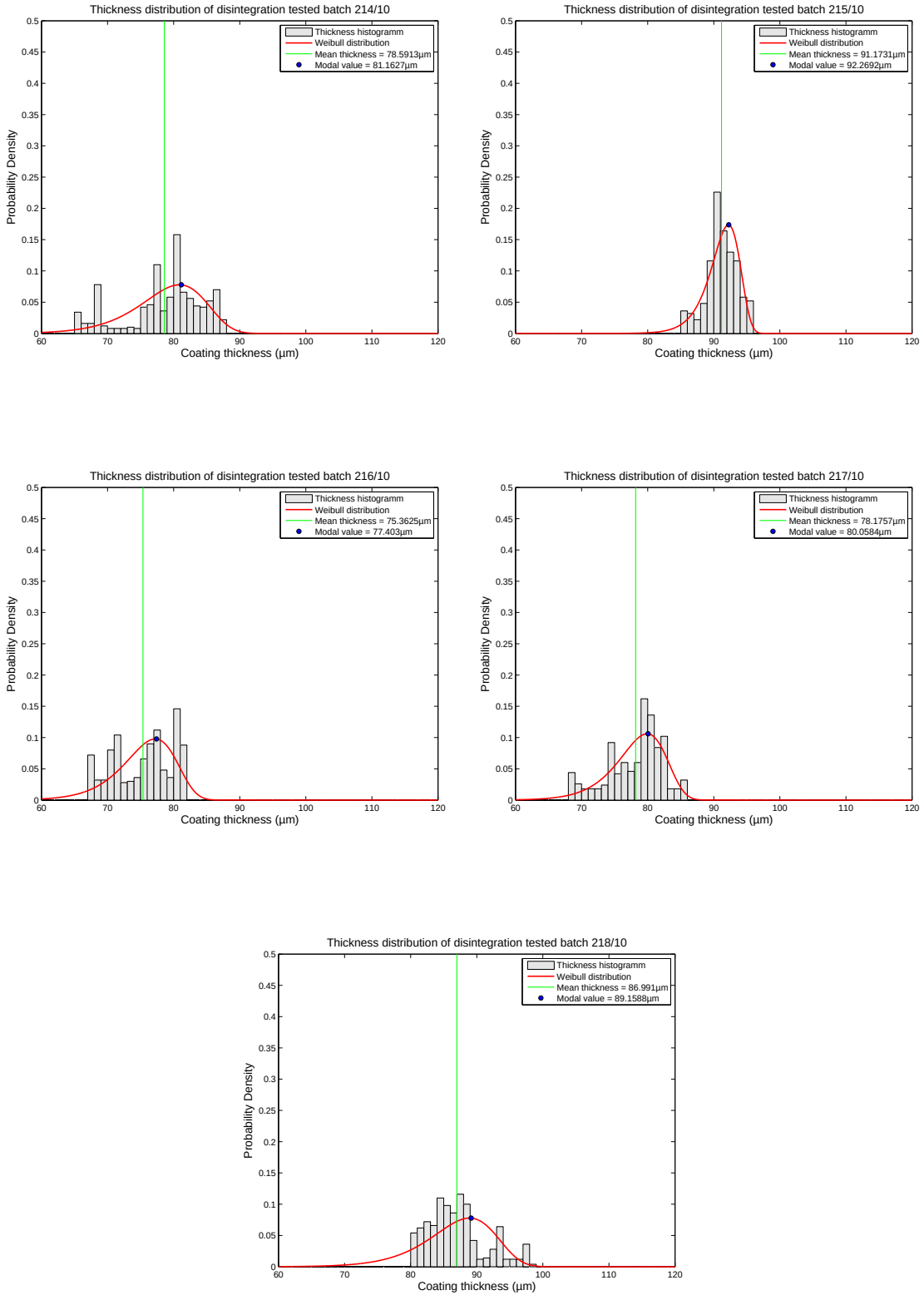

Figure A.4.: Thickness distribution histogram with mean and modal value of disintegration tested tablet A batches.

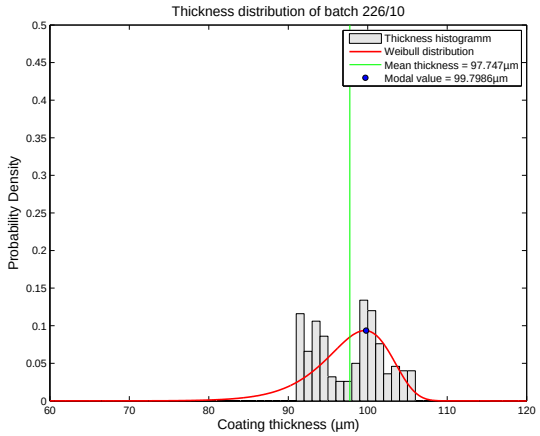
Thickness distribution of batch 226/10
Thickness histogramm
Weibull distribution
Mean thickness = 97.747µm
Modal value = 99.7986µm
Probability Density
Coating thickness (µm)

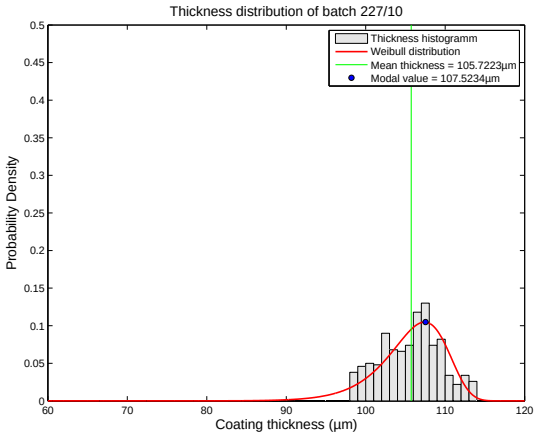
Thickness distribution of batch 227/10
Thickness histogramm
Weibull distribution
Mean thickness = 105.7223µm
Modal value = 107.5234µm
Probability Density
Coating thickness (µm)

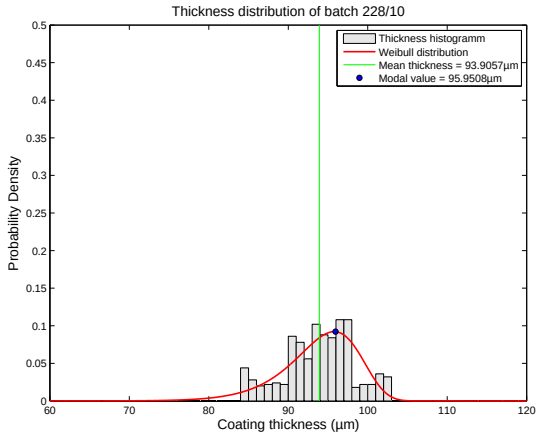
Thickness distribution of batch 228/10
Thickness histogramm
Weibull distribution
Mean thickness = 93.9057µm
Modal value = 95.9508µm
Probability Density
Coating thickness (µm)

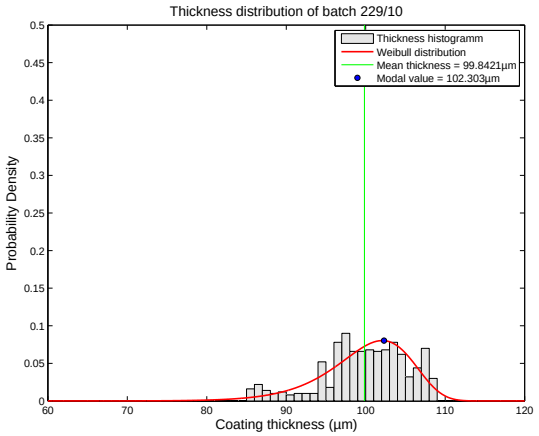
Thickness distribution of batch 229/10
Thickness histogramm
Weibull distribution
Mean thickness = 99.8421µm
Modal value = 102.303µm
Probability Density
Coating thickness (µm)

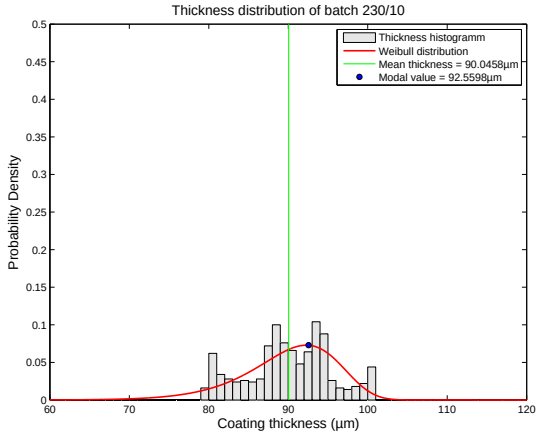
Thickness distribution of batch 230/10
Thickness histogramm
Weibull distribution
Mean thickness = 90.0458µm
Modal value = 92.5598µm
Probability Density
Coating thickness (µm)

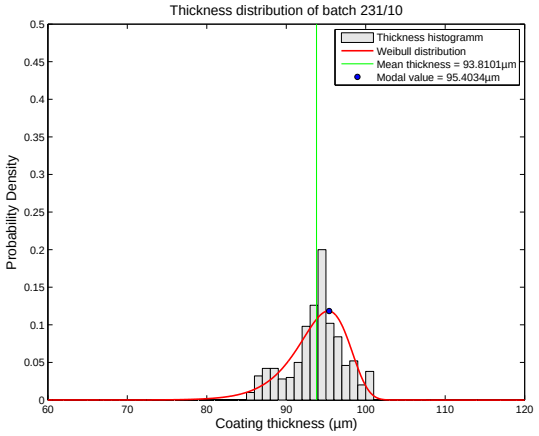
Thickness distribution of batch 231/10
Thickness histogramm
Weibull distribution
Mean thickness = 93.8101µm
Modal value = 95.4034µm
Probability Density
Coating thickness (µm)

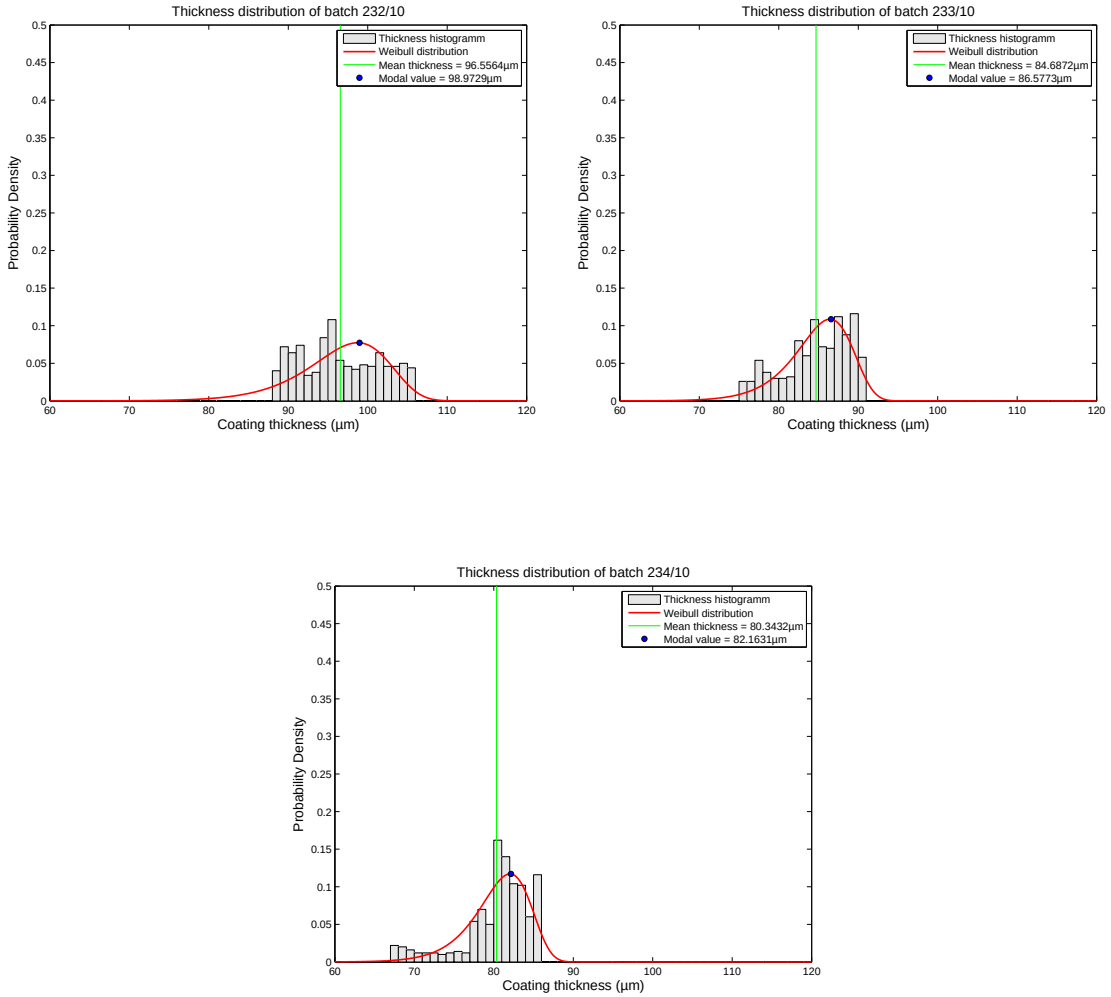

Figure A.5.: Thickness distribution histogram with mean and modal value of tablet B batches.

A.4. OCT Images

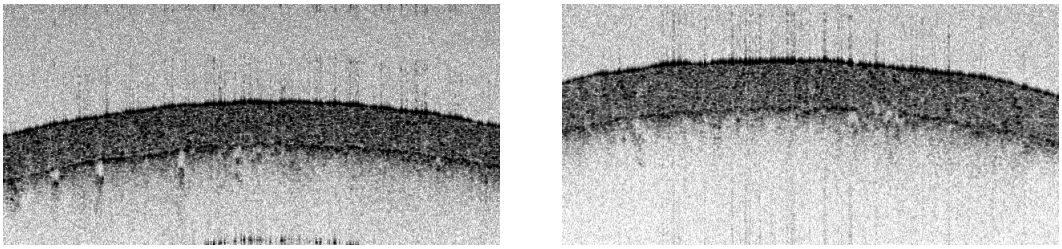

(a) OCT image of 212/10.

(b) OCT image of 213/10.

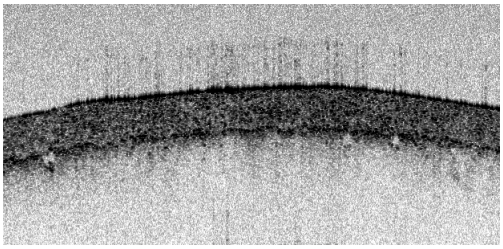

(c) OCT image of 214/10.

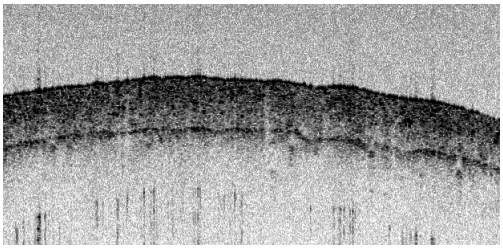

(d) OCT image of 215/10.

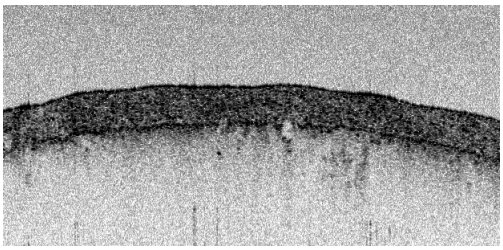

(e) OCT image of 216/10.

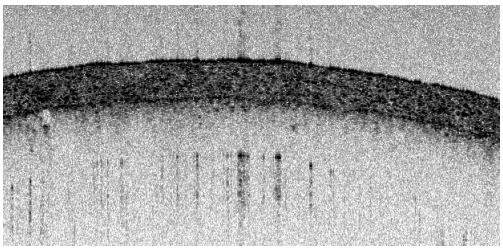

(f) OCT image of 217/10.

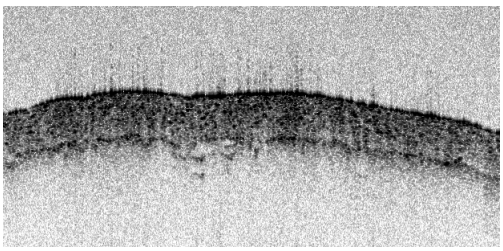

(g) OCT image of 218/10.

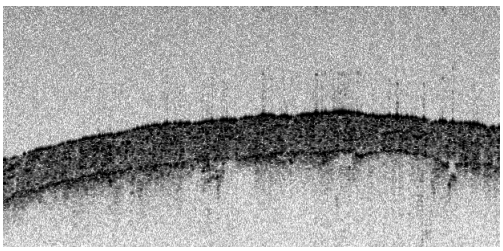

(h) OCT image of 224/10.

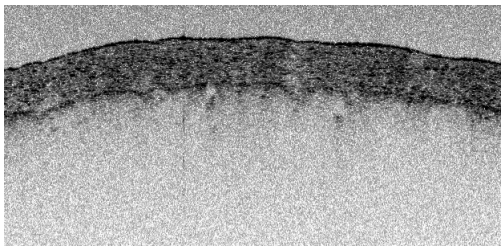

(i) OCT image of 225/10.

Figure A.6.: Batch representative OCT images of tablet A experiments.

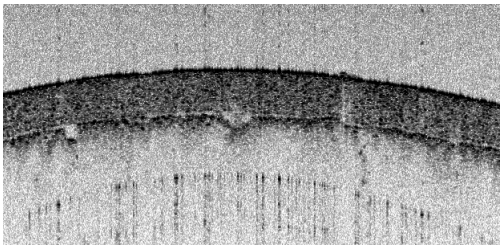

(a) OCT image of 212/10.

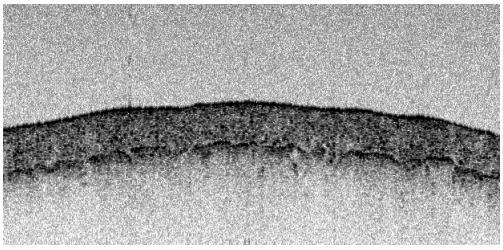

(b) OCT image of 213/10.

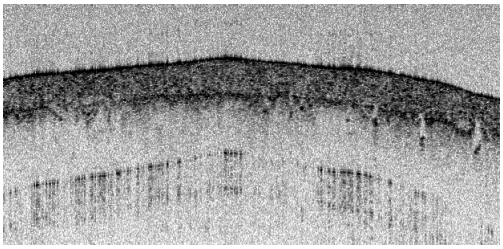

(c) OCT image of 214/10.

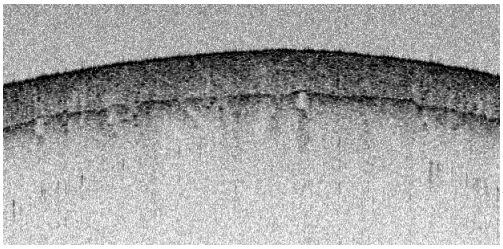

(d) OCT image of 215/10.

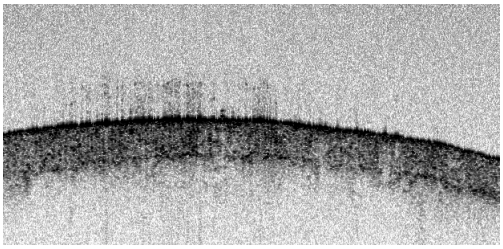

(e) OCT image of 216/10.

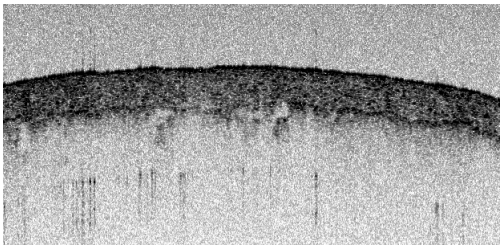

(f) OCT image of 217/10.

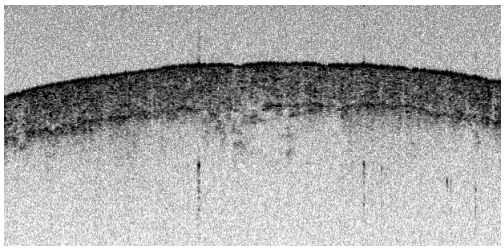

(g) OCT image of 218/10.

Figure A.7.: Batch representative OCT images of disintegration tested tablet A experiments.

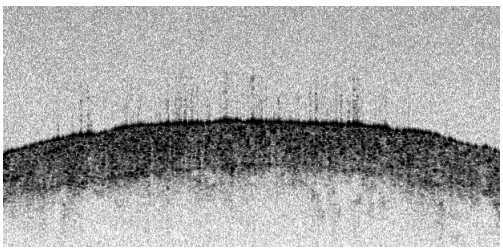

(a) OCT image of 226/10.

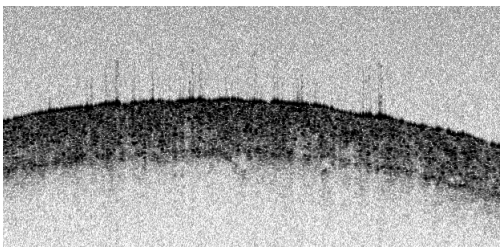

(b) OCT image of 227/10.

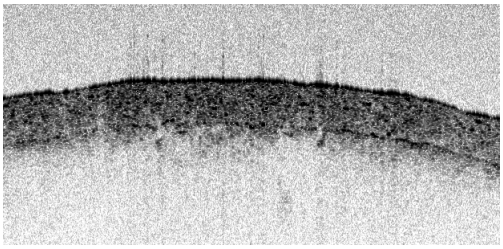

(c) OCT image of 228/10.

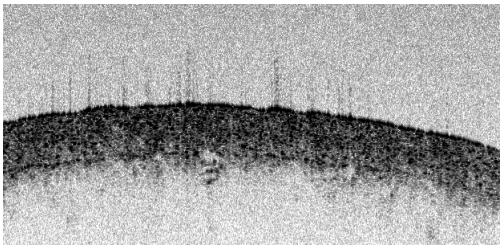

(d) OCT image of 229/10.

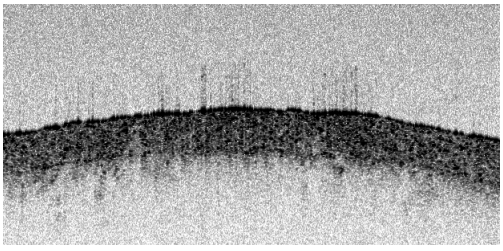

(e) OCT image of 230/10.

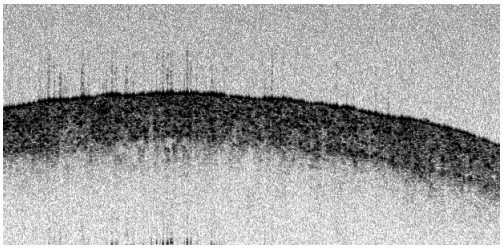

(f) OCT image of 231/10.

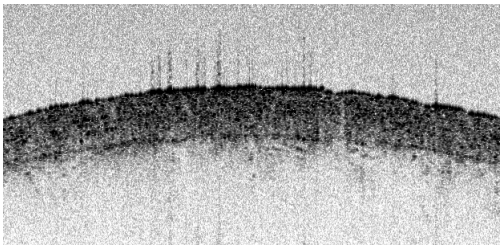

(g) OCT image of 232/10.

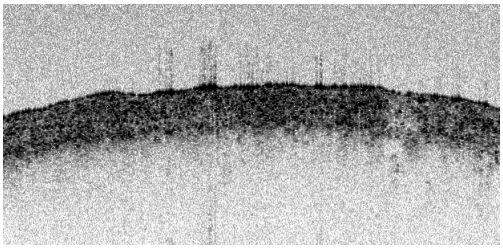

(h) OCT image of 233/10.

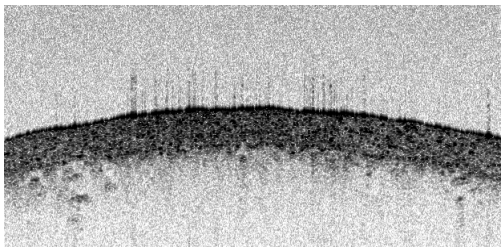

(i) OCT image of 234/10.

Figure A.8.: Batch representative OCT images of tablet B experiments.

A.4. Experimental plan (DoE)

Experimental plan for tablet A (DoE)

				Factors				Responses						
Exp No	Exp Name	Run Order	Incl/Excl	Tablet bed temp (°C)	Spray rate (RPM)	Supply air power (%)	Spray rate (g/min)	Tablet weight (mg)	Coating center MECH (µm)	Coating side MECH (µm)	process time (min)	Coating center IPT (µm)	API release 10min (%)	Coating center MAT (µm)
1	212/10	1	Incl	31	2,5	40	5,27	215,27	91,6	51,02	59	93,19	56,6	98,62
2	213/10	2	Incl	42	2,5	40	4,39	215,67	87,35	50,98	70	101,76	52,2	101,58
3	214/10	3	Incl	23	2,5	40	4,87	216,4	94,65	79,6	56	91,69	73,3	95,78
4	215/10	4	Incl	31	1,5	40	2,35	215,14	84,25	47,47	127	106,84	58,4	107,66
5	216/10	5	Incl	31	3,5	40	7,18	216,17	75,65	72,75	35	86,19	74,7	84,86
6	217/10	6	Incl	31	2,5	60	4,73	215,74	80,45	55,1	57	86,44	77,8	85,4
7	218/10	7	Incl	31	2,5	20	3,83	215,36	90,65	52,73	62	95,85	62,5	89,57
8	224/10	8	Excl	31	2,5	40	4,79	215	77,95	66,53	63	88,02	79	86,84
9	225/10	9	Incl	31	2,5	40	4,67	215,95	84,45	61,42	63	100,68	71,9	96,6

Experimental plan for tablet B (DoE)

				Factors				Responses					
Exp No	Exp Name	Run Order	Incl/Excl	Tablet bed temp (°C)	Spray rate (RPM)	Supply air power (%)	Spray rate (g/min)	Tablet weight (mg)	Coating center MECH (µm)	Coating side MECH (µm)	Process time (min)	Coating center IPT (µm)	Coating center MAT (µm)
1	226/10	1	Incl	31	2,5	40	4,73	161,55	97,95	56,63	68	100,18	97,75
2	230/10	5	Incl	31	2,5	40	5,05	161,37	96,45	57,82	58	89,02	90,05
3	232/10	7	Incl	31	2,5	40	3,7	162,43	99,5	57,23	91	99,6	96,56
4	227/10	2	Incl	42	2,5	40	4,57	161,61	97,6	55,12	75	109,1	105,73
5	234/10	9	Incl	23	2,5	40	3,64	160,98	99,3	62,98	75	81,36	80,35
6	229/10	4	Incl	31	1,5	40	2,49	161,06	95,6	49,7	127	102,68	99,84
7	233/10	8	Incl	31	3,5	40	5,69	162,24	95,15	61,67	53	85,27	84,69
8	231/10	6	Incl	31	2,5	60	4,9	162	100,5	59,97	62	94,93	93,81
9	228/10	3	Incl	31	2,5	20	4,88	161,93	102,3	63,7	66	95,68	93,91

A.5. Image processing algorithm

```
% Program name: image_algorithm.m
% Author: Christoph Schinwald
% Purpose: Automatic OCT image analysis and statistical evaluation
% Date: April 2011, Version 5

clear all;
close all;

number_of_images=10; % number of images investigated
coating_low=60;      % to adjust settings of histogramm
coating_high=120;
fontsize=13;         % adjust fontsize in diagrams

for i=41:(40+number_of_images);
    image_number=num2str(i);

    % select type of tablet:
    type='Tablet A'; cal=3;
%     type='Tablet B'; cal=0;
%     type='Tablet A HCl'; cal=3;

    % select Center or Edge:
    position='Center';
%     position='Edge';

    % select Batch:
    batch='212'; probe='Probe4'; cal_cen=55.95; cal_edg=47.40;
%     batch='213'; probe='Probe4'; cal_cen=61.10; cal_edg=53.05;
%     batch='214'; probe='Probe7'; cal_cen=55.05; cal_edg=46.65;
%     batch='215'; probe='Probe7'; cal_cen=64.15; cal_edg=55.55;
%     batch='216'; probe='Probe2'; cal_cen=51.75; cal_edg=47.65;
%     batch='217'; probe='Probe3'; cal_cen=51.90; cal_edg=48.25;
%     batch='218'; probe='Probe3'; cal_cen=57.55; cal_edg=49.50;
%     batch='224'; probe='Probe0'; cal_cen=52.85; cal_edg=48.45;
%     batch='225'; probe='Probe7'; cal_cen=60.45; cal_edg=50.45;
%     batch='212'; probe='HCl_P1'; cal_cen=56.65; cal_edg=50.35;
%     batch='213'; probe='HCl_P5'; cal_cen=55.10; cal_edg=46.10;
%     batch='214'; probe='HCl_P3'; cal_cen=45.70; cal_edg=42.85;
%     batch='215'; probe='HCl_P0'; cal_cen=52.90; cal_edg=44.35;
%     batch='216'; probe='HCl_P3'; cal_cen=48.20; cal_edg=47.25;
%     batch='217'; probe='HCl_P0'; cal_cen=49.00; cal_edg=43.85;
%     batch='218'; probe='HCl_P3'; cal_cen=54.20; cal_edg=46.70;
%     batch='226'; probe='Probe5'; cal_cen=60.15; cal_edg=49.95;
%     batch='227'; probe='Probe1'; cal_cen=65.45; cal_edg=55.95;
%     batch='228'; probe='Probe9'; cal_cen=57.45; cal_edg=51.40;
%     batch='229'; probe='Probe6'; cal_cen=61.65; cal_edg=53.40;
%     batch='230'; probe='Probe3'; cal_cen=53.45; cal_edg=49.15;
%     batch='231'; probe='Probe5'; cal_cen=57.00; cal_edg=52.05;
%     batch='232'; probe='Probe2'; cal_cen=59.80; cal_edg=53.10;
%     batch='233'; probe='Probe4'; cal_cen=51.20; cal_edg=50.65;
%     batch='234'; probe='Probe6'; cal_cen=48.85; cal_edg=46.35;
```

```
    imagename = ['C:\Dokumente und Einstellungen\diplomand\Eigene Dateien\Area
3\A 3.1\Thickness determination - Matlab Algorithm\Algorithm
V5.0\',type,'\',batch,'_10\Fitted
images\',batch,'_',probe,'_',position,'_',image_number,'_log.bmp'];

    image=imread(imagename);
%     imtool(image);
%     break;

    poly_degree=20;
    res=2.6*1000/1025; % (µm/pixel)
    refraction_index=1.523; % Refraction index for Tablet A coating
    smoothing_window=2; % x pixels above and under the on under investigation

    dimension=size(image);

    image_check=zeros(size(image));
    for col=1:dimension(1,2);
        for row=1:dimension(1,1);
            image_check(row,col)=image(row,col);
        end
    end

    check_mean=0;
    pixel_check = 0;
    pixel_select = 0;
    edge_detector1=zeros(dimension(1,2),1); % For detecting upper edge
    edge_detector2=zeros(dimension(1,2),1); % For detecting lower edge
    edge_detector2=edge_detector2+300;      % start from bottom

    for col=1:dimension(1,2);   % detect upper edge columnwise
        for row=20:(dimension(1,1)-smoothing_window); % start at 20 to exclude
possible black bar at top
            for pixelcheck=1:smoothing_window;
                check_mean=check_mean+image_check((pixelcheck+row-1),col);
            end
            if check_mean <= 200; % 2 pixels lower 200 is quite dark and
therefore coating
                edge_detector1(col,1)=row;  % save pixel position at detector
                break;
            end
            check_mean=0;   % reset
        end
    end

    check_mean=0;   % reset

    for col=1:dimension(1,2);   % detect lower edge columnwise
        for row=(dimension(1,1)):-1:smoothing_window;   % from bottom to top
            for pixelcheck=1:smoothing_window;
                check_mean=check_mean+image_check((row-pixelcheck+1),col);
            end
            if check_mean <= 100; % lower edge is harder to detect, therefore
2 pixels lower 100 is coating
                edge_detector2(col,1)=row;  % save pixel position at detector
                break;
            end
```

```
            check_mean=0;    % reset
        end
    end

    x = (1: 1: 620);
    edge_detector1=300-edge_detector1;  % mirror detected edge
    edge_detector1=edge_detector1';
    p2 = polyfit(x,edge_detector1,2);   % fit first polynom to determine
relevant values
    f2 = polyval(p2,x);

%     plot(x,edge_detector1,'k');
%     hold on;
%     plot(f2,'b'); plot((f2+10),'r'); plot((f2-10),'r');
%     xlabel('Image pixel');
%     ylabel('Image pixel');
%     title('Detection of upper edge');
%     xlim([0 620]); ylim([0 300]);
%     break;

    for col=1:620;  % exclude non-relevant values
        if edge_detector1(1,col) > (f2(1,col)+10) % values more than 10 pixels
bigger than first polynom
            edge_detector1(1,col)=0;    % set 0 if non-relevant
        elseif edge_detector1(1,col) < (f2(1,col)-10) % values more than 10
pixels smaller than first polynom
            edge_detector1(1,col)=0;    % set 0 if non-relevant
        end
    end

    exclude_zero = edge_detector1 ~= 0; % exclude zeros from vector
    edge_detector1_2 = edge_detector1(exclude_zero); % define detector with
relevant values
    x2 = x(exclude_zero);   % define new x-axis
    p1 = polyfit(x2,edge_detector1_2,poly_degree);  % fit polynom for upper
edge
    f1 = polyval(p1,x);

%     plot(x2,edge_detector1_2,'k');
%     hold on;
%     plot(f1,'b');
%     xlabel('Image pixel');
%     ylabel('Image pixel');
%     title('Approximation of upper edge');
%     xlim([0 620]); ylim([0 300]);
%     break;

    edge_detector2=300-edge_detector2;  % mirror detected edge
    edge_detector2=edge_detector2';

    for col=1:620;  % exclude non-relevant values
        if strcmp('Center',position)==1;
            if edge_detector2(1,col) > (f1(1,col)-cal_cen+20) % values more
than 10 pixels bigger than offset (cal) from first polynom
                edge_detector2(1,col)=0;    % set 0 if non-relevant
            elseif edge_detector2(1,col) < (f1(1,col)-cal_cen-20) % values
more than 10 pixels smaller than offset (cal) from first polynom
```

```
                edge_detector2(1,col)=0;    % set 0 if non-relevant
            end
        else
            if edge_detector2(1,col) > (f1(1,col)-cal_edg+20)
                edge_detector2(1,col)=0;    % set 0 if non-relevant
            elseif edge_detector2(1,col) < (f1(1,col)-cal_edg-20)
                edge_detector2(1,col)=0;    % set 0 if non-relevant
            end
        end
    end

%     plot(x,edge_detector2,'k');
%     hold on;
%     plot((f1-cal_cen-20),'r'); plot((f1-cal_cen+20),'r');
%     xlabel('Image pixel');
%     ylabel('Image pixel');
%     title('Detection of lower edge');
%     xlim([0 620]); ylim([0 300]);
%     break;

    exclude_zero = edge_detector2 ~= 0; % exclude zeros from vector
    edge_detector2_2 = edge_detector2(exclude_zero); % define detector with
relevant values
    x2 = x(exclude_zero);   % define new x-axis
    p3 = polyfit(x2,edge_detector2_2,poly_degree);  % fit polynom for lower
edge
    f3 = polyval(p3,x);

%     plot(x2,edge_detector2_2,'k');
%     hold on;
%     plot(f3);% plot((f1-cal_cen-20),'r'); plot((f1-cal_cen+20),'r');
%     xlabel('Image pixel');
%     ylabel('Image pixel');
%     title('Approximation of lower edge');
%     xlim([0 620]); ylim([0 300]);
%     break;

    for a=1:60; % clear first and last columns of polynoms (not good fitted)
        f1(:,1)=[];
        f3(:,1)=[];
        dimension=size(f1);
        col=dimension(1,2);
        f1(:,col)=[];
        f3(:,col)=[];
    end

    x=1:500;
    edgeplot=figure;
    edgedata=plot(x,f1,'b',x,f3,'b');
    xlabel('Pixel');
    ylabel('Pixel');
    title('Reconstruction of film coating edges');
    ylim([0 300]); xlim([0 500]);

    edge_image = ['C:\Dokumente und Einstellungen\diplomand\Eigene
Dateien\Area 3\A 3.1\Thickness determination - Matlab Algorithm\Algorithm
```

```
V5.0\',type,'\',batch,'_10\Edge
images\',batch,'_',position,'_',image_number,'_edge.bmp'];
    print(edgeplot, '-dbmp', edge_image);
    close;

    dimension=size(f1);

    if i==41;
        thickness_vector=zeros(number_of_images,dimension(1,2));  % vector for
number of coating pixels each column
    end

    for col=1:dimension(1,2);
        thickness_vector((i-40),col)=(f1(1,col)-f3(1,col)-cal)*res...
            /refraction_index;  % thickness per column per image
    end

    image_number='';
end

mean_histplot=mean(thickness_vector); % average over rows
skew_hist=skewness(mean_histplot);    % calculate skewness of histogramm
std_dev=std(mean_histplot);           % calculate standard deviation of
histogramm
mean_thickness=mean(mean_histplot);   % average over rows and columns

binWidth=1;
binCtrs=(coating_low+0.5):binWidth:(coating_high-0.5);  % to cover thickness
variation
histplot=figure;
histdata=hist(mean_histplot,binCtrs);

paramEsts1 = wblfit(mean_histplot);
paramEsts2 = cauchyfit(mean_histplot);
[mu,sigma] = normfit(mean_histplot);

n = length(mean_histplot);
prob = histdata / (n * binWidth);
bar(binCtrs,prob,'hist');
h = get(gca,'child');
set(h,'FaceColor',[0.9 0.9 0.9],'EdgeColor','k');
% if strcmp('Center',position)==1;
xlabel('Coating thickness (µm)','FontSize',fontsize);
% else
%     xlabel('Thickness of filmcoating, side of tablet (µm)');
% end
ylabel('Probability Density','FontSize',fontsize);
if strcmp('Tablet A HCl',type)==1;
    batchtitle=['Thickness distribution of disintegration tested batch
',batch,'/10'];
else
    batchtitle=['Thickness distribution of batch ',batch,'/10'];
end
title(batchtitle,'FontSize',fontsize);
xgrid = linspace(coating_low,coating_high,1000); ylim([0 0.5]);
pdfEst1 = wblpdf(xgrid,paramEsts1(1),paramEsts1(2));
pdfEst2 = cauchypdf(xgrid,paramEsts2(1),paramEsts2(2));
```

```
pdfEst3 = normpdf(xgrid,mu,sigma);

weib_modal=paramEsts1(1,1);
weib_fwhm=fwhm(xgrid,pdfEst1);
modalstring=num2str(weib_modal);
Modalname = ['Modal value = ',modalstring,'µm'];
fwhmstring=num2str(weib_fwhm);
fwhmname = ['FWHM = ',fwhmstring];
meanstring=num2str(mean_thickness);
Meanname = ['Mean thickness = ',meanstring,'µm'];

var_wbl=0;
var_cauchy=0;
var_norm=0;

for i=1:50;
    var_wbl=var_wbl+(pdfEst1(1,(i*20)-10)-prob(1,i))^2;
    var_cauchy=var_cauchy+(pdfEst2(1,(i*20)-10)-prob(1,i))^2;
    var_norm=var_norm+(pdfEst3(1,(i*20)-10)-prob(1,i))^2;
end

var_vector=[var_wbl,var_cauchy,var_norm];
% lookup=find(var_vector==min(var_vector));

% if lookup==1
line(xgrid,pdfEst1,'LineWidth',1.5,'Color','r');
hold on;
%plot(mean_thickness,prob(ceil(mean_thickness-
coating_low)),'o','MarkerEdgeColor','k','MarkerSize',5,'MarkerFaceColor','g');
x = mean_thickness; % positionen für die Marker
lim = get(gca,'YLim'); % die Höhe des Markers wird von der Höhe der Axes
abgeleitet:
h = arrayfun(@(x) line([x x],lim,'LineWidth',1,'Color','g'),x); % Marker
zeichen
hold on;
plot(weib_modal,max(pdfEst1),'o','MarkerEdgeColor','k','MarkerSize',5,'MarkerF
aceColor','b');
legend('Thickness histogramm','Weibull
distribution',Meanname,Modalname,'FontSize',fontsize);
% elseif lookup==2
%     line(xgrid,pdfEst2,'LineWidth',1,'Color','r');
%     legend('Thickness histogramm','Cauchy distribution');
% else
%     line(xgrid,pdfEst3,'LineWidth',1,'Color','r');
%     legend('Thickness histogramm','Normal distribution');
% end

skew_wbl=skewness(pdfEst1);
% skew_cauchy=skewness(pdfEst2);
% skew_norm=skewness(pdfEst3);
% skew_vector=[skew_hist,skew_wbl,skew_cauchy,skew_norm];

histname = ['C:\Dokumente und Einstellungen\diplomand\Eigene Dateien\Area 3\A
3.1\Thickness determination - Matlab Algorithm\Algorithm
V5.0\',type,'\',batch,'_10\',batch,'_hist_',position,'.eps'];
print(histplot, '-depsc2', histname);
```

```
histname = ['C:\Dokumente und Einstellungen\diplomand\Eigene Dateien\Area 3\A
3.1\Thickness determination - Matlab Algorithm\Algorithm
V5.0\',type,'\',batch,'_10\',batch,'_hist_',position,'.pdf'];
print(histplot, '-dpdf', histname);
histname = ['C:\Dokumente und Einstellungen\diplomand\Eigene Dateien\Area 3\A
3.1\Thickness determination - Matlab Algorithm\Algorithm
V5.0\',type,'\jpgs\',batch,'_hist_',position,'.png'];
print(histplot, '-dpng', histname);

mean_histplot=mean_histplot';

% open the file with write permission
filename = ['C:\Dokumente und Einstellungen\diplomand\Eigene Dateien\Area 3\A
3.1\Thickness determination - Matlab Algorithm\Algorithm
V5.0\',type,'\',batch,'_10\',batch,'_',position,'.txt'];
fid = fopen(filename, 'w');
fprintf(fid,'Mean thickness: ');
fprintf(fid,'%3.4f ', mean_thickness);
fprintf(fid,'Standard deviation: ');
fprintf(fid,'%3.4f ', std_dev);
fprintf(fid,'Modal value: ');
fprintf(fid,'%3.4f ', weib_modal);
% fprintf(fid,'Skewness (hist, wbl, cauchy, norm): ');
% fprintf(fid,'%3.4f ', skew_hist);
fprintf(fid,'Skewness (hist, wbl): ');
fprintf(fid,'%3.4f ', skew_hist, skew_wbl);
fprintf(fid,'FWHM: ');
fprintf(fid,'%3.4f ', weib_fwhm);
% fprintf(fid,'Variance (wbl, cauchy, norm): ');
% fprintf(fid,'%3.4f ', var_vector);
% fprintf(fid,'Parameters of distributions: (2 x wbl, 2 x cauchy, 2 x norm):
');
% fprintf(fid,'%3.4f %3.4f %3.4f %3.4f ',paramEsts1,paramEsts2,mu,sigma);
fprintf(fid,'histplot data: ');
fprintf(fid,'%3.4f ', mean_histplot);
fclose(fid);
```